THE DETECTION, ELIMINATION AND DAMAGING EFFECT OF SINGLET OXYGEN IN THE PHOTOSYNTHETIC APPARATUS OF PLANTS AND MICROALGAE

PhD Thesis

Presented by

FAIZA BASHIR

Supervisor: Prof. Dr. Imre Vass

Co-Supervisor: Dr. Milán Szabó

Laboratory of Molecular Stress and Photobiology, Institute of Plant Biology

Biological Research Center, Szeged

Doctoral School of Biology

Faculty of Science and Informatics, University of Szeged,

Szeged, Hungary

2021

Szeged

I dedicate this thesis to

my beloved family and my husband

for their constant support and unconditional love.

I love you all dearly.

Table of Contents

LIST OF FIGURES AND TABLES

Tables

ABBREVIATIONS

O_2 - molecular oxygen

$^1O_2$ - singlet oxygen

$^3O_2$ - triplet oxygen

ASG - Aarhus sensor green

ATP - adenosine-5'-triphosphate

CAP - chloramphenicol

Chl - chlorophyll

Cyt-b_6f - cytochrome b_6f complex

DanePy- 3-[N-(b-diethylaminoethyl)-N-dansyl] aminomethyl-2,2,5,5-tetramethyl-2,5 dihydro1H-pyrrole

DCMU - 3-(3,4-dichlorophenyl)-1,1-dimethylurea

DMBQ - 2,5-dimethyl-p-benzoquinone

EPR- electron paramagnetic resonance

Fm - maximum fluorescence in dark

Fo - minimum fluorescence

Fv/Fm - maximum quantum yield of Photosystem II in dark adapted state

His - histidine

LHCI - light-harvesting complex I

LHCII - light-harvesting complex II

NaN_3 - sodium azide

NDH - NAD(P)H dehydrogenase

P680 - reaction center chlorophyll of PSII

P700 -reaction center chlorophyll of PSI

PB - phycobilisome

Phe - pheophytin

PQ - plastoquinone

PQH2 - plastoquinol

PSI - photosystem I

PSII - photosystem II

Q_A, Q_B - primary and secondary quinone molecules

RNO - p-nitrosodimethylaniline

ROS - reactive oxygen species

TyrD- tyrozine-D

TyrZ- tyrozine-Z

SOSG - singlet oxygen sensor green

TEMP - 2,2,6,6-tetramethylpiperidine

TEMPD - 2,2,6,6-tetramethyl-4-piperidone

TEMPD-HCl - 2,2,6,6-tetramethyl-4-piperidone hydrochloride

PAR- photosynthetically active radiation

Fd- ferredoxin;

FR- far-red illumination

PC-plastocyanin

TL- thermoluminescence

RB- rose bengal

Pro- proline

MB- methylene blue

Asc- ascorbate

RC- reaction center

1. INTRODUCTION

1.1. Photosynthesis: an overview

Plants, algae, and cyanobacteria capture sunlight and use it to convert water and carbon dioxide into carbohydrate molecules and oxygen (Renger & Govindjee, 1985), which are essential for the present state of life on Earth. The process of photosynthesis evolved 2.5 to 3 billion years ago, and it is the route by which almost all energy enters the biosphere (Olson, 2006). Photosynthesis is a fundamental biochemical and physicochemical mechanism, and plants use it as a primary source of energy to power their metabolic processes. This process includes harvesting the energy of sunlight, excitation energy transfer, energy transformation, and electron transfer from water to $NADP^+$ (described in detail in section 1.3), ATP formation, and enzymatic reactions that assimilate carbon dioxide and synthesize carbohydrate (Tanaka & Makino, 2009). Photosynthesis can be divided into two types of reactions, the light and the dark reactions. In the light driven reactions, or more precisely called as photophosphorylation, light energy is used by pigment-protein complexes located in the chloroplast thylakoid membrane, to drive the oxygen-evolving complex to form ATP from ADP, reduce electron carrier molecules, such as $NADP^+$ to NADPH, and produce oxygen as a by-product. In dark reactions, or more precisely called as Calvin-Benson-Bassham cycle, the energy of ATP and reducing power of NADPH are utilized to fix carbon dioxide into sugars (Barber, 2007).

An overall equation of the oxygenic photosynthetic reactions is the following:

$$6\ CO_2 + 6\ H_2O + \text{Light energy} \longrightarrow C_6H_{12}O_6 + 6\ O_2$$

The chlorophyll (Chl) molecules in the chloroplast thylakoid membrane absorb the energy of sunlight, which drives the oxygen-evolving complex, where the water splitting reaction takes place (Lichtenthaler, 1987; Olson, 2006; Barber, 2007). Chlorophyll (Chl) absorbs light primarily in the red and blue spectral regions of UV-visible light. A Chl molecule is excited (Chl^*) from its ground state when it receives a photon. To return to its ground state, the excited Chl either re-emits a photon or dissipates its excitation energy as heat, or it drives the photosynthetic electron transport chain (Demmig-Adams & Adams, 1996; Havaux *et al.*, 2000; Vogelmann & Han, 2000; Hendrickson *et al.*, 2004, 2005).

The photosynthetic organisms contain various photosynthetic pigments which absorb the sunlight. Photosynthetic organisms have a variety of chlorophylls, carotenoids, and bilin pigments. The bulk of the pigments function as an antenna complex, collecting light and

transferring it to the reaction centers (RC) of the photosystems, where chemical oxidation and reduction reactions take place. The photosynthetic apparatus is a highly conserved molecular machinery; however, the antenna systems vary substantially among different classes of photosynthetic organisms. In eukaryotes, there is a pigment-protein antenna complex called light harvesting complex II (LHCII) that is associated with Photosystem II (PSII), as well as an antenna complex called light harvesting complex I (LHCI) that is associated with Photosystem I (PSI). PSII of plants and cyanobacteria comprises two chlorophyll *a*-containing core antennas, CP43 and CP47, in addition to the outer antenna (Mori & Yamamoto, 1992; Alfonso *et al.*, 1994). LHCII and LHCI are made up of a complex of hydrophobic membrane-intrinsic polypeptides that bind chlorophyll *a, b,* and carotenoid molecules non-covalently. However, in cyanobacteria the principal light-harvesting complexes are phycobilisomes (PBs), which are peripheral to the thylakoid membranes (Kamennaya *et al.*, 2012), rather than the integral membrane Chl-a/b binding proteins which capture light in plants. Cyanobacteria do not have Chl-containing LHC but they contain bilin proteins (Glazer, 1984; Grossman *et al.*, 1993; Miskiewicz *et al.*, 2002; Tandeau De Marsac, 2003; Liu *et al.*, 2005).

The absorbed light energy by the Chl molecules in the light harvesting antenna complexes is transferred into the Chl *a* molecules in the RC, where it is used to initiate the primary charge separation reaction. In this process, part of the excitation energy transfer takes place through the chlorophyll triplet state (^{3}Chl*), resulting in the formation of singlet oxygen ($^1O_2$), which is a reactive oxygen species (ROS) (described in detail in section 1.7). The photosynthetic machinery generates a variety of ROS during electron transport (Roth, 2014) (described in details in section 1.6). Linear electron flow connects PSII to PSI via cytochrome b_6f complex (Cyt-b_6f). PSII oxidizes two water molecules into one molecule of O_2, along with four protons and four electrons. These electrons are transferred to $NADP^+$ via Cyt-b_6f and PSI by electron transport chain and generated proton gradient drives ATP synthesis via ATPase (details described in section 1.2). The ATP and NADPH are the products of light dependent reactions and they are used as substrates in a series of reduction-oxidation reactions to produce sugars in a step-wise process known as Calvin cycle (van Grondelle & Zuber, 1992; Forti *et al.*, 2003; Renger, 2010).

1.1.1. Chloroplast structure

In plants and algae, photosynthesis takes place in a specialized organelle, called chloroplast. Chloroplast are lens shaped structures with a diameter of 5-10 µm and surrounded by a double membrane (outer and inner envelope) (Staehelin, 1975; Staehelin & van der Staay,

1996; Mustárdy & Garab, 2003). In plants, the thylakoid membrane is divided into two distinct structures: grana and stroma lammelae (Menke, 1962, 1990). The grana regions typically form grana stacks, which are made up of repeating units with paired layers (Nelson & Yocum, 2006). The stroma lammelae connect the grana stacks together. Grana are the stacked regions of thylakoid membrane while stroma lamellae are the unstacked regions of the thylakoid membranes. Thylakoid membranes enclose an inner aqueous phase, called lumen. The photosynthetic complexes embedded in the thylakoid membrane perform light reactions, while the dark reactions occur in stroma. Plants and algae have thylakoid membranes embedded in the chloroplast and arranged into grana stacks linked by stroma-exposed lamellae. On the other hand, cyanobacteria lack chloroplasts; instead, their thylakoid membranes are dispersed throughout the cells and have attached phycobilisomes (Fig. 1.1). Like mitochondria, the chloroplast has its own genome and can synthesize essential proteins for the photosynthetic machinery.

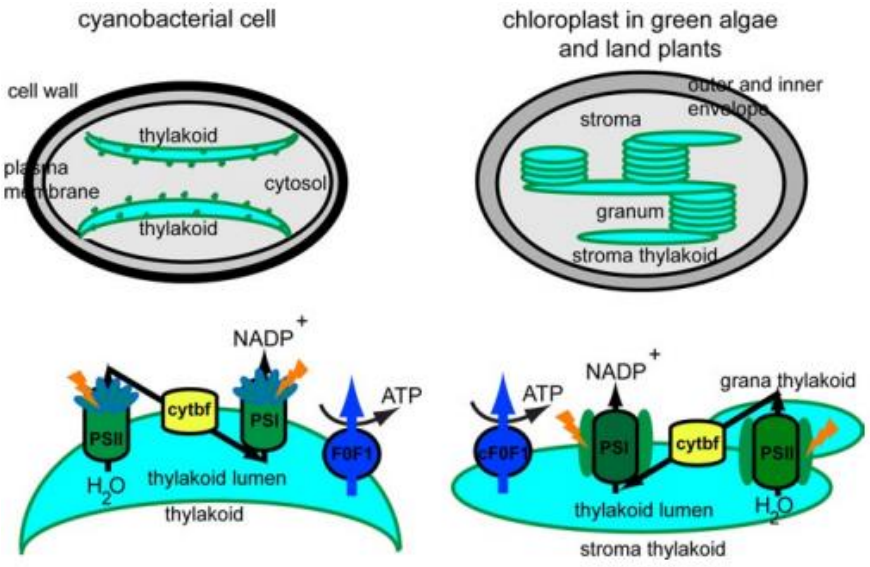

Fig. 1.1. Organization and composition of thylakoid membrane in cyanobacteria and plants (Pfeil *et al.*, 2014).

1.2. Structure and function of photosynthetic apparatus

The photosynthetic apparatus contains four main protein complexes in the thylakoid membrane, namely Photosystem II (PSII), Photosystem I (PSI), cytochrome b_6f complex (Cyt-b_6f) and the ATP synthase (Allen, 1995), which perform the initial, light-dependent steps of the photosynthetic process. These photosystems are embedded in the thylakoid membrane and

include peripheral light-harvesting complexes, pigments, and redox-active cofactors that mediate electron transport reactions. In the thylakoid membrane, these complexes are distributed non-uniformly. The majority of the PSII reaction centers (RC) with their main light-harvesting complex, LHCII, are located in the grana, whereas PSI and its light harvesting complex, the LHCI are found in the stroma membranes and grana margins. ATP synthase is located in the stromal membranes and Cyt-b_6f may exist in both areas of membrane (Andersson & Anderson, 1980; Allen & Forsberg, 2001; Anderson & Chow, 2002; Dekker & Boekema, 2005). According to some studies, Cyt-b_6f, which transports electrons between PSII and PSI, is mainly found in the grana margins (Allen & Forsberg, 2001). PSII complexes are mainly found in stacked part of thylakoid (grana) in chloroplast, while PSI complexes are found in the non-stacked portion of the thylakoid membranes, referred to as lamella (Albertsson, 2001; Rast *et al.*, 2015; Pribil *et al.*, 2018).

1.3. Mechanism of electron transport

The process of oxygenic photosynthesis starts with the light excitation and consequent charge separation both in the RC of PSII and PSI. Anoxygenic photosynthesis differ from oxygenic photosynthesis in that each species has only one type of reaction center. In some photosynthetic bacteria the reaction center is similar to PSII and in others it is similar to PSI. However, neither of these two types of bacterial reaction center is capable of extracting electrons from water, so they do not evolve O_2. The three protein complexes PSII, Cyt-b_6f and PSI are linked in series and the linear electron transfer process between them is usually depicted in the so called Z-scheme (Govindjee, 2004). Photosystem II and I, which are found in oxygenic photosynthetic organisms, each have their own RC Chl molecules, P_{680} and P_{700}, with maximum absorption at 680 and 700 nm, respectively. PSII is composed of various redox components which are responsible for the transfer of electrons from H_2O to the plastoquinone pool (Mn cluster, tyrosine (Tyr), RC P_{680}, Pheophytin (Phe) and plastoquinone (PQ) molecules). In PSII, the photochemical reaction is initiated by charge separation between P_{680} and Phe, creating $P_{680}^{+\bullet}Phe^{-\bullet}$ followed by rapid charge stabilization process. The primary radical pair is stabilized by reduction of Q_A by Phe^- and oxidation of Tyr-Z by $P_{680}^{+\bullet}$ to prevent its rapid recombination.

The first chemical step happens within only a few picoseconds (10-12 ps) when excited P_{680}^* loses an electron to Phe, producing oxidized P_{680} (P_{680}^+) and reduced Phe (Phe^-) in PSII, and excited P_{700}^* loses an electron to A_o, producing oxidized P_{700} (P_{700}^+) and reduced A_o (A_o^-). This is the only step where light energy is converted to chemical energy, precisely oxidation-reduction energy (Govindjee, 2004). The oxygen evolving complex (OEC), which is made up

of four Mn^{2+} and one Ca^{2+} ion, performs the water-splitting reaction on the lumenal side of the PSII complex. Water is split into protons, oxygen and electrons. The electron generated in this reaction is transferred to P_{680}^{+}. Between P_{680} and the OEC complex, a tyrosine residue (Y_z) on the D1 protein serves as an electron transfer intermediate (Fig. 1.2). It reduces P_{680}^{+}, while being reduced by an electron from water splitting (Rutherford, 1989).

From Phe, which is a primary electron acceptor of PSII, electron is transferred to two plastoquinones: Q_A (plastoquinone molecule tightly bound to PSII) and Q_B (plastoquinone molecule loosly bound to PSII) (Rutherford, 1989). Through various heme groups and iron-sulfur clusters, electron will reduce plastocyanin (PC), a small water-soluble copper-containing protein. The reduced PC passes the electron on to PSI. PSI can be described as light-driven plastocyanin-ferredoxin oxidoreductase. After light excitation of the RC (P_{700}) chlorophyll in PSI, charge separation occurs resulting in oxidized P_{700} (P_{700}^{+}). Electrons are transferred from PSI reaction center to the primary acceptor Chl A_0 (chlorophyll a molecule, primary electron acceptor of PSI), then to PhQ A_1 (Phylloquinone) which occupy the quinone binding sites of PSI and finally to iron-sulfur clusters FeS_x, FeS_A, and FeS_B, where they exit PSI and reduce ferredoxin (Fd). Fd is located at the cytoplasmic side and passes the electron on to the membrane-associated flavoprotein ferredoxin: NADP: oxidoreductase (FNR), which in turn catalyzes the reduction of NADP+ to NADPH.

The electrochemical gradient caused by the charge separation across the thylakoid membrane is used by the ATP synthase to produce ATP from ADP and Pi. The stored energy in form of NADPH and ATP is used in the carbon fixation reactions of photosynthesis, which take place in the cytosol or the stroma. The ATP synthase is powered by a proton gradient through the thylakoid membrane. The energetics of the reaction and the distance between the carriers have a crucial role in determining the electron pathway. It is important to remember that reaction conditions during photosynthesis are not always in equilibrium. Electron transport is energetically downhill after primary charge separation (from a lower (more negative) to a higher (more positive) redox potential) (Whitmarsh & Govindjee, 1999). The development of a proton chemical gradient requires free energy, which is provided by the downhill flow of electrons.

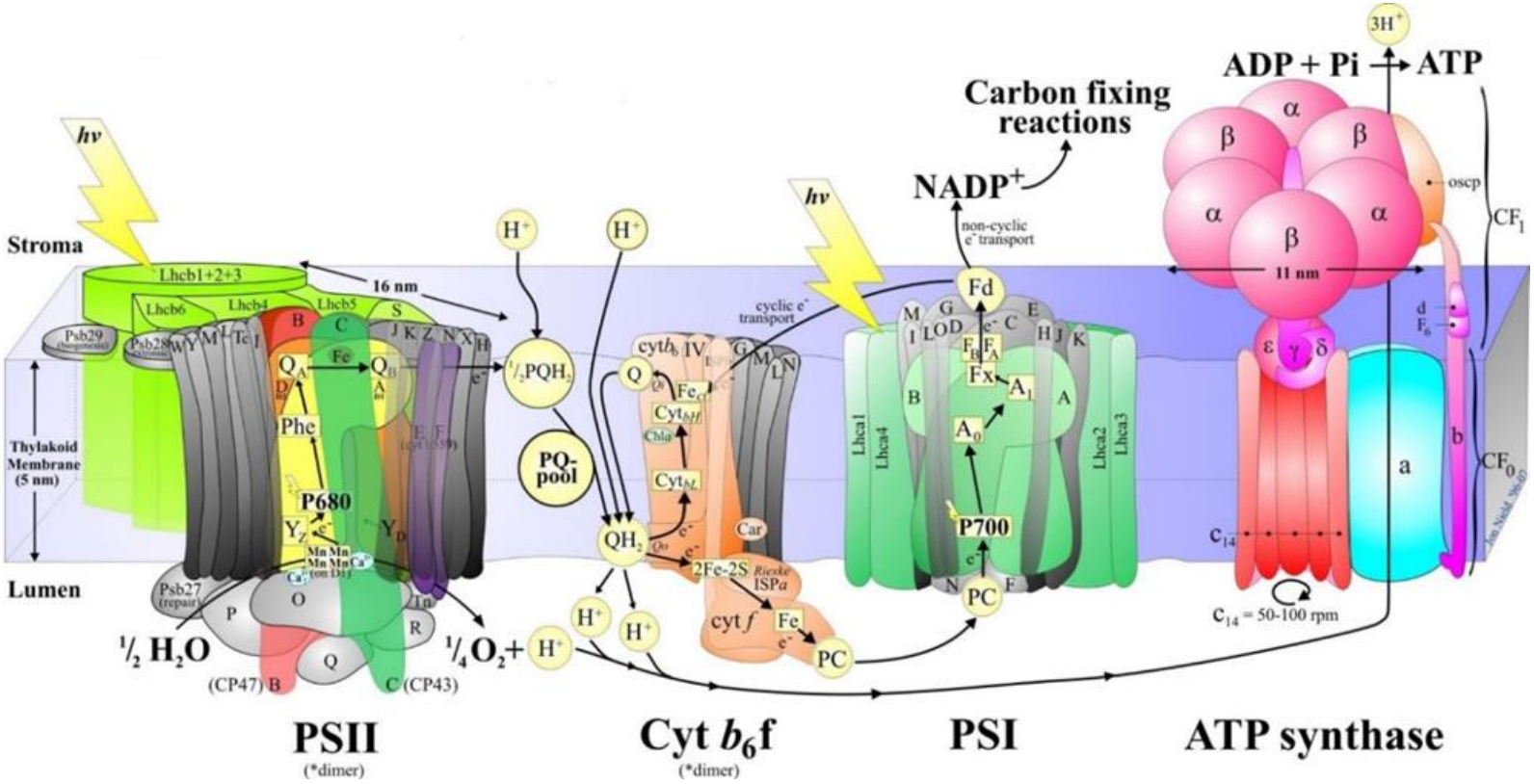

Fig. 1.2. Schematic model of the photosynthetic electron transport chain in the thylakoid membrane of green plants, including structural details on the organization of the protein complexes involved in electron and proton transport. Structural information of PSI, PSI- LHCI, Cyt-b_6f and PSII by (Jordan et al., 2001; Ben-Shem et al., 2003; Stroebel et al., 2003; Ferreira et al., 2004) respectively. Approximate estimated times for the various steps are also indicated in the figure (Govindjee, 2004).

1.4. Structure and function of Photosystem II (PSII)

Photosystem II (PSII), a multi-subunit membrane protein complex, uses light energy to perform the most thermodynamically demanding and unique reaction of photosynthesis, namely the oxidation of water to molecular oxygen and reducing equivalents. Nield and Barber (2006) presented the structure of LHCII-PSII supercomplex of plants at 3.5 resolution and revealed that the molecular mass of PSII dimer is 650 kDa with the depth, length and width of 105 Å, 205 Å, and 110 Å respectively (Nield & Barber, 2006). Each monomer contains more than 20 proteins, of which 16 are intrinsic and four are extrinsic (Hankamer *et al.*, 1997; De Las Rivas & Barber, 2004). The reaction centre of PSII is heterodimer and consists of two homologous proteins named D1 (PsbA) and D2 (PsbD) , which bind cofactors for the electron transport. Closely associated to the D1 and D2 proteins are two chlorophyll-binding proteins called CP43 and CP47 (Kessler & Schnell, 2006; Suorsa & Aro, 2007).

In oxygenic photosynthetic organisms, there are four extrinsic proteins, PsbO, PsbP, PsbQ and PsbR associated with the OEC (Seidler, 1996; De Las Rivas *et al.*, 2007). The OEC complex is located on the lumenal side of the PSII complex (Seibert *et al.*, 1987). The water splitting has its side effects in the RC of PSII: the production of singlet oxygen and of highly oxidising redox components, which may cause damage to the PSII, and especially to its reaction centre D1 subunit (details in section 1.8).

1.5. Photoinhibition, repair and photoprotection

Although light is essential to drive photosynthesis, it can also be a highly energetic and potentially dangerous factor that can harm the photosynthetic apparatus. Light stress to PSII becomes a problem for photosynthetic capacity when the rate of photodamage exceeds the rate of repair process, cauing photodamage and potentially leading to cell death. This process is called photoinhibition. The exact mechanism of photodamage and repair still remains controversial despite intensive research during the last decades (Jones & Kok, 1966; Ohad *et al.*, 1984; Barber & Andersson, 1992; Aro *et al.*, 1993; Nishiyama *et al.*, 2006; Oguchi *et al.*, 2009; Vass & Cser, 2009; Murata *et al.*, 2012; Tyystjärvi, 2013a; Zavafer *et al.*, 2019, 2017).

The most light-sensitive site in the photosynthetic apparatus is the PSII complex in which electron transport activity is impaired and the D1 (and D2) reaction centre protein is degraded, see (Aro *et al.*, 1993). In addition to PSII, PSI (Sonoike & Terashima, 1994; Sonoike *et al.*, 1995; Tiwari *et al.*, 2016; Lima-Melo *et al.*, 2019) as well as the Chl containing light harvesting antenna structures (Zolla & Rinalducci, 2002; Rinalducci *et al.*, 2004, 2008; Lingvay

et al., 2020) can also be damaged by light. PSII is especially vulnerable to light-induced damage, which limits the efficacy of both aquatic and terrestrial photosynthesis. Although the exact mechanism of photodamage and its repair is not fully clarified yet there is a consensus in the literature that ROS are involved in the overall photoinhibition process (Barber & Andersson, 1992; Anderson & Chow, 2002; Nishiyama *et al.*, 2006; Krieger-Liszkay *et al.*, 2008; Vass, 2011, 2012; Fischer *et al.*, 2013). The detrimental effects of light linearly depend on light intensity (Tyystjärvi & Aro, 1996) and can occur at all light intensities (Keren *et al.*, 1997; Kou *et al.*, 2012), therefore plants have evolved a protective repair mechanism, by which light induced loss of photosynthetic activity can be restored. This repair mechanism proceeds via *de novo* synthesis of the light-damaged D1 (and D2) subunit(s) of PSII (Aro *et al.*, 1993; Nixon *et al.*, 2010; Komenda *et al.*, 2012; Li *et al.*, 2018; Murata & Nishiyama, 2018). Due to competing photodamage and repair processes net loss of PSII activity occurs when the rate of photodamage exceeds the rate of repair. Certain protein synthesis inhibitors such as lincomycin and chloramphenicol are used to determine the net photoinhibition, i.e., extent of photodamage in the absence of repair. Unless the rate of damage exceeds the repair rate, photoinhibition does not result in a loss of PSII activity. Only in the absence of concurrent repair can the rate of photodamage be measured. Hence, it is critical to monitor photodamage and protein synthesis-dependent repair rates separately (Nishiyama *et al.*, 2004; Kato *et al.*, 2015).

To survive, the D1 protein undergoes an extensive repair cycle, including degradation and replacement by a newly synthesised protein (Aro *et al.*, 1993). There are two mechanisms of D1 degradation, a donor and an acceptor-side inhibition. The acceptor-side inhibition occurs under high light and is due to an over-reduction of the PQ pool. This in turn leads to the formation of P_{680} triplet state that can cause the formation of singlet oxygen ($^1O_2$) (for details of singlet oxygen production, see section 1.7). The $^1O_2$, produced in the vicinity of the D1 protein, leads to an excessive damage and the need for repair. The donor-side inhibition occurs when the donor-side of PSII can not keep up with the withdrawal of electrons from P_{680}, leading to long lived P_{680}^+ and the oxidised tyrosine electron donor Y_z^+, which causes an inactivation of the PSII electron transport (Aro *et al.*, 1993; Vass, 2012).

Oxygenic photosynthetic organisms have evolved a large array of mechanisms to protect themselves against detrimental effects of light. These include (i) dissipation of excess light energy in the antenna (Ruban *et al.*, 2007) or the PSII RC (Ivanov *et al.*, 2007) before photosynthetic electron transport occurs; (ii) quenching of dangerous Chl triplets and $^1O_2$ by carotenoids (Frank & Cogdell, 1996; Edge *et al.*, 1997; Ramel *et al.*, 2012); and (iii) repair of

the damaged PSII complexes via *de novo* synthesis of the D1 RC protein (Komenda *et al.*, 2007; Nixon *et al.*, 2010).

1.6. Production of reactive oxygen species in the photosynthetic apparatus

Reactive oxygen species (ROS) are chemically reactive molecules containing oxygen. The generation of ROS is important in cellular processes such as infection defense and cellular signaling, and it is linked to damage to cellular components including proteins, lipids, and nucleic acids. Protein complexes in the electron transport chain react with molecular oxygen to produce ROS. The chloroplast and mitochondria are the main sources of ROS production in plant cells (Apel & Hirt, 2004; Laloi & Havaux, 2015). Singlet excited oxygen, free radicals (superoxide and hydroxyl ions), and peroxides are all examples of ROS. When cells are exposed to stressful environments, these ROS are generated (Asada, 2006). PSI and PSII RCs in chloroplasts are the primary source of ROS generation. The reduction of O_2 results in superoxide anion (O_2^-) formation and its disproportionation produces H_2O_2 and O_2 upon dismutation by superoxide dismutase (Jakob & Heber, 1996; Asada, 1999), while $^1O_2$ is created when ground-state O_2 interacts with Chl triplets produced either in the RC of PSII complex or in the light-harvesting antenna (Krieger-Liszkay, 2005; Asada, 2006; Krieger-Liszkay *et al.*, 2008). To protect the thylakoid membrane, rapid scavenging of ROS, which are formed in thylakoids prior to diffusion to surrounding compartments from their generation site, is critical.

1.7. Production of $^1O_2$ in the photosynthetic apparatus

$^1O_2$ is a highly reactive excited state of molecular oxygen (Ogilby, 2010). It is an important ROS in biological systems because it damages proteins, lipids, and nucleic acids. It is less stable than triplet oxygen ($^3O_2$) and can be created in various ways, but the most common way is by transferring energy from a photosensitized pigment or triplet state of dye molecule to triplet oxygen (Hirakawa *et al.*, 2011; Fischer *et al.*, 2013). Photons are absorbed mainly by Chl in the light harvesting antenna complex and the excitation energy is transferred to the RC of PSII, where charge separation occurs between the excited RC assembly (P680*) and Phe. The formation of the primary radical pair/charge-separated state ($P_{680}^{+\bullet}Phe^{-\bullet}$) between the excited RC Chl assembly (P_{680}^{*}) and the Phe molecule is a primary event during PSII electron transfer, which is accompanied by rapid charge stabilization processes. To avoid rapid recombination, the primary radical pair is stabilized by reducing Q_A with Phe and oxidizing Tyr^Z with $P_{680}^{+\bullet}$

(Vass, 2011). The singlet spin configuration ($^1[P680^{+\bullet}Phe^{-\bullet}]$) is used to construct the $[P680^{+\bullet}Phe^{-\bullet}]$ state, which then recombines to $^1P680^*$ (Phe). Spin conversion, on the other hand, will convert $^1[P680^{+\bullet}Phe^{-\bullet}]$ to the triplet $^3[P680^{+\bullet}Phe^{-\bullet}]$, resulting in excited $^3P_{680}$ after recombination. The interaction of the excited triplet $^3P_{680}$ with ground state triplet oxygen produces $^1O_2$ under light stress conditions (Vass, 2011, 2012).

1.8. $^1O_2$ dependent mechanism of photodamage

Production of $^1O_2$ has been demonstrated in isolated photosynthetic complexes (Macpherson *et al.*, 1993; Hideg *et al.*, 1994a; Telfer *et al.*, 1999) and intact photosynthetic systems (Hideg *et al.*, 1998; Flors *et al.*, 2006; Rehman *et al.*, 2013, 2016b). It has also been shown that photolerance in highly light tolerant algal species is accompanied by decreased $^1O_2$ production (Treves *et al.*, 2016; Virtanen *et al.*, 2021). However, the exact sites and mechanisms of ROS action in photoinhibition are debated. According to one idea, ROS, including $^1O_2$, affects only the repair of PSII by inhibiting translation elongation of the *psbA* gene, thereby preventing *de novo* synthesis of photodamaged D1 protein (Nishiyama *et al.*, 2001, 2004, 2006). Other results however, have demonstrated a clear correlation between the rate of $^1O_2$ formation and the rate of PSII photodamage in various experimental systems (Rehman *et al.*, 2013; Bersanini *et al.*, 2014; Hakkila *et al.*, 2014; Sedoud *et al.*, 2014; Treves *et al.*, 2016) pointing to the role of $^1O_2$ as an agent that damages directly the function and structure of the PSII complex (Vass & Cser, 2009)

Previous research has shown that $^1O_2$ can cause damage to the repair cycle as well as cleavage of the D1 and D2 RC subunits (Okada *et al.*, 1996). Other studies find that $^1O_2$ has an indirect damaging effect in *Synechocystis* cells by inhibiting the PSII repair cycle rather than specifically damaging the PSII complex (Nishiyama *et al.*, 2001, 2004, 2006). In comparison to these findings, direct PSII damage has been seen in intact tobacco leaves infiltrated with Rose Bengal (Hideg *et al.*, 2007), and several other groups support direct PSII damage caused by $^1O_2$ (Aro *et al.*, 1993, 1994; Kirilovsky *et al.*, 1994; Dobáková *et al.*, 2007; Vass & Aro, 2008; Allahverdiyeva *et al.*, 2013; Kerfeld & Kirilovsky, 2013; Tyystjärvi, 2013b; Hakkila *et al.*, 2014). Reduction of the PQ molecules in the lipid phase of the membrane due to saturation of electron sinks, especially the Calvin–Bensson cycle, is a crucial step in the excess excitation dependent pathway of photodamage (Fig. 1.3). Excitation back pressure is created when the PQ pool and Q_B are reduced and the $Q_A^{-\bullet}$ is stabilized, resulting in increased $^3P680$ and $^1O_2$ formation (Vass, 2012). The intrinsic rate constant of primary charge separation is 50-300 ns^{-1}

after a single photon excitation (Govindjee, 2004). Since the frequency of the charge separation events, i.e. the number of charge separtion events which occur in a unit time linearly depends on light intensity the produced amount of $^1O_2$, as well as the induced photodamage is expected to increase linearly with increasing light intensity even after reaching saturation of photosynthetic electron transfer (Vass, 2011, 2012), which can explain the experimentally observed linear light depency of the rate of photoinhibition (Tyystjärvi & Aro, 1996).

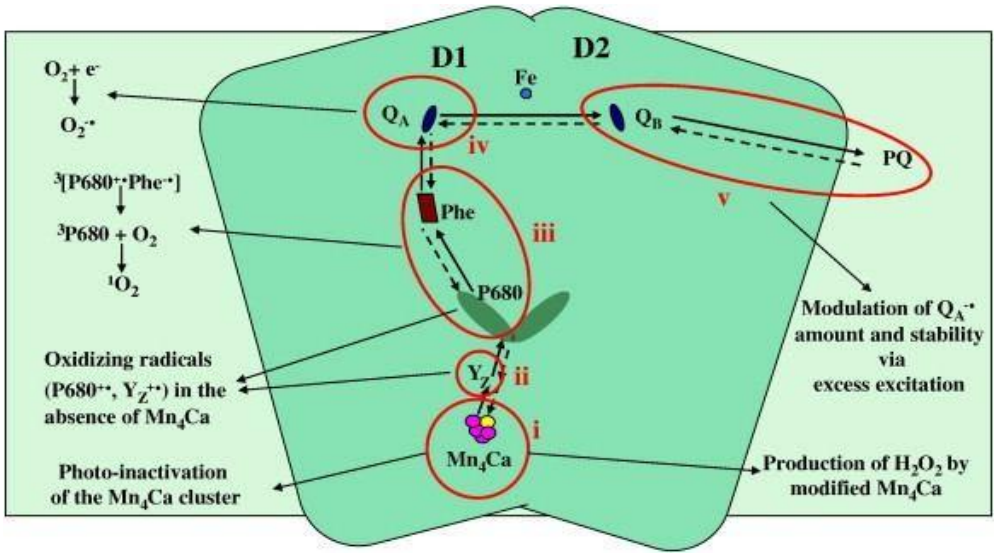

Fig. 1.3. Light -induced photodamage in the PSII complex of photosynthetic apparatus (Vass, 2012).

Besides ^{3}Chl-dependent intracellular $^1O_2$ production, $^1O_2$ can also be produced externally by energy transfer from the triplet state of a photosensitized pigment or dye molecule. Externally produced $^1O_2$ can be generated by externally added photosensitizers, (i.e., Rose Bengal, Methylene Blue) and its role in PSII photodamage can be assessed. The exact sites and mechanism of action of $^1O_2$ in photoinhibition are debated and the main question of this debate is does $^1O_2$ directly damages the PSII or it only affects the PSII repair? The generation of $^1O_2$ by externally added photosensitizers is one useful method for assessing the role of $^1O_2$ in PSII photodamage. Kovács et al., compared the ability of different $^1O_2$ photosenzitizers to penetrate into plant cells (Rose Bengal, Methylene Violet, Neutral Red, and Indigo Carmine). Rose Bengal (RB), which can be excited by green light with only a minor impact on photosynthetic electron transport, was found to be the most effective $^1O_2$ generating photosensitizer, causing PSII activity loss and D1 protein degradation (Kovács *et al.*, 2014). Similar findings were

previously obtained using tobacco leaves infiltrated with RB (Hideg *et al.*, 2007). However, in these studies, very high RB concentrations (100 µM and 1 mM, respectively) were needed to ensure penetration into the tobacco leaf, and no information about the actual level of $^1O_2$ within the cells or in the thylakoid membranes was available. As a result, it is impossible to rule out the possibility that unnaturally high $^1O_2$ levels caused unspecific PSII harm. $^1O_2$ production in the presence of a few micromolar RB concentrations has been shown to induce growth retardation and specific gene expression in the green alga *Chlamydomonas reinhardtii* (Leisinger *et al.*, 2001; Fischer *et al.*, 2004), however, direct PSII damage was not demonstrated in these studies

1.9. Involvement of ROS in the breakdown of coral symbiosis

Symbiodinium, a photosynthetic dinoflagellate, is the crucial symbiotic component of reef building corals and primary producer in the aquatic ecosystem on earth (Murray *et al.*, 2016). Dinoflagellate is any diverse flagellate protists comprising the Phylum Dinoflagellata, typically characterized by being single-celled and with two dissimilar flagella during at least part of their life cycle. In terms of light harvesting, *Symbiodinium* have a unique array of pigments and pigment proteins arranged in a unique thylakoid membrane and plastid (Larkum & Vesk, 2003). There are two major types of light harvesting proteins in *Symbiodinium*, (i) a membrane bound protein (Chl *a*, Chl c_2, peridinin protein complex: acpPC) and (ii) a water-soluble peridinin-chlorophyll protein (PCP) complex. Peridinin has an in vivo absorption spectrum extending up to 540 nm and adds greatly to the absorption capacity of dinoflagellates by light absorption in the blue-green region of the spectrum; thus PCP significantly augments the light-harvesting capacity of the dinoflagellate (Larkum, 2003).

Coral reef ecosystems represent essential habitats for a wide variety of marine animals (Steele *et al.*, 2011). Reef building corals are among the most biologically diverse group, which belong to the Class Anthozoa (Phylum Cnidaria), form an endosymbiosis with dinoflagellate algae from the genus *Symbiodinium* (Family Symbiodiniaceae), that reside within the endodermal tissue of the anthozoan host (Bertucci *et al.*, 2013). In this symbiotic relationship, *Symbiodinium* provides organic compounds to the host (Anthozoan) and in return it gets inorganic compounds and protection from the host, making them pivotal for coral physiology (Yellowlees *et al.*, 2008). Symbiodiniaceae not only drive coral productivity and reef growth (Muscatine & Porter, 1977; Muscatine, 1990), but their physiological, biochemical, morphological and genetic diversity can also determine the thermal bleaching thresholds of

their coral host (Howells *et al.*, 2012; Yuyama *et al.*, 2012; Levin *et al.*, 2016). Cultured *Symbiodinium* exhibit daily morphological changes between a flagellated (motile) stage during the day to a non-flagellated spherical (coccoid) stage at night. *Symbiodinium* cells in the motile stage have thin thecal plates (Loeblich & Sherley, 1979; Trench & Blank, 1987), and thus, some *Symbiodinium* species have been formally described with thecal plate tabulations for species criterion (Hansen & Daugbjerg, 2009; Jeong *et al.*, 2014). However, the differences in thecal tabulations between genetically distant species are small (Lee *et al.*, 2015), therefore, molecular grouping has been commonly used. As a result, *Symbiodinium* has been classified into groups (clades A–I) and each clade consists of numerous subclades or types (Pochon & Gates, 2010). However, more recent molecular and taxonomic analyses indicated the necessity to reassign *Symbiodinium* clades as individual genera within the class Symbiodiniaceae (LaJeunesse *et al.*, 2021). Therefore, a new taxonomic nomenclature applies for the previously defined clades, only clade A referred to as *Symbiodinium*, which is consistently applied in the thesis.

The symbiotic relationship between the coral host and its symbiotic partner is very sensitive to environmental stresses such as ocean acidification and increased temperature, but also to pollutions, pathogens and changes in salinity (Pandolfi *et al.*, 2011). Because of the ecological stressors, the beneficial interaction between the coral host and its algal symbiont may separate, prompting the expulsion of the zooxanthellae (dinoflagellate, the photosynthetic partner in corals, e.g., *Symbiodinium*) and lead to a phenomenon known as coral bleaching (Brown, 1997; Franklin *et al.*, 2004). The mechanisms of expulsion of the *Symbiodinium* is still not fully known. However, the role of ROS, such as $^1O_2$, the superoxide anion radical, hydrogen peroxide and hydroxyl radical which are generated under heat and light stress in symbiotic breakdown has been extensively studied (Lesser *et al.*, 1990; Lesser, 1996; Brown *et al.*, 2002; Downs *et al.*, 2002; Richier *et al.*, 2005; Weis, 2008; Hawkins *et al.*, 2015). Among those, one of the very important ROS is the $^1O_2$, which is highly reactive. Previous studies have shown that the increased production of $^1O_2$ occurs primarily under high light stress conditions, which will ultimately result in the inactivation of PSII and photoinhibition (Hideg & Schreiber, 2007; Triantaphylidès *et al.*, 2008; Triantaphylidès & Havaux, 2009) (see details in the section 1.6). Rehman *et al.*, (2016) used the histidine-mediated chemical trapping method and fluorescein derivative singlet oxygen specific fluorescent dye, Singlet Oxygen Sensor Green (SOSG) for the detection of $^1O_2$ in cultured *Symbiodinium* cells and showed that $^1O_2$ production was increased under light and heat stress (Rehman *et al.*, 2016b). Their study also demonstrated that SOSG is not permeable to *Symbiodinium* cells, which makes it nearly impossible to investigate the adverse effects of intracellularly generated $^1O_2$ in these cells.

1.10. $^1O_2$ detection methods

In vitro and in vivo, a variety of spectroscopic and microscopic techniques have been used to detect the formation of $^1O_2$ in photosynthetic species. In vitro $^1O_2$ detection allows for the quantification of $^1O_2$ formation, while in vivo techniques allow for the spatiotemporal characterization of $^1O_2$ within plant cells. Chemical trapping and fluorescence probes can be used either in vitro or in vivo.

1.10.1. Chemical trapping

Histidine- or imidazole-mediated chemical trapping

Chemical entrapment based on uptake of O_2 due to the reaction of $^1O_2$ with histidine or imidazole is carried out in isolated PSII RC (Telfer et al., 1994) and in *Synechocystis* cultures (Rehman et al., 2013). Fig 1.4A shows a generalized scheme for the histidine (His) mediated chemical trapping method for $^1O_2$ detection in intact *Synechocystis* cells (Rehman et al., 2013). This method relies on the interaction of the produced $^1O_2$ with the aromatic side chain of His or imidazole, which results in the formation of a His oxidation product that lowers the concentration of dissolved O_2 in the suspension. The amount of ROS trapped should be proportional to the amount of O_2 taken up from the medium, as measured by an oxygen electrode. For His it has been proposed that the endoperoxide species is formed through a Diels–Alder process (Méndez-Hurtado et al., 2012). The Diels–Alder reaction is the reaction between a conjugated diene and an alkene (dienophile) to form unsaturated six-membered rings. Since the reaction involves the formation of a cyclic product via a cyclic transition state, it is also referred to as a cycloaddition. The proposed intermediate species and products for the reaction between His and $^1O_2$ are shown in Fig 1.4 B.

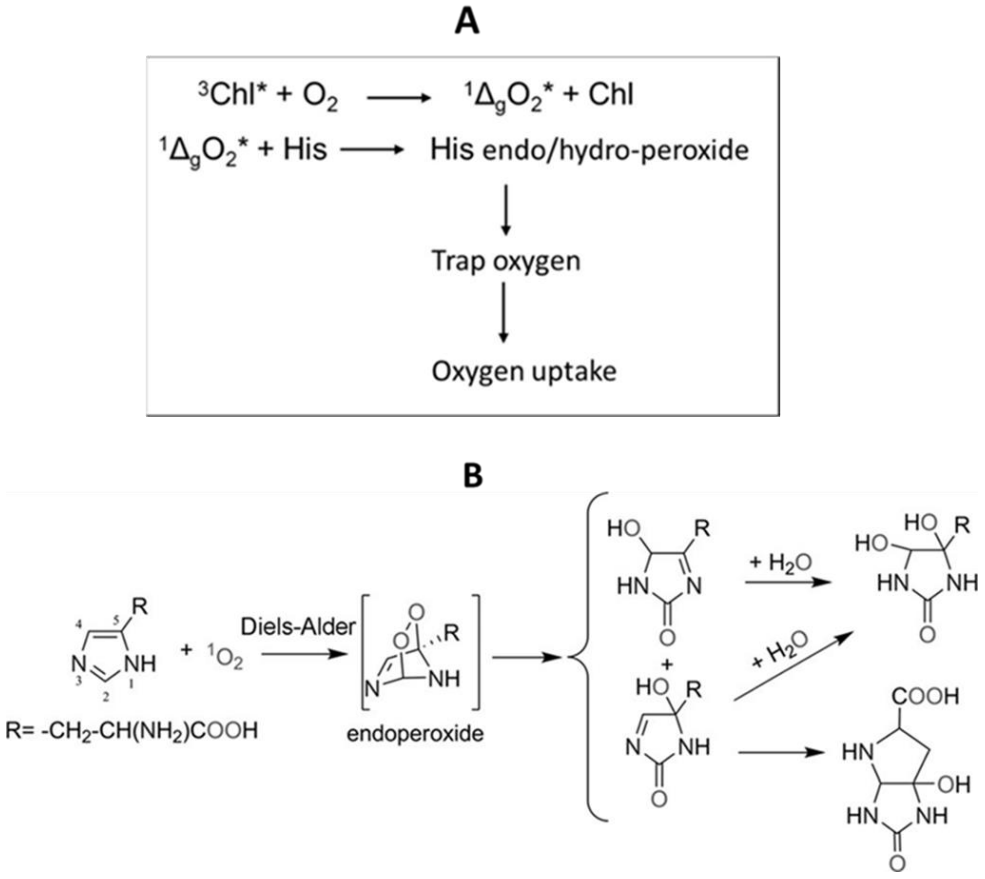

Fig. 1.4. A) The scheme of His-mediated oxygen uptake in Synechocystis cell suspension (Rehman *et al.*, 2013). *B) The chemical reaction of His with singlet oxygen* (Méndez-Hurtado *et al.*, 2012).

Time-resolved $^1O_2$ phosphorescence

Time resolved phosphorescence, which is measured at 1270 nm, is a direct detection tool for $^1O_2$ (Macpherson *et al.*, 1993). Because of the low efficiency of $^1O_2$ phosphorescence and the association with Chls, this detection method can only be used for isolated PSII cores. Since the luminescence peak of $^1O_2$ is at 1270 nm, the hydration artifact must be carefully isolated from the original $^1O_2$ signals (Macpherson *et al.*, 1993).

Dye bleaching technique

To detect $^1O_2$ in isolated PSII RC complexes, a dye bleaching technique was previously developed (Telfer *et al.*, 1994). The bleaching of pnitrosodimethylaniline (RNO) by the intermediate endo-peroxide of His was the basis for this technique. The reaction between O_2

and His causes RNO bleaching, which can be measured photometrically at 440 nm. However, in the case of Chl-rich samples, this approach appears to be inconvenient.

EPR spin trapping technique

EPR (electron paramagnetic resonance) spin trapping, which was previously used in thylakoid membrane particles by using 2, 2, 6, 6-tetramethylpiperidine (TEMP), is another useful technique for $^1O_2$ detection (Hideg *et al.*, 1994a,b). This approach uses a $^1O_2$ reaction with TEMP and TEMP derivatives as a starting point (Lion & Gandin, 1980). As a result, a paramagnetic nitroxide radical is formed, which can be detected using EPR spectroscopy. The EPR measurement of the nitroxide radical in biological samples is time-consuming. Other probes with higher hydrophilicity, such as TEMPD-HCl (Fischer *et al.*, 2006) and TEMPD (2,2,6,6-tetramethyl-4-piperidone) (Hideg *et al.*, 2011), could be used for EPR spin trapping. TEMPD-HCl is preferred on TEMPD because the hydrochloride form is more stable in storage. Since it is less sensitive for in vivo experiments, this technique has only been used successfully in isolated functional photosynthetic membranes. The drawback of these probes is their impermeability in intact cyanobacterial and algal cells.

1.10.2. Fluorescent probes

Fluorescent probes can also be used to detect $^1O_2$ in intact plant systems, and fluorescence imaging techniques can be used to measure changes in fluorescence of these particular $^1O_2$ probes. Dansyl-dependent (DanePy) (Hideg *et al.*, 2006) and Singlet Oxygen Sensor Green reagent (SOSG) (Flors *et al.*, 2006) fluorescent probes based on endoperoxide formation have been used to monitor $^1O_2$ formation in photosynthetic organisms for the past two decades. These probes are made up of an anthracene moiety (electron donor) that uses electron transfer to quench the fluorescence of the fluorochrome (electron acceptor). When the anthracene moiety traps $^1O_2$, the oxygen adduct formed fails to act as an intramolecular electron donor, and the fluorescence is recovered.

DanePy

DanePy (3-[N-(b-diethylaminoethyl)-N-dansyl]aminomethyl-2,2,5,5-tetramethyl-2,5-dihydro-1H-pyrrole) has previously has been used to detect $^1O_2$ in isolated thylakoid membrane particles as well as intact leaves (Hideg *et al.*, 1998, 2001; Hideg & Schreiber, 2007). As DanePy reacts with $^1O_2$, it loses its fluorescence. This probe has some drawbacks because it involves UV range excitation (Kálai *et al.*, 1998), which likely inhibits cell metabolic activity.

Another drawback of DanePy is partial quenching of $^1O_2$ fluorescence, which can result in artifacts (Hideg, 2008). Therefore, this probe is only useful for detecting high levels of $^1O_2$.

SOSG (Singlet Oxygen Sensor Green) fluorescence Probe

Since the mid-2000s, Singlet Oxygen Sensor Green (SOSG) has been released and tested on plants (Flors *et al.*, 2006; Hideg, 2008). SOSG, unlike other fluorescent and chemiluminescent $^1O_2$ commercially available probes, meets the criteria for high selectivity and specificity. It is very specific for $^1O_2$ and does not react to other ROS which are produced in the chloroplast in stress conditions (Pospíšil, 2016). When SOSG reacts with $^1O_2$, SOSG endoperoxide (SOSG-EP) is formed which emits green fluorescence with excitation and emission maxima in the ranges of 504–508 nm and 525–536 nm, respectively, investigated by (Ragàs *et al.*, 2009; Gollmer *et al.*, 2011; Kim *et al.*, 2013).

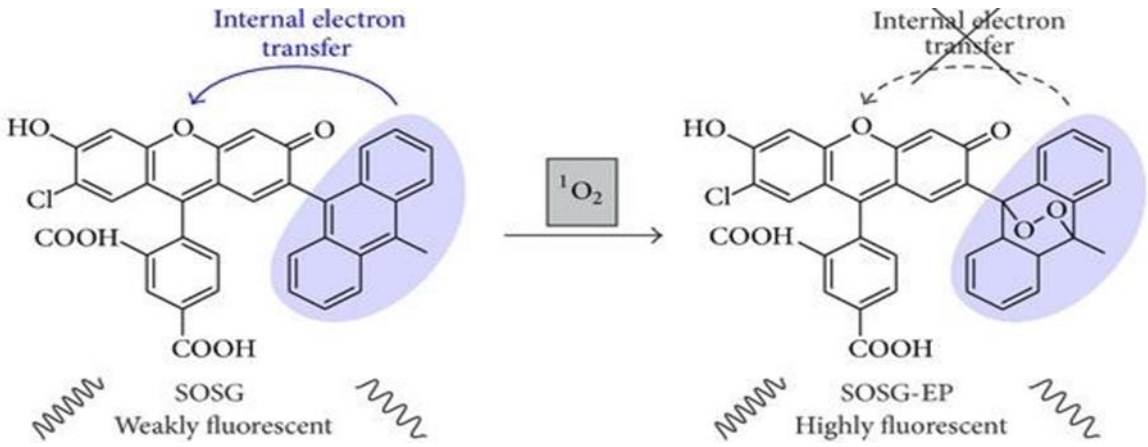

Fig. 1.5. The chemical structure of SOSG and its mechanism of reaction with singlet oxygen (Gollmer *et al.*, 2011)

Since SOSG spectral properties are close to those of fluorescein, it can be observed using a broad variety of fluorescence and confocal microscope systems with standard filters. However, SOSG is known to have a number of disadvantages (including uneven penetration and photosensitization) that must be considered. SOSG was originally designed to be a cell-impermeable probe, but subsequent studies have revealed that it can be localized in most cell compartments under various stress conditions (Flors *et al.*, 2006; Hideg, 2008; Mor *et al.*, 2014). The photosensitization of SOSG adds to the limitations of its use in light-dependent studies. SOSG has been shown to produce $^1O_2$ when exposed to UV radiation (355 nm) and

visible light (532 nm) respectively (Ragàs *et al.*, 2009). Later, it was discovered that SOSG-EP has a far higher efficiency as a photosensitizer than SOSG (Gollmer *et al.*, 2011).

A thorough analysis of SOSG photochemistry revealed that singlet excited SOSG converts to triplet excited SOSG through intersystem crossing, with the triplet excitation energy being transferred to molecular oxygen to form $^1O_2$ (Kim *et al.*, 2013). The $^1O_2$ could be formed by SOSG and its intermediate reaction product endoperoxide (SOSG-EP) (Hideg *et al.*, 2007). The formation of $^1O_2$ is photosensitized by these endoperoxides. It is worth noting that SOSG has been tried in the *Synechocystis* cells and to induce the SOSG fluorescence signal (Sinha *et al.*, 2012), the cells were illuminated for a long time under photonhibitory conditions (3h at 1000 µmole photons $m^{-2}s^{-1}$). In *Synechocystis*, longer illumination of SOSG causes an artifactual fluorescence increase in the absence of an exogenous $^1O_2$ source due to internal electron transfer (Ragàs *et al.*, 2009). The SOSG has been used to detect $^1O_2$ in microalgal cultures (Flors *et al.*, 2006; Driever *et al.*, 2009), and in single cells of the green alga *Chlamydomonas reinhardtii* (Prasad *et al.*, 2018a). However, SOSG has limited penetration into cyanobacterial cells, or can be penetrated in intact cyanobacterial cells only with mild heating and pressure infiltration (Prasad *et al.*, 2018b). $^1O_2$ is clearly a potential competitor among the ROS that could be accumulated in the *Symbiodinium* cells from its coral host (Rehman *et al.*, 2016b). SOSG has been found to be impermeable in *Symbiodinium* (Rehman *et al.*, 2016b); or only partially permeable (Wietheger *et al.*, 2018) in these cells.

Aarhus Sensor Green (ASG)

Because of the photosensitization of SOSG and SOSG-EP, researchers set out to find a fluorescent probe with specificity and sensitivity similar to SOSG but without the negative trait of photosensitization (Ragàs *et al.*, 2009). Aarhus Sensor Green (ASG) (a tetrafluoro-substituted fluorescein derivative covalently bound to a 9,10-diphenyl anthracene moiety) was discovered and used on mammalian cells by Pedersen and colleagues (Pedersen *et al.*, 2014). Aarhus Sensor Green has spectral properties that are identical to SOSG, but without the negative feature of photosensitization. Despite this, ASG has not been tested on plants and is not currently available for regular use.

Other $^1O_2$ sensors

Thus developing new $^1O_2$ sensors remained a goal of research teams. More alternatives to SOSG exist in chemical systems, such as FRET-based ratiometric monitoring of $^1O_2$ with

acene-doped conjugated polymer nanoparticles (Frausto & Thomas, 2017) or Bodipy-based energy transfer cassette (Erbas-Cakmak & Akkaya, 2014) for $^1O_2$ detection in solutions. Tang et al. recently suggested an alternative indocyanine green (ICG), an NIR tricarbocyanine probe that decomposes after reaction with $^1O_2$ (Tang *et al.*, 2016). However, the absorption and emission peaks of ICG at ~807 nm and ~822 nm, respectively, make it less convenient for the fluorescence microscopy.

1.11. Singlet oxygen detection in cell wall removed microalgae (*Symbiodinium*) in microfluidic chamber

With coral reefs under severe threat from climate change (Baker *et al.*, 2008; Ainsworth *et al.*, 2016), a better understanding of *Symbiodinium* biology is urgently needed. As discussed in the previous section (section 1.8), ROS are involved in the coral bleaching. The fluorescein derivative singlet oxygen specific fluorescent dye, SOSG is impermeable to *Symbiodinium* cells, as discussed in the (section 1.9), which makes it nearly impossible to investigate the adverse effects of intracellularly generated $^1O_2$ in these cells. The impermeability of these fluorescent probes is due to the complex cell wall structure of these species. Therefore, cell wall-free cells are required to investigate the ROS consequences in these cells. Cell wall free mutants in *Symbiodinium* do not exist, therefore protoplast preparation by enzymatic digestion of the cell wall has to be attempted. Protoplast, a cell without cell wall, is a significant tool in research. Protoplast technology has extensive applications in plants and microalgae for nuclear transformation, somatic hybridization, in vitro cell culturing and plant regeneration (Carlson, 1973; Noda *et al.*, 2017). Various methods and procedures have been developed and successfully applied to a range of algal species whereas isolation and regeneration of viable protoplasts in *Symbiodiniaceae* has just recently been established (Levin *et al.*, 2017) and attempted to perform transformation of the nuclear genome of *Symbiodinium* (to date, the nuclear transformation of *Symbiodinium* genome was found to be unsuccessful, Nimmo *et al.*, 2019). The major structural element of the cell wall of *Symbiodinium* is cellulose associated with proteins/glycoproteins, therefore *Symbiodinium* cell wall can be digested with cellulase enzymes (Markell *et al.*, 1992). However, the cell wall organization of dinoflagellates is complex due to the existence of several pellicles and thecal plate layers (Morrill & Loeblich III, 1981; Wakefield *et al.*, 2000), which might represent a significant hindrance in cell wall digestion using cellulase enzymes. Previously described protoplast isolation and regeneration protocol efficaciously resulted in viable protoplast, but the procedure of cell wall digestion and regeneration of cell wall was time consuming, making it less suitable for further experiments.

Furthermore, the lack of high resolution real time analysis of the protoplast formation process on single cell level hinders the understanding the efficacy and physiological features of protoplast formation and therefore the application of protoplast technology as a biotechnology tool remains far from routine in *Symbiodiniaceae*.

The protoplast formation encounters the challenges of immense enzyme costs and low output during the production optimization in laboratory or pilot scale processes. To solve this problem, microfluidic methods have demonstrated their high throughput and minimal cost in various microbial applications, for example, screening and directed evolution of yeast strains (Chen *et al.*, 2017; Huang *et al.*, 2018) and detection of pathogens (Foudeh *et al.*, 2012). Numerous microfluidic screening systems have been attempted to grow microalgae and study their growth rate at microscale (Juang & Chang, 2016). Microfluidic technology enables studying the growth and single cell heterogeneity of microalgae (Westerwalbesloh *et al.*, 2019; Castaldello *et al.*, 2019) production of various compounds such as extracellular polymeric substances (Kim *et al.*, 2018) or pigments (Yao *et al.*, 2020).

Several microfluidics based approaches have also been applied to investigate chemoattraction and chemotaxis behavior of marine phytoplankton and bacteria (Seymour *et al.*, 2008) and diseases caused by bacterial infections in corals (Gibbin *et al.*, 2018). To obtain the ideal growth conditions for microalgae, microscale photobioreactors have been developed and applied, which have a high potential for strain optimization and phenotype assays (Castaldello *et al.*, 2019). Microfluidics based methods also allowed the trapping and characterization of plant protoplasts and monitoring their regeneration (Sakai *et al.*, 2019). By manipulating the geometry of the microfluidic channels and adjusting the flow rate, it is possible to optimize the protoplast yield from plant cells (Hung & Chang, 2012). Recently, a microfluidics based single cell phenotyping assay has been developed for various *Symbiodiniaceae*, offering a high-throughput capability to monitor single-cell photophysiological changes under heat stress (Behrendt *et al.*, 2020). However, protoplast isolation from intact algal cells trapped in microfluidic chambers and the single cell monitoring of the cell wall regeneration along with their physiological/photosynthetic capacity has not been established so far. By generating the protoplast, these fluorescent dyes could be introduced inside the cells and thus $^1O_2$-mediated effects can be studied.

1.12. Elimination/quenching of $^1O_2$

As mentioned in the previous sections, various ROS are produced in photosynthetic organisms under environmental stresses. These species damage proteins, lipids, and other macromolecules, and essential cellular functions, including photosynthetic apparatus. Several ROS scavenging molecules are found in plant cells, and they are used to eliminate or inactivate harmful reactive oxygen species. These include antioxidant enzymes like superoxide dismutase (SOD) and catalase (CAT), which remove O_2 and H_2O_2, respectively, and low molecular mass antioxidant metabolites (e.g., ascorbate, tocopherol, and glutathione).

Proline (Pro) is an essential antioxidant metabolite that accumulates in large amounts in plant cells in response to stress conditions such as water deficiency, salinity, UV radiation, and heavy metals (Szabados & Savouré, 2010; Meena *et al.*, 2019). Pro has long been thought to be an inert, compatible osmolyte that protects subcellular structures and macromolecules from osmotic stress (Csonka & Hanson, 1991; Hare & Cress, 1997; Kishor *et al.*, 2005). Several investigations have suggested that Pro has antioxidant properties, implying that it can scavenge ROS and act as a $^1O_2$ quencher (Smirnoff & Cumbes, 1989; Matysik *et al.*, 2002). Pro treatment has been shown to reduce ROS levels in fungi and yeast, protecting programmed cell death (Chen & Dickman, 2005), protect human cells from carcinogenic oxidative stress (Krishnan *et al.*, 2008), and reduce lipid peroxidation in heavy metal-exposed algae cells (Mehta & Gaur, 1999). Pro pretreatment reduced Hg^{2+} toxicity in rice (Oryza sativa) by scavenging ROS, such as H_2O_2 (Wang *et al.*, 2009). The damaging effects of $^1O_2$ and hydroxyl radicals (OH) on PSII can be reduced by Pro in isolated thylakoid membranes (PSII) (Alia *et al.*, 1997). Pro reduces the levels of various ROS types in intact plant systems and leads to cellular osmotic change as a compatible solute (Akhter Banu *et al.*, 2010). While there is consensus in the literature that Pro can directly or indirectly remove OH and H_2O_2 in vivo (Akhter Banu *et al.*, 2010), its function in scavenging $^1O_2$ is debated: some studies reported that Pro is an effective $^1O_2$ quencher (Alia *et al.*, 1997; Matysik *et al.*, 2002). In contrary, Signorelli and colleagues presented indicating that Pro did not scavenge $^1O_2$ (Signorelli *et al.*, 2013). The debate over Pro's ability to interact with $^1O_2$ most likely stems from a misunderstanding of the physical and chemical mechanisms of $^1O_2$ removal, (as seen in Fig 1.6).

As described in section 1.7, photosensitization is the most common way for $^1O_2$ to form. $^1O_2$ can also be formed via chemical pathways, but the resulting molecule has the same properties as that formed by photosensitization. The initial step of $^1O_2$ elimination is the

formation of a charge-transfer complex with a quencher or scavenger molecule. The charge-transfer complex can relax via two distinct mechanisms (Ramel *et al.*, 2012):

(1) In physical quenching mechanism, the quencher molecule deactivates $^1O_2$ to the triplet unreactive ground state ($^3O_2$), while the quencher gains energy via spin-orbit coupling mediated intersystem crossing to a triplet excited state, and then loses readily its energy to the environment and returns to its original state (Fig 1.6). The quencher in this process acts like a catalyzer and the O_2 molecule is not consumed, only its reactivity is lost.

(2) In chemical mechanism, a chemical reaction occurs from the charge-transfer complex between $^1O_2$ and the quencher (also called scavenger) molecule. The scavenger is oxidized and consumed in the process, unless enzymatic recycling of the oxidized scavenger can occur, as is the case with ascorbate. Importantly, oxygen is absorbed in this step because it is involved in a chemical reaction with the scavenger (Fig 1.6). There is controversery regarding the role of Pro as a $^1O_2$ scavanger, so we revisited whether or not Pro can interact with $^1O_2$ and by which mechanism Pro quenches the $^1O_2$.

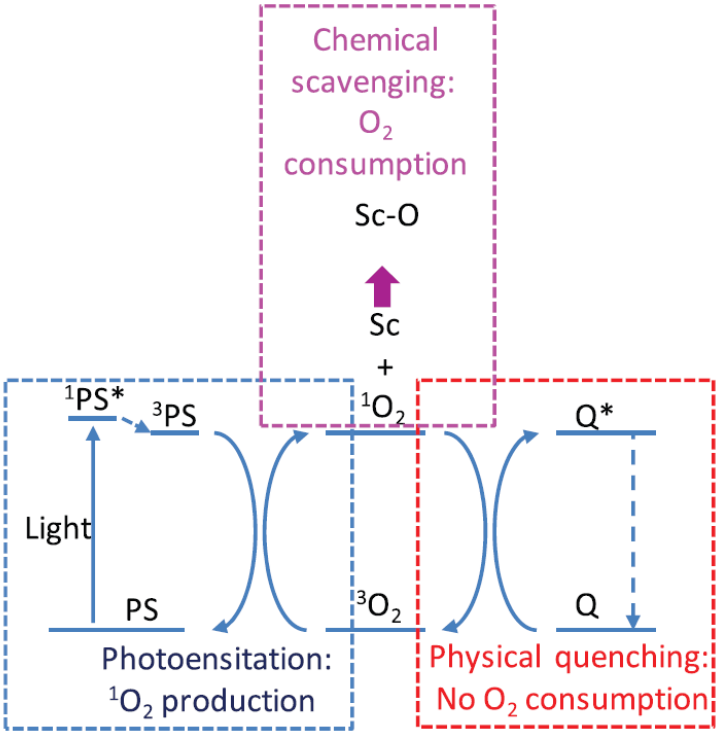

Fig. 1.6. Summary of pathways involved in photosensitized $^1O_2$ production and its elimination. PS, Q, and Sc stand for photosensitizer, physical quencher, and chemical scavenger molecules, respectively. Sc-O represents the oxidation product, which is formed during the chemical reaction between the scavenger and $^1O_2$ (Rehman *et al.*, 2021)

2. AIMS

The general aim of the PhD work was to gain knowledge on the mechanisms of photodamage and photoprotection of the photosystem II complex in plants and microalgae with special emphasis on the singlet oxygen detection, damage and scavenging processes. The specific aims of this study were:

1. To develop a method for the detection of intracellularly produced singlet oxygen in microalagal cells by preparing physiologically competent protoplasts

2. To investigate the role of proline as a singlet oxygen scavenger and understand the mechanism of quenching

3. To characterize the damaging effect of externally produced singlet oxygen on Photosystem II in isolated thylakoid membranes and intact *Chlorella sorokiniana* cells

3. MATERIALS AND METHODS

3.1. Biological materials

3.1.1. *Chlorella sorokiniana* cell culture

Chlorella sorokiniana cells from the Culture Collection of Autotrophic Organisms (CCALA, Trebon, Czech Republic) were propagated in BG-11 growth medium and grown at 24 °C at the irradiance of 60-70 µmol photons m^{-2} s^{-1} white light, in 500 mL flasks containing 200 mL of BG-11 kept on an orbital shaker. Four days old cultures in the exponential growth phase (A750 of 0.2-0.3) were used for the experiments. The chlorophyll concentration (Chl a+b) was determined by a UV-1601 (SHIMADZU) spectrophotometer after extracting the pigments with Acetone: DMSO 1:1. Chl a+b content was calculated according to (Shoaf & Lium, 1976). After extracting the pigments with Acetone: DMSO 1:1, the chlorophyll concentration (Chl a+b) was determined using a UV-1601 (SHIMADZU) spectrophotometer. Cells were harvested by centrifugation at 6500 g for 5 min and re-suspended in fresh BG-11 medium at a concentration of 5 µg of Chl mL^{-1} for chlorophyll fluorescence imaging and oxygen uptake measurements. The cells were kept under normal growth conditions for one hour before measurements.

3.1.2. *Symbiodinium* cultures

The *Symbiodinium* sp. culture (strain CCMP2467, clade A1) was obtained from the National Center for Marine Algae and Microbiota (NCMA), Bigelow Laboratory for Ocean Sciences USA. *Symbiodinium* sp. CCMP2467 was originally derived from the coral *Stylophora pistillata*. Strain CCMP2467 is an A1 type based on the nuclear internal transcribed region 2 (ITS2) (Aranda *et al.*, 2016). Cells were grown in F/2 medium at 25° C at a light intensity of 50 µmol photons m^{-2} s^{-1}, with a light: dark period of 12 h : 12 h. The growth rate and the number of cells were determined by LUNA automated cell counter (Biosystems) every day. The cells were collected during their exponential growth phase by centrifugation at 2000 g for 4 min and resuspended in the fresh F/2 medium for the experiments.

3.2. Thylakoid membrane preparation

Thylakoid membranes were isolated from fresh spinach leaves as described earlier (Anderson, 1981) and stored in −80 ˚C for further experiments. For the experiments, thylakoid membranes were taken from −80 ˚C and thawed while keeping on ice in the dark. Melted thylakoid was resuspended in a buffer solution containing 50 mM HEPES (4-(2-Hydroxyethyl)

piperazine-1- ethanesulfonic acid) (pH 7.5), 5 mM $MgCl_2$, 10 mM $CaCl_2$, and 0.4 M sorbitol. Thylakoid membranes were stored on ice until used for experiments.

3.3. Protoplast isolation and regeneration procedures from *Symbiodinium*

In order to produce protoplast, the protocol by (Levin *et al.*, 2017) was applied with some modifications. *Symbiodinium* cells were taken from one-week old culture (exponential phase) and 4 mL of the culture suspension (~10^5 cells/ml) was centrifuged at 2000 g for 4 min. Pellet was dissolved in the digestion medium, which was prepared by mixing 4% cellulase Onozuka RS (Duchefa Biochemie, Haarlem, Netherlands) and 1% macerozyme R-10 (Duchefa Biochemie, Haarlem, Netherlands) in pre-cooled sterile F/2 medium. Enzyme solution was centrifuged at 10,000 g for 10 min at 4 °C in order to remove any potential impurities of the enzyme powder and the supernatant was sterile filtered by using 0.22 µm sterile syringe filter (Merck Millipore Ltd.). D-sorbitol (Molar chemicals KFT) was sterile added as osmoticum to a final concentration of 0.5 M in the enzyme solution just before initiating the protoplast isolation. After adding in the enzyme solution, cells were incubated at 30 °C in the dark for 24 hours on the shaking incubator at 100 rpm. After 24 hours, protoplasts were centrifuged for 4 min at 200 g and pellet was resuspended in the washing medium (0.5 M sucrose, 0.5 M D-sorbitol, and 25 mM $CaCl_2$) solubilized in sterile F/2. The protoplasts in washing solution were incubated in the dark on the shaking incubator at 30 °C for 3 hours. The protoplasts were pelleted and washing step was repeated. To avoid the microbial contamination, 100 µg mL^{-1} kanamycin was used during washing step. Followed by washing, protoplasts were resuspended in the regeneration medium prepared by adding 25 mM $CaCl_2$ and 0.5 M D-sorbitol in culture medium (pH 7.0), and recurred to *Symbiodinium* growth conditions (50 µmol photons m^{-2} s^{-1}, 25 °C, and 12 h light : 12 h dark cycle).

3.4. Microfluidics setup and monitoring

The microfluidic device was prepared with the specifications according to the cells size of *Symbiodinium* (approx. 10 µm). It is composed of an array of traps with three different sizes, with the purpose of assessing the suitability of trapping and monitoring *Symbiodinium* cells in traps of varying volumes. All traps were found to be suitable for monitoring single cells throughout the whole process of protoplast formation and regeneration. The microfluidic devices were designed using the free open source KLayout software (ref: www.klayout.de). The chips were fabricated using soft lithography techniques (Qin *et al.*, 2010). Briefly, a master mold was created from SU-8 2015 photoresist (Microchem cortp., Westborough MA, USA) on

a silicon substrate by laser direct writing using a Heidelberg µPG 101 micro pattern generator (Heidelberg Instruments GmbH, Heidelberg, Germany). The master mold was replicated by casting of Sylgard 184 polydimethylsiloxane (The Dow Chemical Company, Midland MI, USA). After punching access holes into the cured PDMS pieces, they were bound to glass coverslips by oxygen plasma treatment using a Harrick PDC-002 plasma cleaner (Harrick Plasma, Ithaca NY, USA).

The setup is composed of three parts, the microfluidic device, a tubing system and a syringe pump. Cell cultures were diluted two fold (cell density was diluted from ~10^5 cells/ml diluted to $5x10^4$ cells/ml) and were loaded from the inlet by using a pipette. The microfluidic device was mounted on the microscope stage and a long tube was inserted in the inlet hole, while a smaller tube was inserted in the outlet hole (Fig. 3.1). The inlet tube was attached to a syringe (Omnifix-F Solo Luer 1 mL, B. Braun) containing the media and/or the enzyme mounted on a syringe pump (SyringeTwo-SKU 4000, New Era Pump Systems, Inc. USA). Different flow rates, 20, 40, 60, 80, 100 (µL h^{-1}) were applied to investigate the impact of flow rate on the dynamics and efficiency of protoplast formation. The images were captured with 25X objective (Hund Wetzlar, Helmut Hund GmbH, Wetzlar, Germany) by using a light microscope (H 600/12, Hund Wetzlar, Helmut Hund GmbH, Wetzlar, Germany) equipped with a microQ digital camera (UCMOS08000KPB, ToupTek Photonics Co., Ltd., Hangzhou, China). ToupView, a camera control software (ToupTek Photonics Co., Ltd., Hangzhou, China) was used to continuously capture the images every 10 s. The changes in the morphology and cell size throughout the process of protoplasting and cell wall regeneration were analyzed with the Matlab software (The MathWorks Inc., Natick, MA, USA). A microscopy version of a Pulse Amplitude Modulation Chlorophyll fluorescence imaging system (Imaging-PAM M-Series Chlorophyll Fluorometer, Microscopy version, Heinz Walz GmbH, Effeltrich, Germany) was attached to the microscope and single cell photophysiology and morphology was monitored under identical conditions, on the same cells.

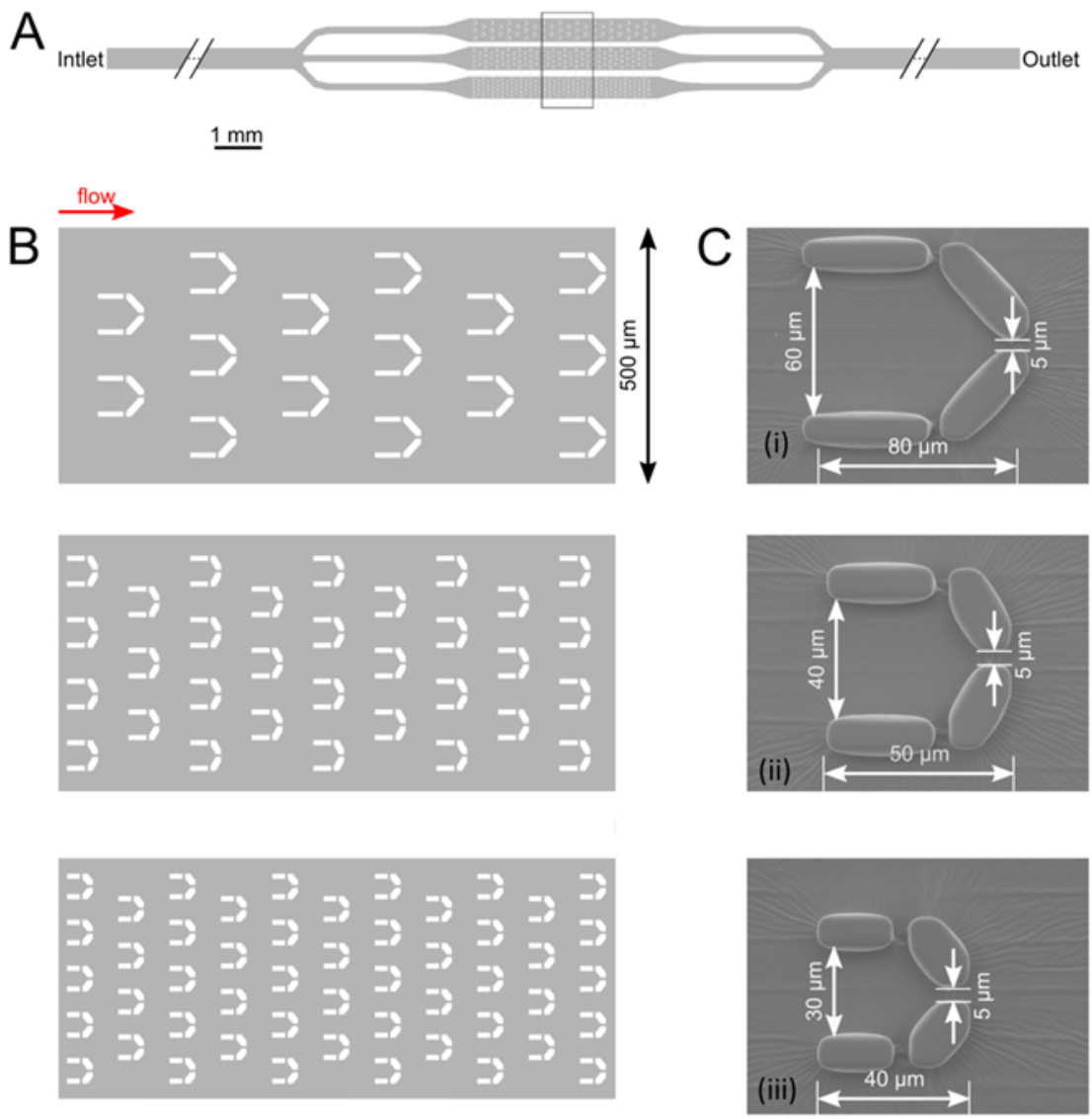

Fig. 3.1. Schematics of the microfluidic device for single cell protoplast preparation and analysis. (A) Overview of the microfluidic device showing the inlet, trifurcated branches and the outlet. (B) The detailed trifurcated part containing traps of different sizes. The right side shows the inlet which leads to the open side of the traps. From the inlet, culture medium and cells are injected into the device and medium after passing through the traps leaves the device at the outlet. The red arrow shows the flow direction. (C) Schematic representation of single traps with three different sizes. (i) Large trap with 60 µm width (ii) Medium sized trap with 40 µm width, (iii) Small trap with 30 µm width. For single cell monitoring, the medium sized traps were used in most experiments. All the traps have a 10 µm wall thickness with 5 µm gaps.

3.5. Single cell chlorophyll fluorescence measurements (Microscopy Imaging PAM analysis)

Single cell chlorophyll fluorescence was determined by pulse-amplitude modulated imaging (PAM) microfluorometry (Imaging-PAM M-series Chlorophyll Fluorometer Heinz Walz GmbH, Germany). Imaging-PAM measures the maximum quantum yield of photosystem II (PSII) physiological heterogeneity among each culture at the single cell level. Non-biological fluorescence standard was used to equalize the maximum fluorescence yield (F_m) to minimum fluorescence yield (F_0) in the absence of variable fluorescence from biological samples, in order to avoid potential artefacts due to high sensitivity mode (this high sensitivity mode is required to obtain variable fluorescence image of cells with appropriate S/N). Once the steady state fluorescence yield (F_0) stabilized, a saturating pulse of blue (460 nm) light was applied and F_v/F_m ([F_m-F_0/F_m) was imaged (measuring light intensity = 4, gain = 10, frequency = 1, damping = 5, F_0 averaging n = 3) after 3 min of dark adaptation.

3.5. Calcofluor white (CFW) staining

Cell wall digestion and regeneration was confirmed by the calcofluor white (CFW) (50 µM) (Sigma-Aldrich) staining. CFW specifically stains the cellulose in the cell wall. The permeabilization of the cell membrane and cell wall for staining was improved by treating the cells with 30 µL of mixture containing 20 % dimethyl sulfoxide (DMSO) and 10 % potassium hydroxide for 5 min before CFW staining (Levin *et al.,* 2017). Cells were imaged by a Leica SP5 confocal laser scanning microscope (LSM) using the HCX PL APO 63X oil immersion objective using sequential scan with 405 nm excitation and 415-485 nm emission detection for cellulose detection and an excitation of 543 nm and 639-778 nm emission detection for chlorophyll fluorescence detection.

3.6. Morphometric analysis of protoplast formation

In order to analyze the morphological changes of protoplasts, an automated image analysis procedure was developed (Matlab version 2018b). The sequential images collected during the protoplast formation were segmented using RGB (Red, Green, Blue) parameters, and the area, eccentricity, major and minor axis of the cells were calculated according to Image Processing Toolbox (The Mathworks Inc., Natick, MA, USA) functions. The procedure allows to display these morphological parameters the time, therefore the kinetics of the morphological changes during protoplast formation can be visualized. Where applicable, the curves of the

time-dependent morphological changes were fitted with logistic function (using OriginPro 2018, OriginLab Corp. Northampton, MA, USA), according to the following equation:

$$y = \frac{A_1 - A_2}{1 + (x / x_0)^p} + A_2$$

where, A_1 is the asymptote of the initial value, A_2 is the asymptote of the final value, x_0 is the value of the sigmoid midpoint, p is the power (sigmoidicity).

3.7. Singlet oxygen imaging

a) In vitro singlet oxygen imaging

A fluorescence stereo microscope (Olympus, SZX12) was used for $^1O_2$ imaging in aqueous solutions and thylakoid membranes. SOSG reagent was used for the detection of $^1O_2$ production in vitro as described previously (Flors *et al.*, 2006; Rehman *et al.*, 2016b). MB was used as a $^1O_2$ source for in vitro light-induced production of $^1O_2$. SOSG at a concentration of 10 µM was mixed with buffer, 1 µM MB, and different concentrations (10–200 mM) of Pro and illuminated with 2300 µmol photons m^{-2} s^{-1} intensity of visible light for 5 min to induce $^1O_2$. Two-microliter drops of each sample were mounted on microscope slides. Imaging of green fluorescence, which is emitted by SOSG after capturing $^1O_2$, was performed using excitation at 460-490 nm and emission 510-590 nm. Olympus Fluoview image analysis software was used to quantify average green fluorescence signals from the images obtained.

b) Subcellular localization of Singlet Oxygen Sensor Green (SOSG)

The intact cells and protoplast cells were stained with 100 µM SOSG dye and incubated for 30 min in the dark followed by light illumination for 5 min under 2300 µmol photons m^{-2} s^{-1} visible light (Rehman *et al.*, 2016a). Then the cells were washed 2 times and images were taken by using 488 nm excitation and 510-590 nm emission with a Leica SP5 confocal laser scanning microscope (Leica, Heidelberg, Germany). SOSG staining was tested both in the plate protoplast experiment where cells were treated with the enzyme in a small petri plate (details mentioned in the protoplast isolation and regeneration procedures) and microfluidic chamber. The cells were washed 2 times with washing solution to remove the excess dye. First, the cells were imaged without light treatment and then they were illuminated with the light on the microscope stage to follow the changes in SOSG fluorescence intensity in the same cells after light illumination. The distribution pattern of $^1O_2$ in the intact cells and protoplast was

quantified by using Leica Microsystems LAS-X software. The SOSG fluorescence was quantified by drawing a transect on the cells and then signal intensity was obtained in the graphical form by using the Leica software. Z- stacks were also captured by using confocal microscope and then 3D image of the cells was created by using Image J.

3.8. Oxygen evolution/uptake measurements

In order to investigate the role of Pro as a $^1O_2$ quencher, O_2 uptake measurements were performed by a Hansatech DW2 O_2 electrode. The rate of light-induced $^1O_2$ production in solution was detected by measuring the rate of O_2 uptake as described earlier (Telfer *et al.*, 1994; Rehman *et al.*, 2013) in the presence of the $^1O_2$ sensitizer MB 1 μM, and chemical scavengers histidine (His) and physical quenchers Sodium azide (NaN_3) or Pro. The efficiency of Pro- and ascorbate (Asc)-mediated chemical quenching of $^1O_2$ was tested by measuring the O_2 uptake rate during illumination in the presence 1 μM MB and different concentrations of Pro or Asc. In contrast, the efficiency of Pro as physical $^1O_2$ scavenger was tested by measuring its effect on the rate of chemical trapping of $^1O_2$ by 5 mM His. The efficiency of physical scavenging of $^1O_2$ by Pro was compared with that of the known $^1O_2$ physical quencher, NaN_3.

In order to investigate the $^1O_2$ mediated photodamage, oxygen evolution/uptake measurement were carried out by using a 4-channel FireStingO2 (FSO2-4) fiber optical oxygen meter with optode sensors (Robust oxygen probe, OXROB10) (PyroScience GmbH, Aachen, Germany). A 4- channel optode was used to ensure that all the 4 samples (control and treated) were measured under similar conditions. Oxygen measurements were performed in 1x1 cm plastic cuvettes, which were placed under identical illumination (green-white light, 240 μmol photons m^{-2} s^{-1}) and incubation conditions that were applied for the multiwell plate experiments. The cuvettes were mounted 45° onto a plastic platform, to allow homogeneous light penetration to the samples. The optodes were placed into the cuvettes containing the samples and sealed with plastic stoppers. Before measurements, 2-point calibration was performed using air-saturated water and deoxygenated water (with Na_2SO_3) according to the manufacturers' specifications. 2 mL cultures with the Chl content of 5 μg of Chl mL^{-1} were loaded into the cuvettes, and measurements in the presence or absence or RB, and in the presence or absence of lincomycin were performed. Dark respiration was measured for 5 min in complete darkness, then oxygen evolution/uptake rate (depending on the applied conditions) was measured for 5 min after switching on the light. To determine $^1O_2$ production by O_2 uptake, 5 mM His was applied. Oxygen evolution/uptake rates are expressed in μmol O_2 mg Chl^{-1} h^{-1}.

3.9. EPR measurements

EPR spin trapping was used for $^1O_2$ detection as described earlier (Hideg *et al.*, 1994a) using TEMPD as a spin trap (Fischer *et al.*, 2006; Hideg *et al.*, 2011). For in vitro studies, TEMPD was mixed at a concentration of 100 mM with 10 μM MB and with different concentrations of Pro, and the production of $^1O_2$ was induced by illumination of samples for 3 min with 2300 μmol photons m^{-2} s^{-1} intensity of visible light. The reaction of the $^1O_2$ generated with 100 mM TEMPD resulted in paramagnetic nitroxide radical formation (Lion & Gandin, 1980), which was detected by EPR spectroscopy, using a Bruker ECS-106 X-band EPR spectrometer. The data were quantified and normalized as the percentage of the decrease of the EPR signal versus Pro concentration. For detection of $^1O_2$ in isolated thylakoids TEMPD, at a concentration of 100 mM, was added to 300 μg Chl mL^{-1} thylakoid suspension containing different amounts of added Pro. The mixture was illuminated with 2300 μmol photons m^{-2} s^{-1} intensity of visible light. The reaction of $^1O_2$ produced by illumination of the thylakoids was detected by EPR spectroscopy by using Bruker ELEXSYS- II E580a X-band spectrometer.

3.10. Experimental procedure for the Rose Bengal assay

Samples (in triplicates) were incubated in the presence of 0 μM, 1 μM, 5 μM and 10 μM RB in 24 well plates (Vision Plate™ 24 Well, 4titude, Brooks Life Sciences, U.K.), which were placed in a temperature controlled incubation chamber (temperature was maintained at 24 °C for *Chlorella* cells and at 4 °C for isolated thylakoid membranes, using a water circulation heater-chiller, Julabo). The illumination was provided from the top by a LED array using green light in combination with white light (240 μmol photons m^{-2} s^{-1}) in order to excite the RB dye in the 520-550 nm spectral range, without providing excess excitation to the photosynthetic processes. In *Chlorella* cells the light treatment was performed both in the absence and presence of 300 μg mL^{-1} lincomycin, which inhibits protein synthesis dependent PSII repair. At the indicated time points, the well plates containing the samples were transferred for chlorophyll fluorescence imaging. The same experiment was also performed in complete darkness, under identical experimental conditions that were applied for light treatment but without applying the LED illumination.

3.11. Chlorophyll fluorescence imaging and measurements of the maximum quantum yield of PSII

Chlorophyll fluorescence of the samples incubated in the well plates was assessed by pulse amplitude modulated imaging (PAM) MAXI (Imaging-PAM M-series Chlorophyll

Fluorometer Heinz Walz GmbH, Germany). The minimum fluorescence in dark adapted state, F_0, was measured using a weak measuring light (ML settings=4, PPFD < 0.3 μmole photons m^{-2} s^{-1}) and maximum fluorescence, F_m, was measured by applying a saturation pulse (SP setting=10, length: 0.8 s, PPFD: approx. 2000 μmol photons m^{-2} s^{-1}). The maximum quantum yield of PSII was calculated as $F_v/F_m=(F_m-F_0)/F_m$. Samples were dark-adapted for 5 min before the measurements. The software ImagingWin was applied to select circular areas of interest for individual wells, in which F_0 and F_m were measured and F_v/F_m was calculated. The ML intensity was adjusted so that the F_0 signal did not drop below 0.1, to allow reliable measurements of F_0 and F_m. In order to ensure homogeneity of the chlorophyll fluorescence signal, an image correction was performed according to the manufacturer, which enabled homogeneous signal intensity across the imaged area. Despite all corrections, some heterogeneity of the incident irradiance in the individual wells always remains, therefore minor spatial variations in the amplitude of F_0 and F_m cannot be completely avoided. However, this can be compensated by the ratio calculation of maximum quantum yield of PSII (F_v/F_m), which eliminates the spatial heterogeneity of the amplitude of the basic fluorescence parameters (Schreiber *et al.*, 2007). RB in the thylakoid buffer or in the culture medium did not show any autofluorescence with the 450 nm ML and SP light source of the PAM system in the 1- 10 μM concentration range, as RB does not absorb light in this spectral region, therefore it does not interfere with the Chl fluorescence imaging measurements.

4. RESULTS

4.1. Detection of intracellularly produced singlet oxygen in *Symbiodinium* cells

4.1.1. Protoplast isolation and regeneration

In order to determine the optimal enzyme concentration and mixture required for the protoplast formation in the microfluidic chambers, a preliminary cell wall digestion assay was performed. 3 KU of the cellulase resulted in the cell wall digestion of a small fraction of cells (only 15% of the cells were protoplasted) and the protoplast formation process required approx. 48 hours, consistent with the previous findings (Levin *et al.*, 2017). In order to make the protoplast process more efficient and faster, different enzyme concentrations were tested and complete cell wall digestion was obtained by using 4% (6 KU) of cellulase with 1% (1.5 KU) macerozyme (Fig. 4.1) after 24 hours, which accompanied by a significant increase in the longitudinal and traversal length of the cells (major and minor axis, respectively) (Fig. 4.1C). *Symbiodinium* cells are spindle shaped normally, they acquire bean shape when they are just added in the digestion medium and finally become rounded with increased diameter on completion of protoplast formation process (Fig 4.1A & Fig 4.1B).

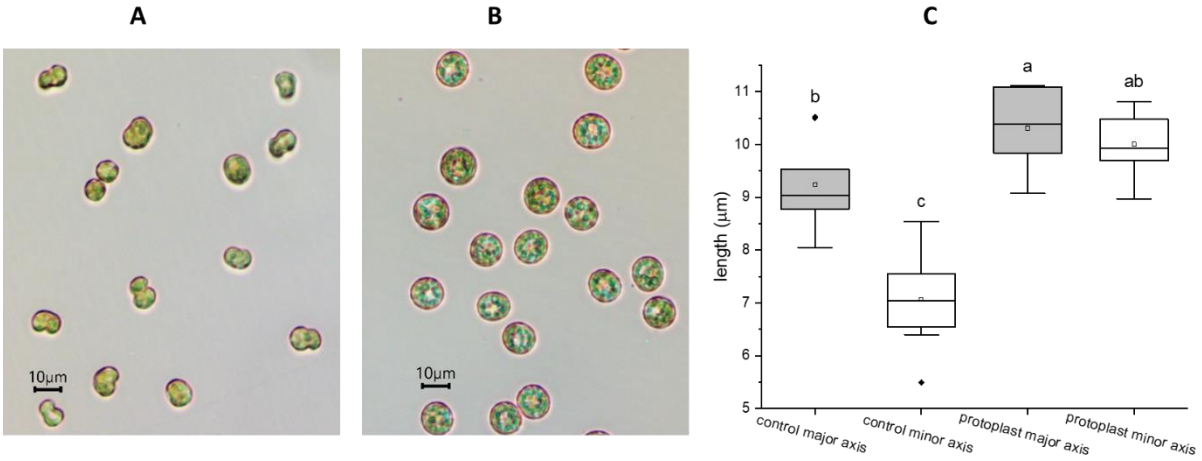

Fig. 4.1. Light microscope images of untreated (control)(A) and treated (protoplast)(B) Symbiodinium cells from the digestion assay experiment. Statistical analysis of the changes in cell morphology (major and minor axis) (C) (scale bar 10µm).

Protoplast formation was confirmed by the lack of Calcofluor White (CFW) staining as it gives blue fluorescence when it reacts with cellulose of intact cells (Fig. 4.2, displays

examples for each condition). A pronounced blue fluorescence was observed in the cell wall of control cells (Fig. 4.2 panel a), but in the protoplast, the lack of CFW fluorescence indicated the digestion and removal of the cell wall (Fig. 4.2 panel b). Regeneration of cell wall was also confirmed with the reappearance of CFW fluorescence of newly synthesized cell wall of the regenerated protoplast (Fig. 4.2 panel c). Protoplast formation was also confirmed by incubating protoplasts in distilled water; in distilled water protoplasts exhibited bursts, because water entered the cell which caused cell rupture, as the turgor pressure could not be maintained due to the absence of cell wall (Fig. 4.2 panel d). These results were applied as initial conditions for the protoplast isolation and regeneration procedure in microfluidic chambers.

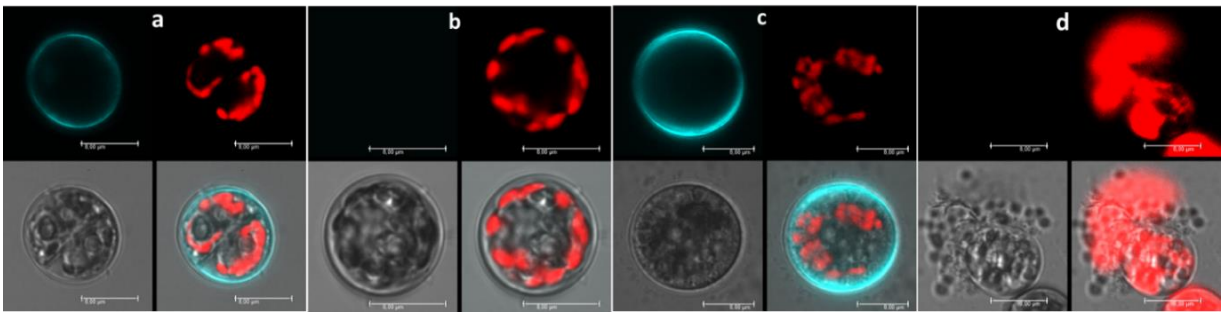

Fig. 4.2. a) Control cells stained with CFW b) Protoplast stained with CFW c) CFW staining after regeneration of cell wall d) ruptured protoplast in distilled water. (In each panel, 1st channel (top left) shows CFW fluorescence, 2nd (top right) is chlorophyll fluorescence, 3rd (bottom left) is transmission and 4th (bottom right) is merged image) (scale bar 8 µm).

4.1.2. Protoplast investigation in microfluidic chambers

The microfluidic system was designed and applied to investigate the efficiency and time course of protoplast formation and regeneration of cell wall under well controlled environmental conditions, considering medium, temperature, and flow rate. The cells were captured in the individual traps, which allowed the characterization of the morphological and physiological changes in single cells throughout the entire loading, enzyme digestion and regeneration process, as well as SOSG staining. *Symbiodinium* cells acquired changes in the morphology during the process of protoplast formation. Cells became rounded due to decrease in eccentricity and on the completion of protoplast formation, they acquired fully round shape (Fig 4.3).

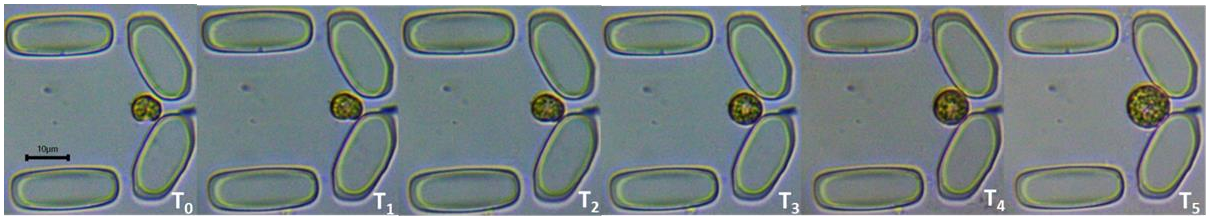

Fig. 4.3. Symbiodinium cells morphological changes before, during and after enzyme treatment. Cells in the trap of microfluidic device (T_0 control cells before enzyme treatment showing oval shape in normal conditions, T_1 cells after 4 hours of enzyme treatment, T_2 cells after 8 hours of enzyme treatment, T_3 cells after 15 hours of enzyme treatment, T_4 cells after 25 hours of enzyme treatment, T_5 cells after 30 hours of enzyme treatment increased in the diameter and getting rounded, T_6 cells after 40 hours of enzyme treatment more rounded and with enhanced diameter (flow rate was 20 µL h^{-1}, capture rate, 60 seconds). Scale bar represents 10 µm.

4.1.3. *Symbiodinium* cells motility pattern in the microfluidic traps

Most of the cells (~70%) stopped moving after loading in the chamber, indicating that cells were possibly under shear stress, however motility was regained after four hours. Cells were motile before enzyme treatment (pre-digestion) (Fig 4.4), and *Symbiodinium* cells maintained the regular cell cycle (Fujise *et al.*, 2018) in the traps, indicating that the trapping procedure and the maintenance method of single cells in the traps did not influence the physiological activity of *Symbiodinium*. However, the enzyme digestion procedure caused marked changes in morphology of trapped *Symbiodinium* cells, the sequence of which could be recorded over time. The cells lost motility on day 1 postdigestion (Fig. 4.4), potentially due to cell cycle arrest (Wang *et al.*, 2008; Pozdnyakov & Skarlato, 2012), or incidental mechanical loss of flagella (Bricheux *et al.*, 1992) during the cell wall digestion procedure. The cells were in the dividing phase and moving forms before enzyme treatment but after 1 hour of enzyme treatment, cells stopped moving and cell division also halted, however, some of the cells still divided in the protoplast phase (Fig. 4.5B see below). The motility of cells recovered after 2 days incubation in the regeneration medium and the number of motile cells increased when they were incubated in the culture medium. In culture medium, after 2 days, some of the cells were moving but most of them were in the division phase (Fig. 4.5C see below). On day 3 in the culture medium, all of the cells divided into very actively moving daughter cells. Changes in the morphology and size of the cells were observed during the process of protoplast formation.

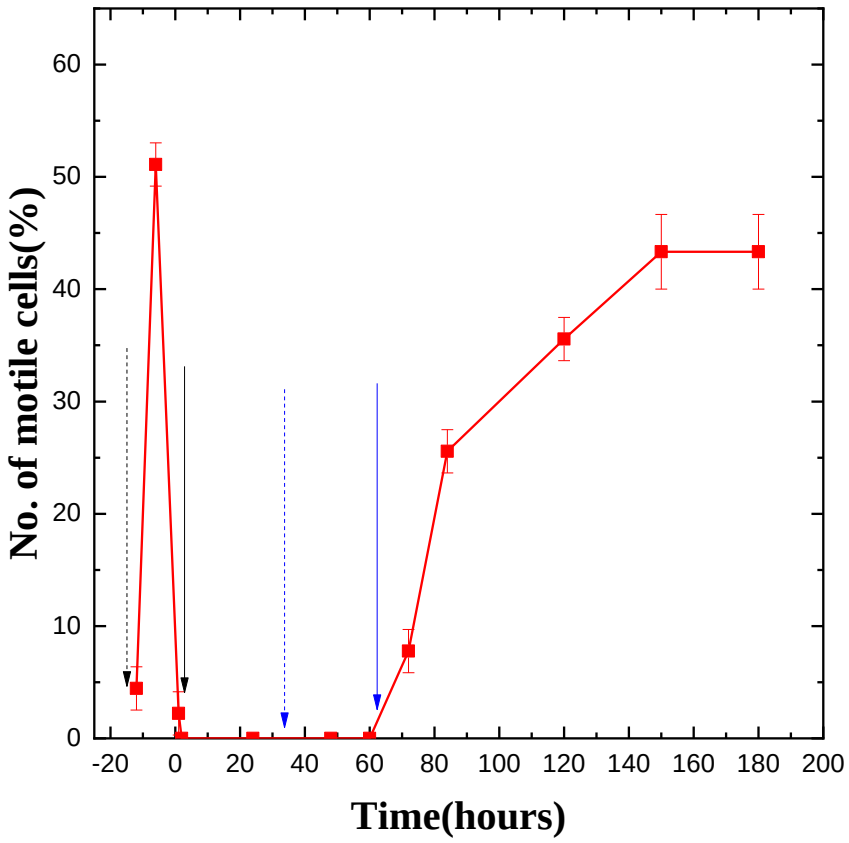

Fig. 4.4. Symbiodinium cells motility pattern before, during and after enzyme treatment. The black dotted line on day -1 marks when cells were loaded in the chamber and black solid line on day 1 marks when enzyme solution was given to the cells. The blue dotted line on day 2 marks when regeneration medium was applied and blue solid line marks when cells were returned to culture medium. (mean ± SE, n = 3).

4.1.4. Pattern of cell division and morphological differences in the control cells, protoplast and after regeneration of cell wall

Enzyme treatment was given when the cells were at the active dividing phase, as during dividing phase dinoflagellates shed their thecal plates and external membranes so cell wall digestion is potentially more efficient (Morrill & Loeblich III, 1981). Some divisions were also observed during enzyme treatment, where protoplast divided into two very rounded non-motile daughter cells (Fig. 4.5B) as opposed to the cell division of non-digested control cells, where two spindle shape motile daughter cells are formed (Fig. 4.5A). This non-motile daughter cells formation occurred within approx. 60 min as compared to cells in non-dividing phase, in which protoplast formation takes 25-35 hours (Fig 4.3). The protoplast formation, i.e. the complete

rounding of the daughter cells was faster in dividing vs. non-dividing cells (Fig 4.5A and 4.5B), indicating that actively dividing cells are more efficiently protoplasted than non-dividing cells.

Cell division pattern was observed to be different in the cells after regeneration of cell wall than in the normal cell division. In normal cells division, mother cell divided into 2 or 4 daughter cells (Fig 4.5A), but after regeneration more than 4 daughter cells were found to be formed with maximum division into 8 daughter cells with cell size smaller than normal daughter cells (Fig 4.5C). In intact cells, the division process into 2 motile daughter cells was completed in 3 minutes (Fig 4.5A), however, in the protoplast state the division process required 3 hours to complete and it resulted in two very rounded and non-motile cells instead of motile and spindle shaped daughter cells (Fig 4.5A, 4.5B). These daughter cells expanded in size after cell division. These results indicate that *Symbiodinium* cells that are undergoing cell wall digestion are able to divide (albeit slower), and the daughter cells formed during cell wall digestion procedure are prone of protoplast formation with higher efficiency than non-dividing cells. This could be important for further optimization of protoplast preparation procedure, i.e. by means of culture synchronization the protoplast yield could be enhanced in *Symbiodinium*.

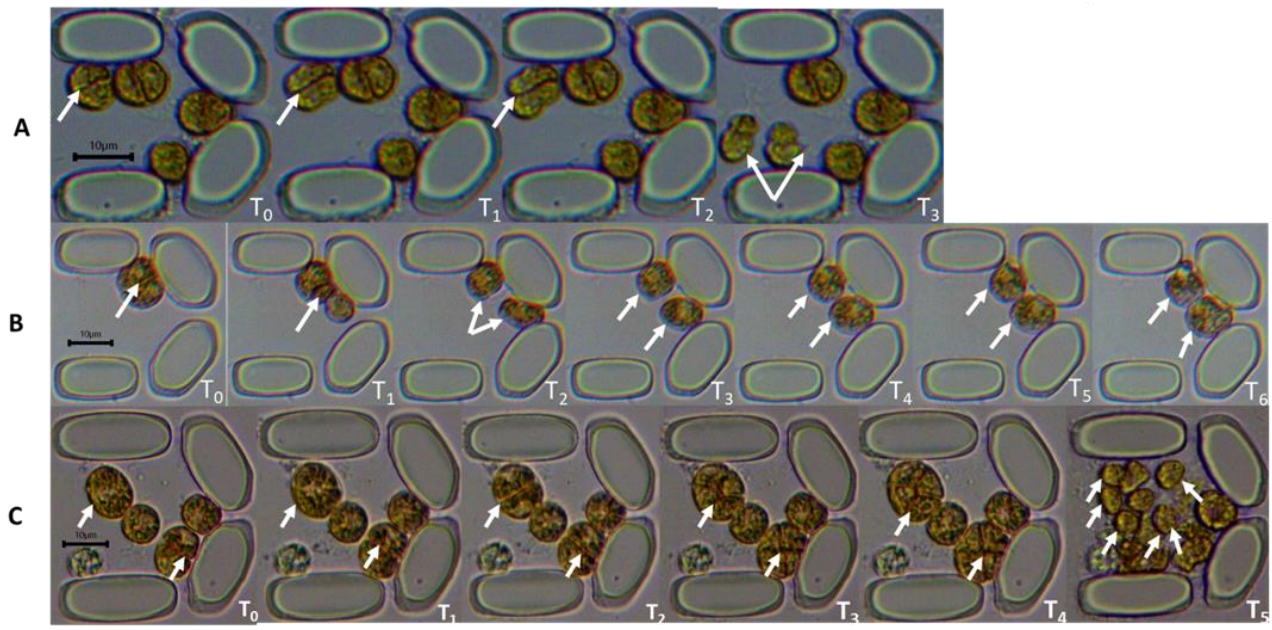

Fig. 4.5. Pattern of cell division and morphological differences in the control cells, protoplast and after regeneration of cell wall. A) Cell division of intact cells into two motile daughter cells shown by arrows. B) Cell division of protoplast into two daughter cells. C) Pattern of cell division after regeneration of cell wall into more than 4 daughter cells shown by arrows. (In panel a, To is the cell before division and T_1, T_2, T_3, are the times series of the cell division

process after 60, 120 and 180 seconds respectively. In panel b, T_0 is the state of cell before enzyme treatment and T_1, T_2, T_3, T_4, T_5 and T_6 is the time after 120, 140, 150, 165 and 185 min of enzyme treatment. In panel c, T_0, T_1 and T_2 is the protoplast after 1, 2 and 3 days in regeneration medium (RM) respectively while T_3, T_4 and T_5 are the cells after 1, 2 and 3 days in culture medium. Scale bar represents 10 µm.

In order to investigate the regeneration capacity of the protoplasts after removal of digestion solution, the changes in cell morphology and cell cycle were monitored under continuous flow of regeneration medium. After the addition of the digestion enzyme solution, all the moving forms are converted into non-moving forms in the plate as well as in the microfluidic traps. Cells were kept in the regeneration medium for two days followed by incubation in the culture medium. After one day in the culture medium, cells regained division ability. All the cells regained motility after 2 days in the culture medium, and the complete cell wall regeneration of the protoplast occurred in 4 days. Protoplast formation and regeneration in the microfluidic chamber was also confirmed by CFW staining, which indicated that no staining could be observed in protoplasts and CFW staining re-appeared in regenerated cells and the cell wall is resynthesized.

4.1.5. Time-resolved morphometric analysis of protoplast formation

In order to investigate and quantify the morphological changes over time during the protoplast formation, an automated image processing and analysis procedure was applied on individually trapped cells. In a typical experiment, after addition of digestion solution, the area (Fig. 4.6B), major and minor axis (Fig. 4.6D and Fig. 4.6E, respectively) of the cells increased, until an equilibrium state in these parameters were attained. In the case of the applied flow of 40 µL h^{-1} the equilibrium state was attained after approx. 35 hours, however, the time dependency of these morphological changes were dependent on the flow rate (see below Fig 4.7 and Fig 4.8). The eccentricity of the cells exhibited a decrease (Fig. 4.6C), indicating that the cells became more rounded over time. However, the time required to attain equilibrium state of the eccentricity parameter could not be unequivocally assigned. It has to be noted that minor changes in cell morphology occurred after loading the cells in the microfluidic chambers, indicating that loading stress might have perturbed cell morphology (indicated by the time period after loading but before the start of the cell wall digestion). The curves of the morphological parameters could be reasonably well fitted with a logistic (sigmoid) function,

and the x_0 value (representing the midpoint of the timescale of the changes) can be used as a quantitative descriptor of the time scale of protoplast formation (Fig 4.6).

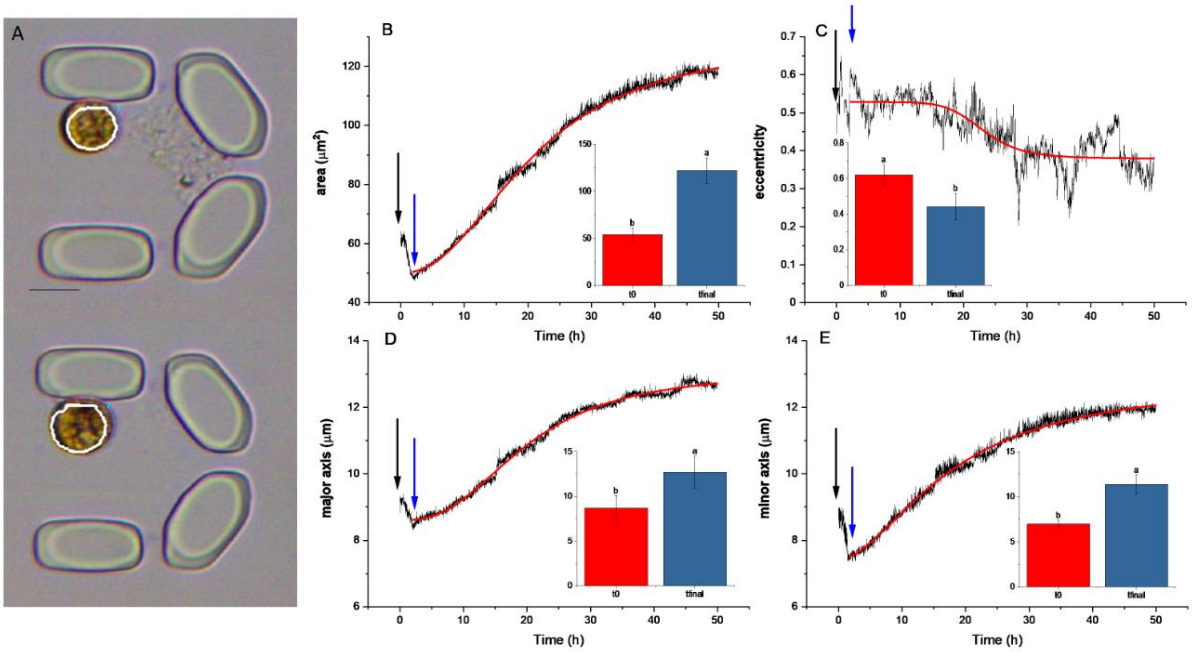

Fig. 4.6. Morphometric analysis of protoplast formation over time in the microfluidics chamber. A) original images of traps showing the selected areas of interest of single cells applied for morphological analysis. The same cell is shown over time at the beginning (top image) and at the end (bottom image) of the experiment. B) area, C) eccentricity, D) major axis, E) minor axis of cells. Insets show the changes in the parameters after approx. 35 hours, when the changes attain the equilibrium state (mean±S.D., n=10, different letters indicate significant differences (p=0.05)). Black solid arrow indicates the phase when cells were loaded in the microfluidic traps. Blue solid arrow represents when enzyme solution was applied to the cells. The red curves represent the logistic fitting of the original data. The applied flow rate was 40 µL h^{-1}. Scale bar represents 10 µm

In order to investigate whether the protoplast formation process could be accelerated using the microfluidics approach, different flow rates were tested (20, 40, 60, 80 and 100 µL h^{-1}) for the control cells (without enzyme treatment) and enzyme digestion process under identical conditions. Control cells at various flow rates does not show any morphological changes; however, protoplast formation process was faster at higher flow rate. Elevated flow rates resulted in similar trajectories of the time-dependent changes of morphological parameters

during the digestion process, and protoplast formation time was found to be significantly shorter only at the 100 µL h^{-1} flow rate (Fig. 4.7).

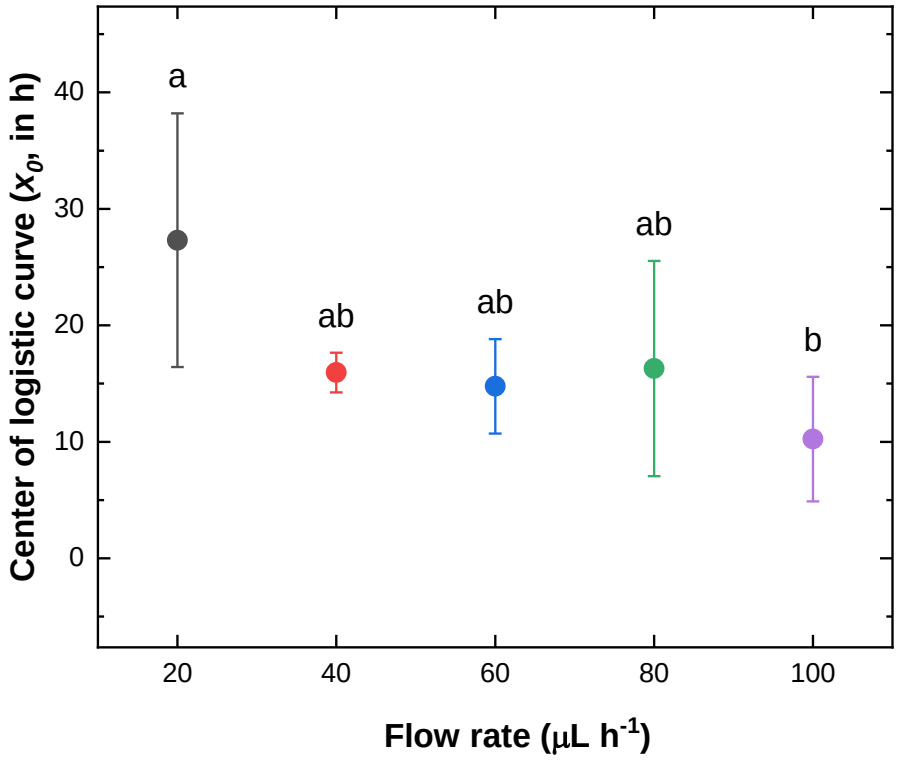

Fig. 4.7. The time course of protoplast formation with various flow rates (µL h^{-1}) (mean ± SD, n = 10) in microfluidic system.

The original traces depicting the time course of the relative changes in area, eccentricity, major and minor axis at different flow rates are shown in Fig 4.8. Increased flow rate caused faster protoplast formation. Protoplast formation was observed in some cells even after 10 hours with the 100 µL h^{-1} flow rate that was the highest flow rate used. With the 100 µL h^{-1} flow rate, this process was completed in 15 hours (Fig. 4.8e) and with 80 µL h^{-1} flow rate the protoplast formation occurred after 20 hours (Fig. 4.8d). With 60 µL h^{-1} and 40 µL h^{-1} flow rate, protoplast formation occurred in 26 and 35 hours respectively (Fig. 4.8b, 4.8c). The longest time for protoplast formation was observed with 20 µL h^{-1} flow rate, which was 40 hours (Fig. 4.8a).

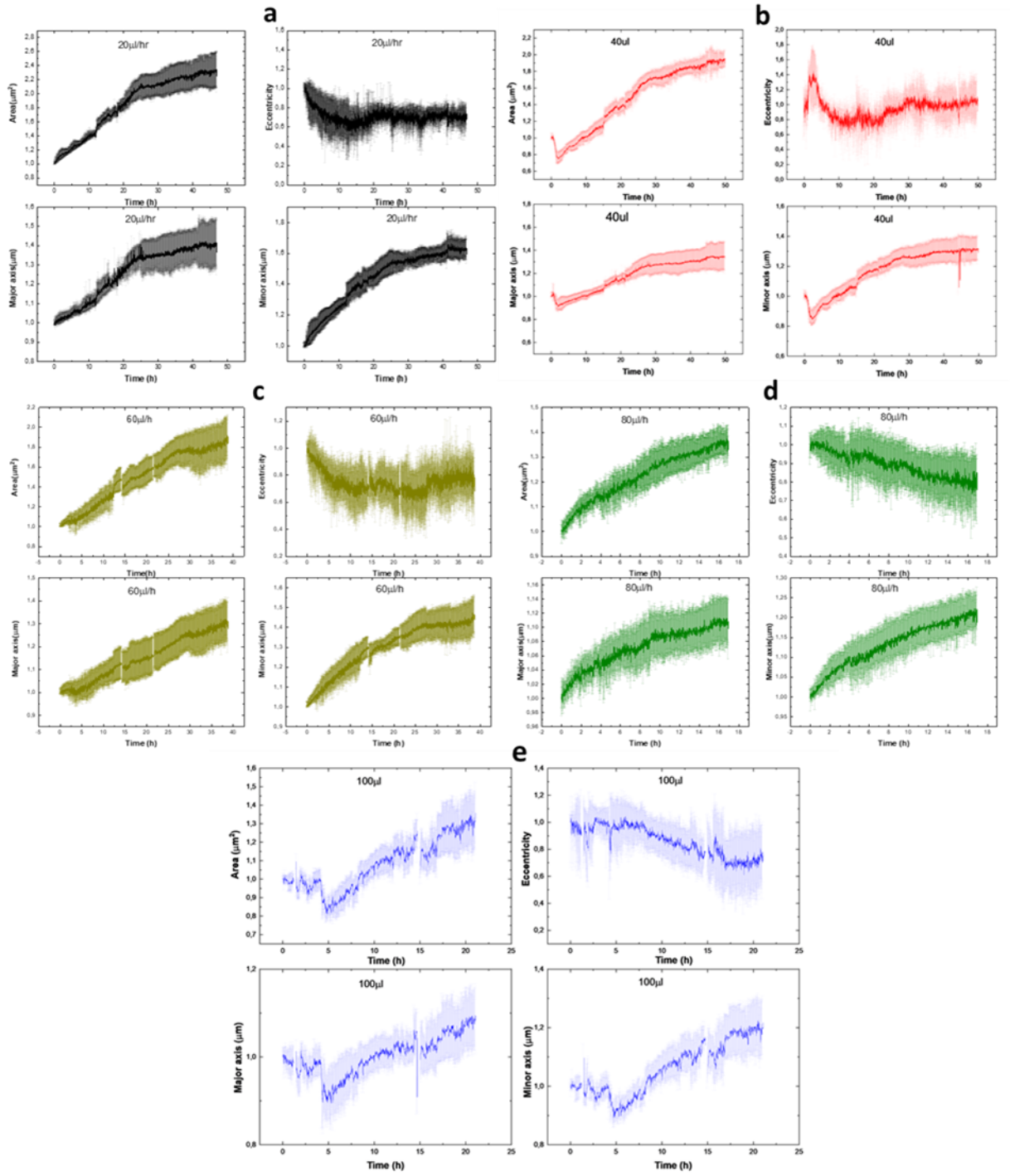

Fig. 4.8. The time course of the relative changes in area, eccentricity, major and minor axis of protoplast at different flow rates. a) morphology changes under 20 μL h^{-1} flow rate b) morphology changes under 40 μL h^{-1} flow rate c) morphology changes under 60 μL h^{-1} flow rate d) morphology changes under 80 μL h^{-1} flow rate e) morphology changes under 100 μL h^{-1} flow rate (mean±S.D., n=10).

4.1.6. Photosynthetic competence of protoplasts

Although the timescale of the morphological changes could be monitored at different flow rates, it was also an important question to clarify whether the protoplasts retained physiological or photosynthetic competency across the applied range of the flow rate, and whether the applied flow rate influenced the maximal quantum efficiency of PS II (F_v/F_m). F_v/F_m of cells before the enzyme treatment was impacted by the applied flow rate; higher flow rate resulted in reduced F_v/F_m particularly in the 80-100 µL h^{-1} flow range (Fig. 4.9). During protoplast formation, the decrease of F_v/F_m as a function on flow rate was more pronounced. F_v/F_m largely (but not fully) recovered in the regeneration phase, when the digestion solution was replaced with regeneration medium, indicating that the enzyme digestion procedure did not affect the PSII activity.

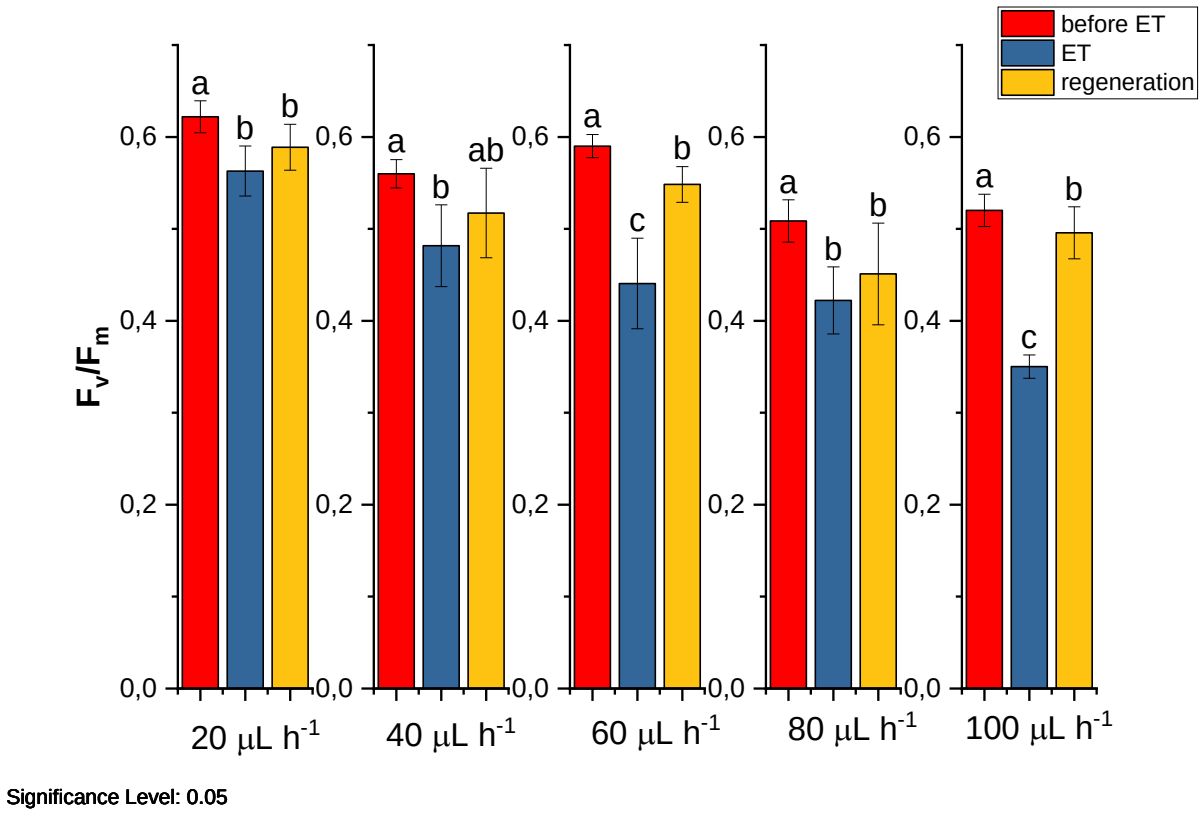

Fig. 4.9. Effect of various flow rates on maximum quantum yield of PSII in control, during protoplast and after regeneration of cell wall (mean ± SD, n = 10) in microfluidic system.

4.1.7. Singlet Oxygen Sensor Green (SOSG) labeling in *Symbiodinium*

Intact cells did not exhibit any internal staining, whereas a strong external SOSG fluorescence was observed when the cells were exposed to light for 5 min (Fig. 4.10), in agreement with (Rehman *et al.*, 2016a). The protoplasts exhibited very light internal SOSG fluorescence without light treatment, but after 5 min illumination intracellular SOSG fluorescence increased significantly (Fig. 4.10c and 4.10d). The SOSG was relatively evenly distributed in the cytoplasm (transect shown in Fig. 4.10d) and also showed some co-localization with chloroplasts, as indicated by the orange color on the merged images (Fig. 4.10d, panel (iv)). It is also observed to co-localize completely with chloroplast, as shown by the orange colour in the merged image (Fig. 4.11A, panel (iv)) .

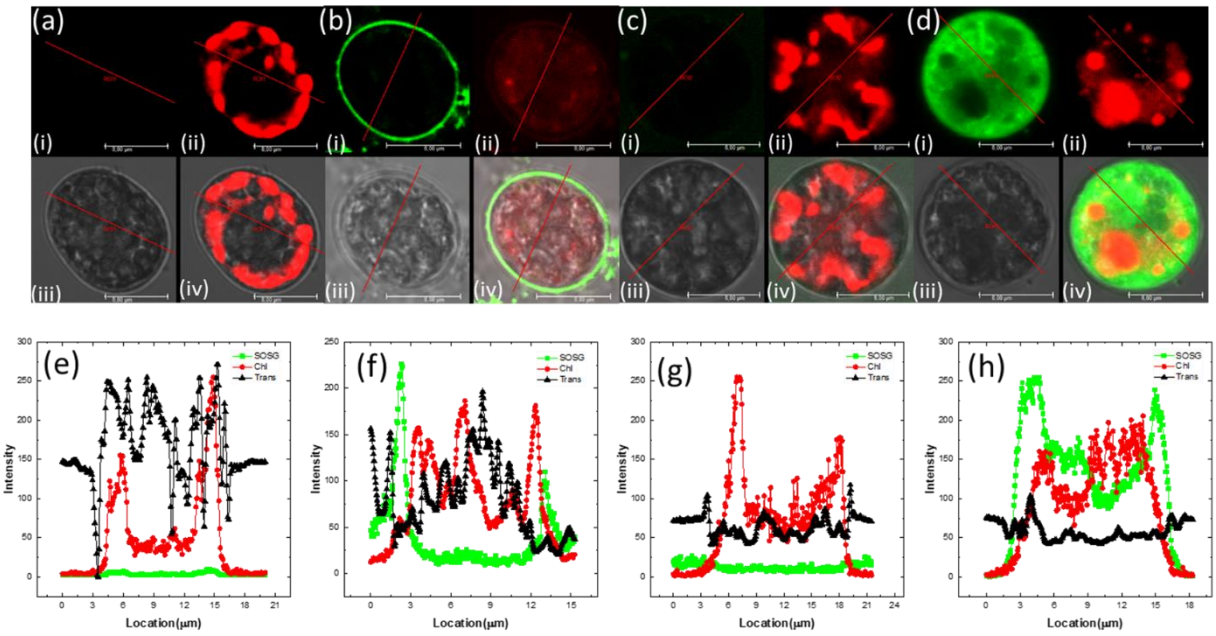

Fig. 4.10. Confocal microscopy imaging of Symbiodinium intact cells and protoplast stained with singlet oxygen sensor green (SOSG). Four detection channels are represented: (i) SOSG fluorescence; (ii) chlorophyll (Chl) fluorescence; (iii) transmission; (iv) merged images of the three signals (scale bar 8 µm). (a) Laser scanning microscopy (LSM) imaging of cells without light treatment. (b) LSM imaging of cells which were exposed to light (2300 µmol photons m^{-2} s^{-1} for 5 min. (c) LSM imaging of protoplast without light treatment (d) LSM imaging of protoplast which were exposed to light (2300 µmol photons m^{-2} s^{-1}) for 5 min, (e), (f) (g) and (h) show the intensity distribution of the four detection channels at the indicated transect lines for (a), (b), (c), and (d), respectively. (Scale bar 8 µm)

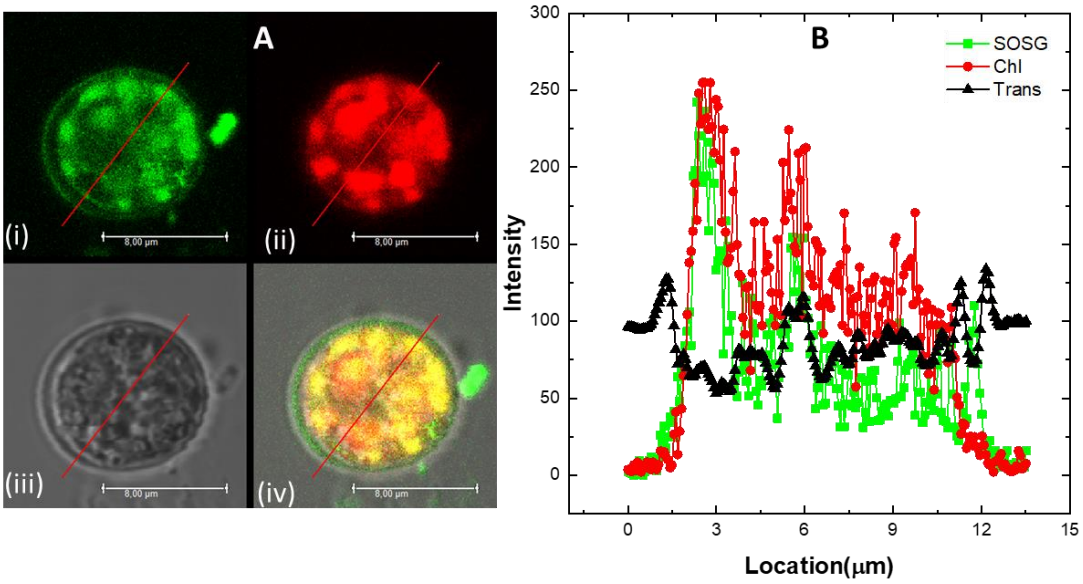

Fig. 4.11. Confocal microscopy imaging of Symbiodinium protoplast stained with singlet oxygen sensor green (SOSG) and illuminated with light showing SOSG fluorescence co-localized with chlorophyll fluorescence. Four detection channels are represented: (i) SOSG fluorescence; (ii) chlorophyll (Chl) fluorescence; (iii) transmission; (iv) merged images of the three signals (scale bar 8 µm). (A) Laser scanning microscopy (LSM) imaging of protoplast which were exposed to light (2300 µmol photons m^{-2} s^{-1}) for 5 min. (B) The intensity distribution of the three detection channels at the indicated transect lines for (i), (ii) and (iii) respectively. (Scale bar 8 µm).

To confirm $^1O_2$ production in the protoplast, SOSG staining was done in combination with His and results showed that SOSG fluorescence was strongly quenched due to the $^1O_2$ uptake by His. This can be clearly seen in Fig. 4.12 that *Symbiodinium* protoplast showed strong SOSG fluorescence when illuminated with light due to the production of $^1O_2$; however, this fluorescence disappeared when SOSG was used together with His, indicating $^1O_2$ uptake by His.

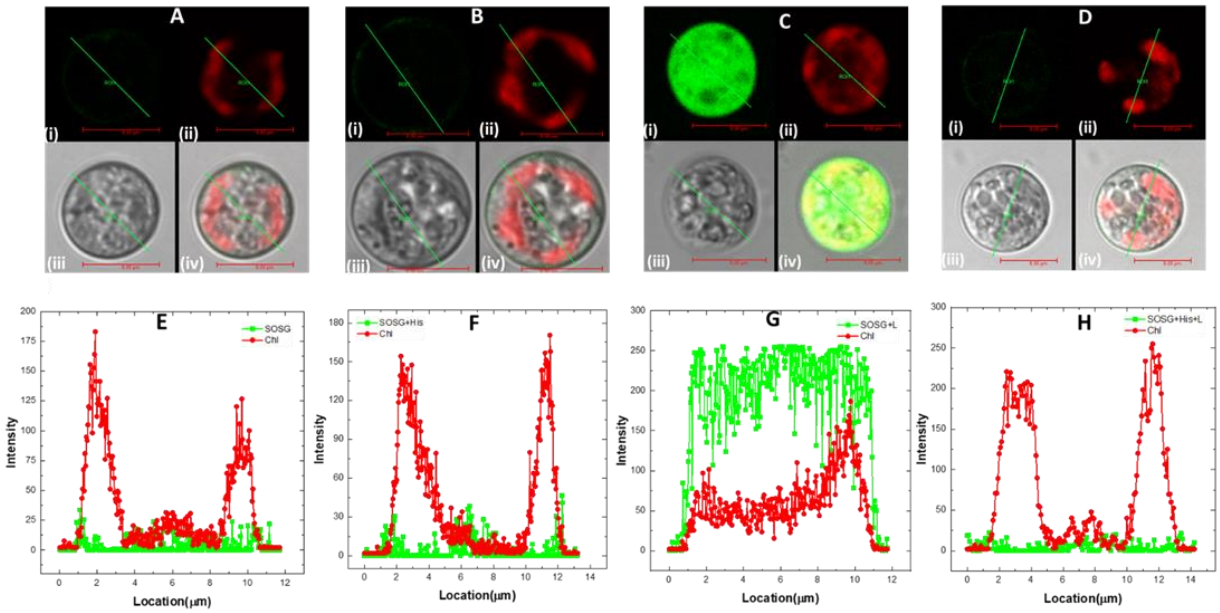

Fig. 4.12. Confocal microscopy imaging of Symbiodinium protoplast stained with singlet oxygen sensor green (SOSG) with and without histidine (His). Four detection channels are represented: (i) SOSG fluorescence; (ii) chlorophyll (Chl) fluorescence; (iii) transmission; (iv) merged images of the three signals (A) Laser scanning microscopy (LSM) imaging of SOSG stained protoplast without light treatment. (B) Laser scanning microscopy (LSM) imaging of SOSG+His stained protoplast without light treatment. (C) Laser scanning microscopy (LSM) imaging of SOSG stained protoplast which were exposed to light (2300 µmol photons m^{-2} s^{-1}) for 5 min. (D) Laser scanning microscopy (LSM) imaging of SOSG+His stained protoplast which were exposed to light (2300 µmol photons m^{-2} s^{-1}) for 5 min, (E), (F) (G) and (H) show the intensity distribution of the four detection channels at the indicated transect lines for (A), (B), (C), and (D), respectively. (Scale bar 8 µm).

3D reconstitution of the Z-scanning images of the protoplast confirmed that SOSG penetrated into the protoplasts and revealed the intracellular spreading pattern of $^1O_2$. Fig. 4.13A shows the X-Y-Z distribution of the SOSG in the protoplast. Fig. 4.13B shows the 3D rendered Z stack image series of SOSG stained protoplast. These images show the same protoplast with different rotation angles. Actually, only half of the cell is shown, and the middle image shows the plane of protoplast at approx. the middle optical section (Fig. 4.13A, Fig. 4.13B).

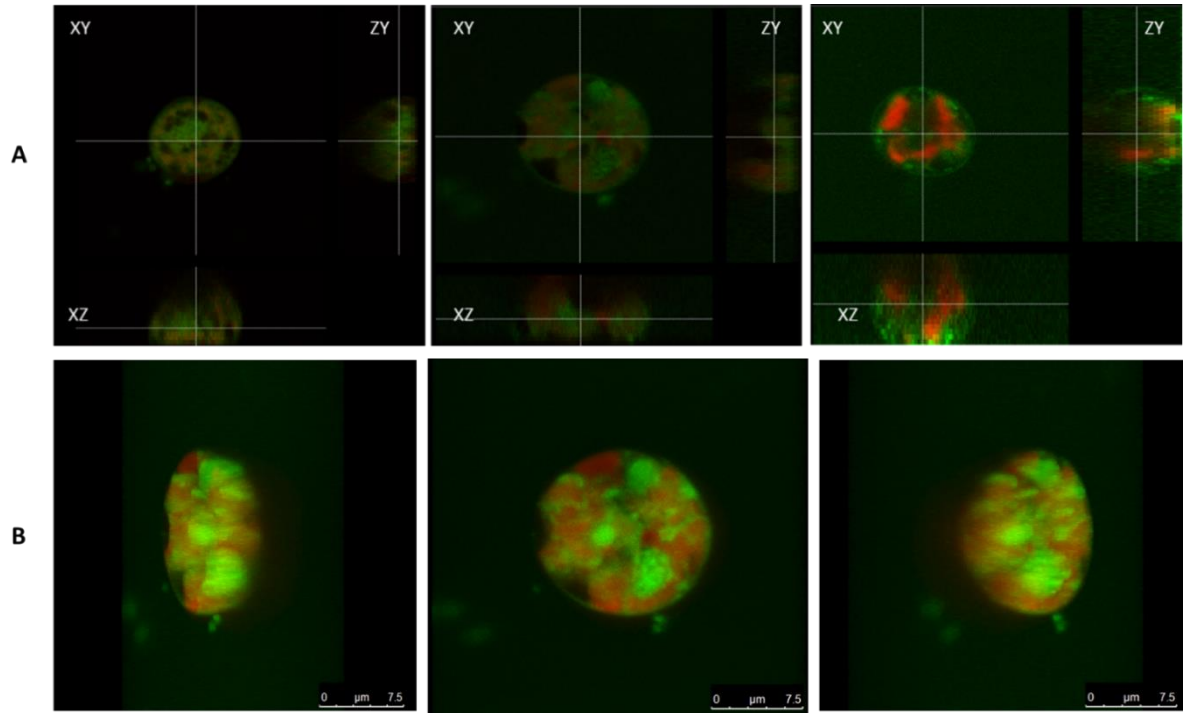

Fig. 4.13. A) Confocal Z sectioning of SOSG stained on 3 individual protoplasts. XY, ZY and XZ display the orthogonal sectioning images of the Z scans across the respective axes. B) 3D projection of confocal Z-stack image series showing the penetration and intracellular localization of SOSG dye and the co-localization of SOSG dye with Chl autofluorescence in protoplast.

In order to demonstrate the applicability of the SOSG dye in trapped *Symbiodinium* protoplasts, SOSG staining and confocal microscopy analysis was performed in protoplasts that were directly trapped, stained and illuminated in the microfluidics chambers (Fig. 4.14). Before illumination, protoplasts displayed characteristic red autofluorescence originating from the Chl molecules in the chloroplasts, however only a weak green fluorescence originating from SOSG could be observed (Fig. 4.14A). Illumination caused a strong quenching of Chl autofluorescence and an intensification of the SOSG fluorescence (Fig. 4.14B). An increase in the SOSG fluorescence was observed after light treatment, shown by plotting intensity profile of SOSG stained protoplast before and after light treatment (Fig 4.14C); however, Chl autofluorescence was strongly quenched after light treatement (Fig 4.14D).

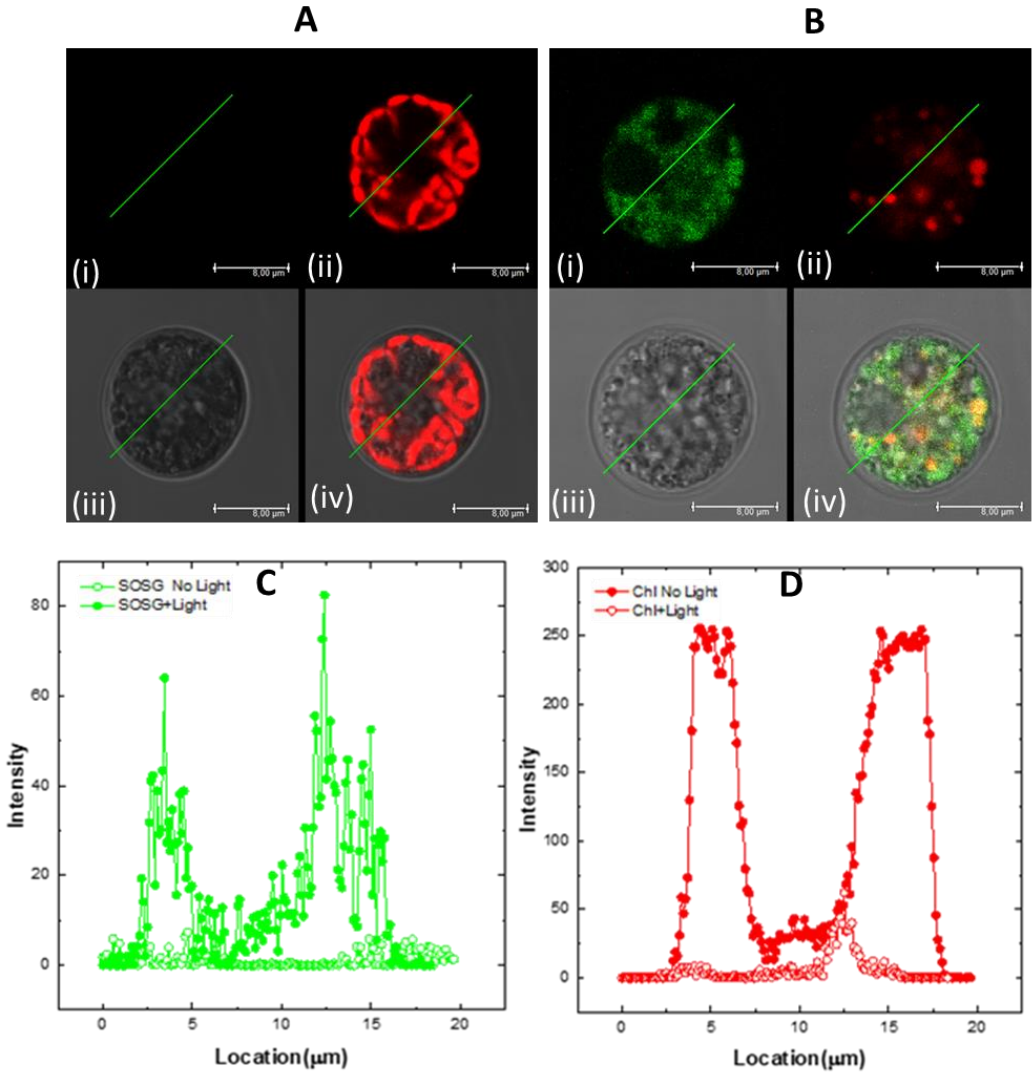

Fig. 4.14 (A) LSM imaging of SOSG stained protoplast before light treatment (B) LSM imaging of the same SOSG stained protoplast after 5 min light treatment in the microfluidic system. (C) *The intensity distribution of the SOSG detection channel and (D) chlorophyll detection channel at the indicated transect lines for (A) and (B). (Scale bar 8 μm).*

4.2. Elimination/scavenging of singlet oxygen by proline

4.2.1. Proline is a $^1O_2$ quencher in vitro, and acts via a physical mechanism

To investigate the role of proline as $^1O_2$ quencher, EPR spin trapping technique was used. In this method, TEMPD spin trap was used which forms TEMPO-D, a stable paramagnetic product upon reaction with $^1O_2$. $^1O_2$ was generated by the photosensitization process by using the MB (photosensitizer) (Fig 4.15A). The characteristic TEMPO-D signal was practically absent in the absence of MB. Only a small residual signal (less than 2%–3% of that obtained in the presence of MB) could be detected (Fig 4.15A). The size of the TEMPO-D signal shrank when Pro was present during illumination of the mixture containing TEMPD + MB in an aqueous buffer (Fig 4.15A), and this effect had a sigmoidal concentration dependency (Fig 4.15C). The data in Fig 4.15(C) also show that ca. 75 mM Pro can decrease the TEMPO-D signal by 50%.

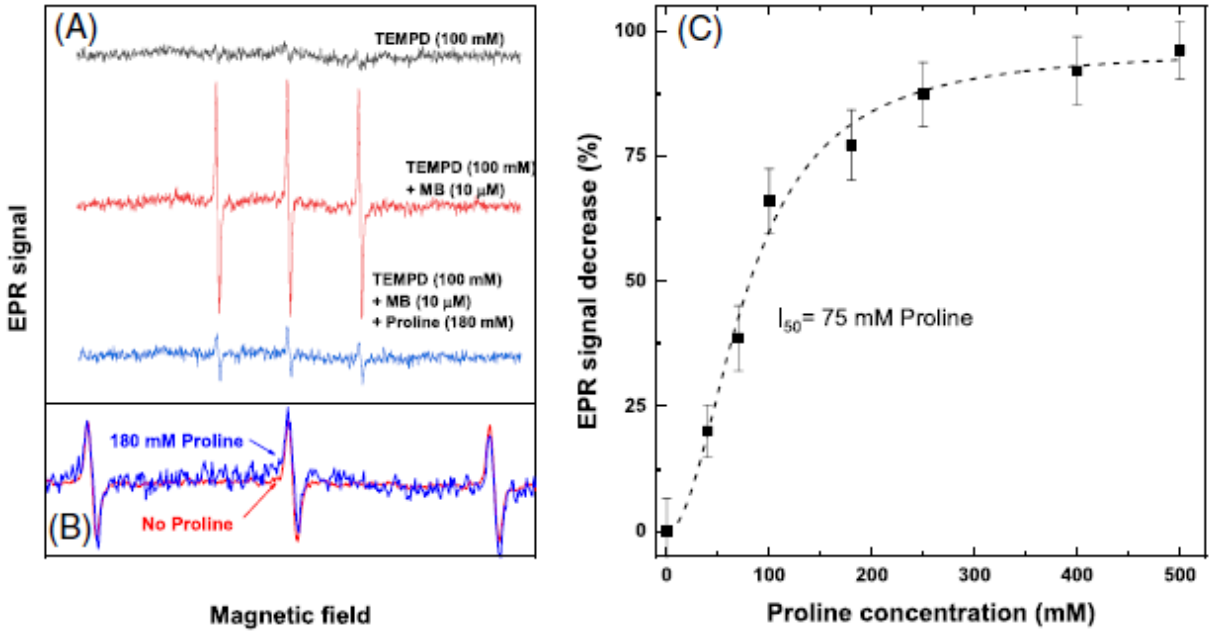

Fig. 4.15. $^1O_2$-scavenging effect of proline detected in vitro by electron paramagnetic resonance (EPR) spin trapping. (A) EPR signals in the dark (upper trace) with 100 mM 2,2,6,6-tetramethyl-4-piperidone (TEMPD, after illumination with 10 µM methylene blue (MB) (middle trace), and after illumination with 10 µM MB + 180 mM proline (lower trace). (B) Loss of EPR signal amplitude as a function of proline concentration relative to the peak amplitude of the TEMPO-D signal obtained in the presence of MB without proline. The proline concentration that causes the TEMPO-D signal to be quenched by 50% is also shown. Using electron

paramagnetic resonance (EPR) spin trapping, the $^1O_2$-scavenging effect of proline was observed in vitro.

To investigate the $^1O_2$ scavenging activity of Pro, Signorelli et al. used O_2 uptake method (Signorelli *et al.*, 2013). The principle of this method is that when $^1O_2$ interacts with a chemical quencher, it absorbs an O_2 molecule and forms a chemical bond, lowering the amount of dissolved O_2 (Fig 4.16). Using a sensitive O_2 electrode, this O_2 uptake effect can be easily observed. Signorelli et al. did not observe any effect of Pro on the rate of O_2 uptake, when $^1O_2$ was genertaed by MB during the illumination and concluded that Pro did not scavange $^1O_2$ at all (Signorelli *et al.*, 2013). When we performed the same experiment, we found similar results (Fig 4.16, diamonds). However, the addition of chemical quenchers of $^1O_2$, i.e., His or Asc to the reaction mixture (Bodannes & Chan, 1979; Méndez-Hurtado *et al.*, 2012), resulted in substantial O_2 uptake (Fig 4.16. circles and triangles, respectively).

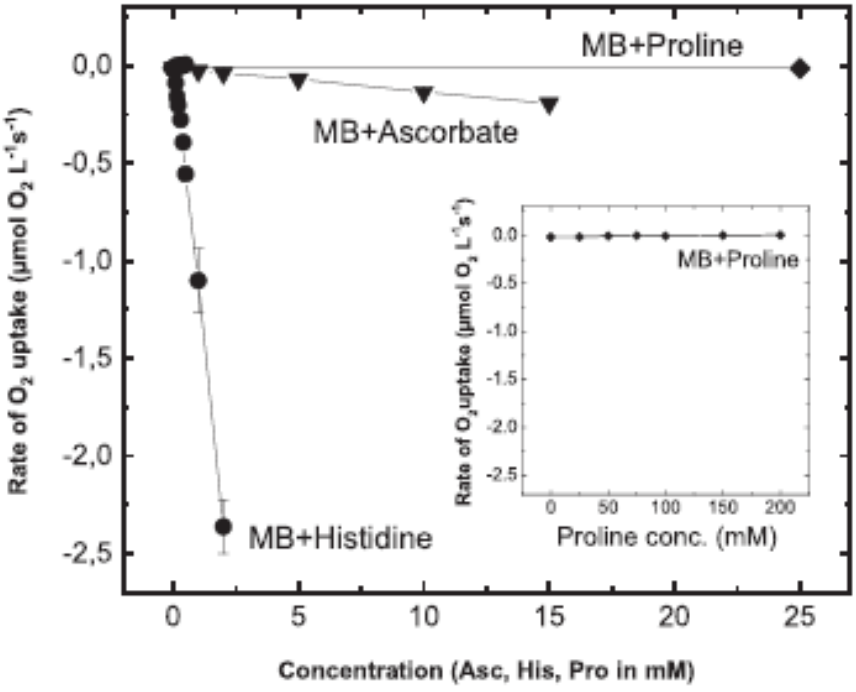

Fig. 4.16. $^1O_2$-scavenging effect of proline detected by oxygen uptake. $^1O_2$ was generated by illuminating 1 µM methylene blue (MB) in the oxygen electrode chamber, and the rate of oxygen uptake due to oxidation of histidine (circles), ascorbate (triangles), and proline (diamonds) was plotted as a function of the concentrations of the respective scavengers. The data represent the

means of three independent measurements with the indicated standard deviations. The inset shows the data on a wider concentration range for proline.

Our data regarding the lack of O_2 uptake in the presence of $^1O_2$ and Pro, is in agreement with Signorelli et al. (Signorelli *et al.*, 2013), and demonstrate that Pro indeed does not act as a chemical scavenger of $^1O_2$. However, this observation does not rule out the $^1O_2$-quenching activity of Pro by the physical mechanism, which proceeds via energy transfer and results in the conversion of the excited $^1O_2$ to ground state $^3O_2$ (Fig 4.17). To answer this question, we combined His with NaN_3, a well-known physical quencher of $^1O_2$ (Hall & Chignell, 1987). NaN_3 converts $^1O_2$ back to its ground state $^3O_2$ without consumption of $^1O_2$; therefore, no O_2 uptake is induced. The presence of NaN_3, on the other hand, reduces the amount of $^1O_2$ available for chemical trapping by His (Rehman *et al.*, 2013). Therefore, the extent of O_2 uptake decreases if the concentration of the physical quencher (NaN_3) increases at the same MB and His concentration (Fig 4.17, triangles). When the same competition experiment was performed with Pro instead of NaN_3, a decrease of O_2 uptake due to $^1O_2$ capture by His was also observed, and this effect was enhanced with increasing Pro concentrations (Fig 4.17, circles). These results demonstrate that Pro functions as a physical quencher of $^1O_2$, reducing the amount of $^1O_2$ available for chemical reactions with His.

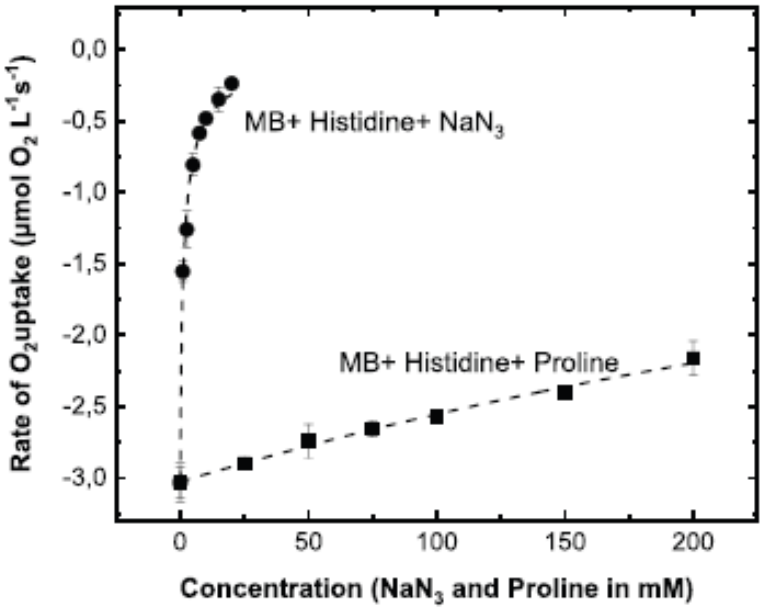

Fig. 4.17. Effect of NaN_3 and proline on the rate of chemical scavenging of $^1O_2$ by histidine. $^1O_2$ was generated by illuminating 1 µM methylene blue (MB) in the oxygen electrode chamber,

and the rate of oxygen uptake due to chemical scavenging of $^1O_2$ by 5 mM histidine was measured in the presence of various concentrations of NaN_3 (triangles) and proline (circles). The data represent the means of three independent measurements with the indicated standard deviations.

Along with EPR and O_2 uptake data, we have employed a third technique to demonstrate that Pro can eliminate $^1O_2$. The fluorescent reporter dye SOSG increases its blue-green fluorescence yield after capturing $^1O_2$ (Flors *et al.*, 2006). Illumination of SOSG alone also induces a fluorescence yield increase, since the chromophore acts as photosensitizer and produces some $^1O_2$ which is captured by the same or other dye molecules, and this results in a background fluorescence signal (Ragàs *et al.*, 2009). However, illumination of SOSG in the presence of MB induces a significant fluorescence yield increase (Fig 4.18(A)). When different amounts of Pro were also present in the reaction mixture, the extent of SOSG fluorescence yield enhancement was reversed (Fig 4.18(A)), resulting in a saturation-type Pro concentration dependence, with ca. 80 mM half inhibitory Pro concentration (Fig 4.18(B)). This effect further demonstrates that Pro competes with various chemical traps of $^1O_2$ (TEMPD, His, SOSG) due to its physical $^1O_2$-quenching activity.

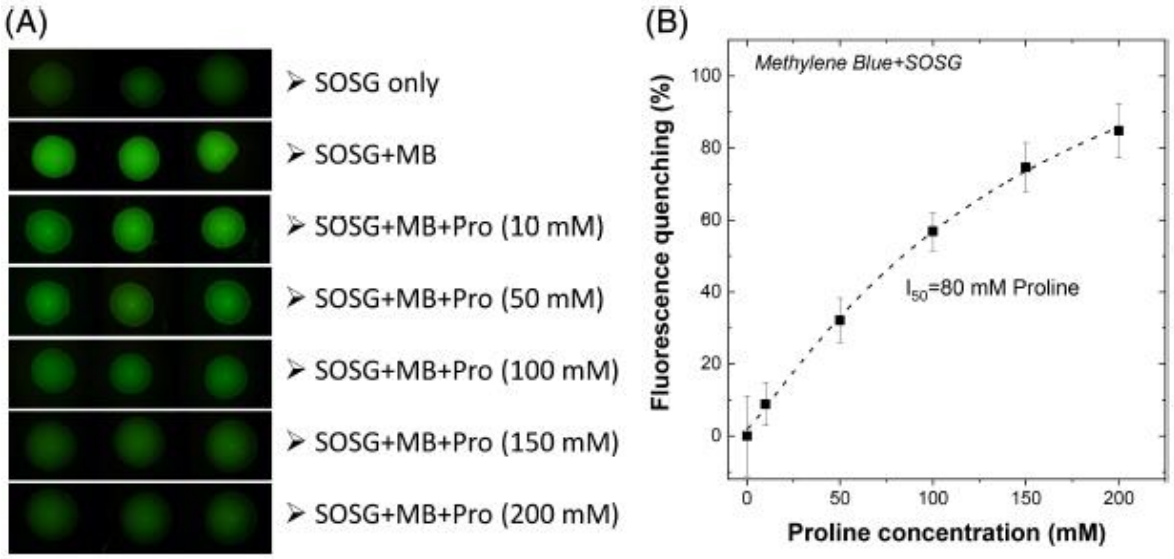

Fig. 4.18. $^1O_2$-scavenging effect of proline in vitro detected by the fluorescent probe singlet oxygen sensor green (SOSG). (A). SOSG fluorescence was detected by a fluorescence stereo microscopy using 460–490 nm excitation and 510–590 nm detection on 2 µL droplets spotted on a microscope slide either alone (top row) or after illumination in the presence of 1 µM methylene blue (MB) and different concentrations of proline (Pro) with 2300 µmole photons

m^{-2} s^{-1} intensity visible light. (B) Fluorescence quenching due to proline-induced $^1O_2$ quenching was quantified by measuring average fluorescence intensities of SOSG-containing droplets, and the change of fluorescence intensity relative to the control sample that contained only SOSG and MB was plotted as a function of proline concentration. The data represent the means of three independent measurements with the indicated standard deviations. The proline concentration which results in 50% quenching of the SOSG signal is also shown.

4.2.2.Proline can eliminate $^1O_2$ from photosynthetic systems

Since intact and isolated photosynthetic systems are known to produce $^1O_2$ upon illumination (Hideg *et al.*, 1994b; Krieger-Liszkay, 2005; Krieger-Liszkay *et al.*, 2008; Rehman *et al.*, 2013), we wanted to check whether or not Pro is active in eliminating the $^1O_2$ produced during photosynthetic processes. When thylakoids were illuminated in the presence of TEMPD and various concentrations of Pro, the size of the TEMPO-D EPR signal, which indicates the amount of captured $^1O_2$, decreased with increasing Pro concentration (with half-inhibitory concentration ca. 80 mM) (Fig.4.19).

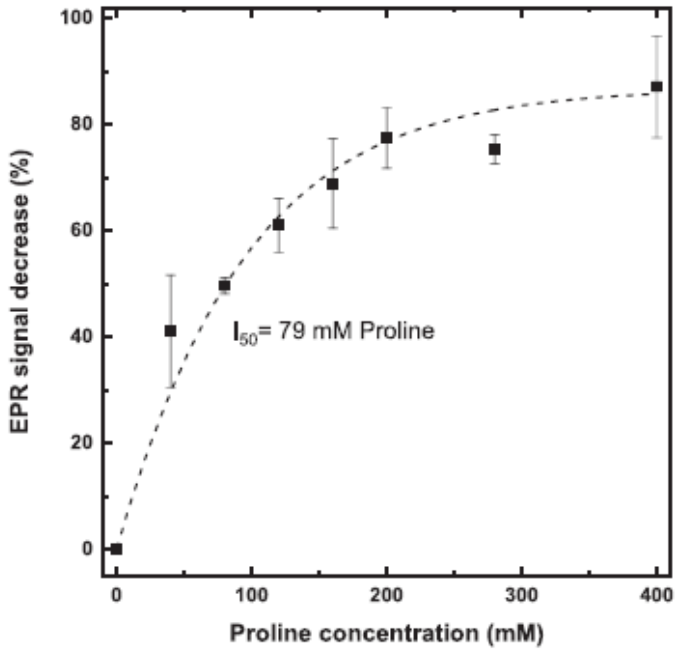

Fig. 4.19. $^1O_2$-scavenging effect of proline detected by electron paramagnetic resonance (EPR) spin trapping in isolated thylakoids. EPR signals were measured as in Fig 4.13 in the presence of 100 mM 2,2,6,6-tetramethyl-4-piperidone (TEMPD) and different concentrations of Pro, but instead of methylene blue (MB) isolated thylakoids (300 µg mL^{-1}) were used for photosensitized production of $^1O_2$ by illumination 2300 µmol photons m^{-2} s^{-1} intensity visible light. The loss of

the TEMPO-D EPR signal amplitude, compared to the control obtained without proline, is plotted as a function of proline concentration. The data are the means of three independent measurements with the indicated standard deviation. The proline concentration which results in 50% quenching of the TEMPO-D signal is also shown.

Similar results were obtained when SOSG was used as $^1O_2$ sensor. A large increase in the yield of the blue-green fluorescence was observed, demonstrating the production of $^1O_2$ by illuminated thylakoids (Fig 4.20 A). This effect is consistent with the well-known production of $^1O_2$ by Chl-containing photosynthetic complexes embedded in thylakoid membranes in response to light. The SOSG fluorescence was suppressed when increasing concentrations of Pro were present during illumination (Fig 4.20(A)), and the magnitude of this effect was inversely proportional to the concentration of Pro, with a half-inhibitory concentration of 75 mM (Fig 4.20 B). This finding demonstrates Pro's ability to remove $^1O_2$ formed in thylakoids and its ability to function as a natural $^1O_2$ quencher in plant systems.

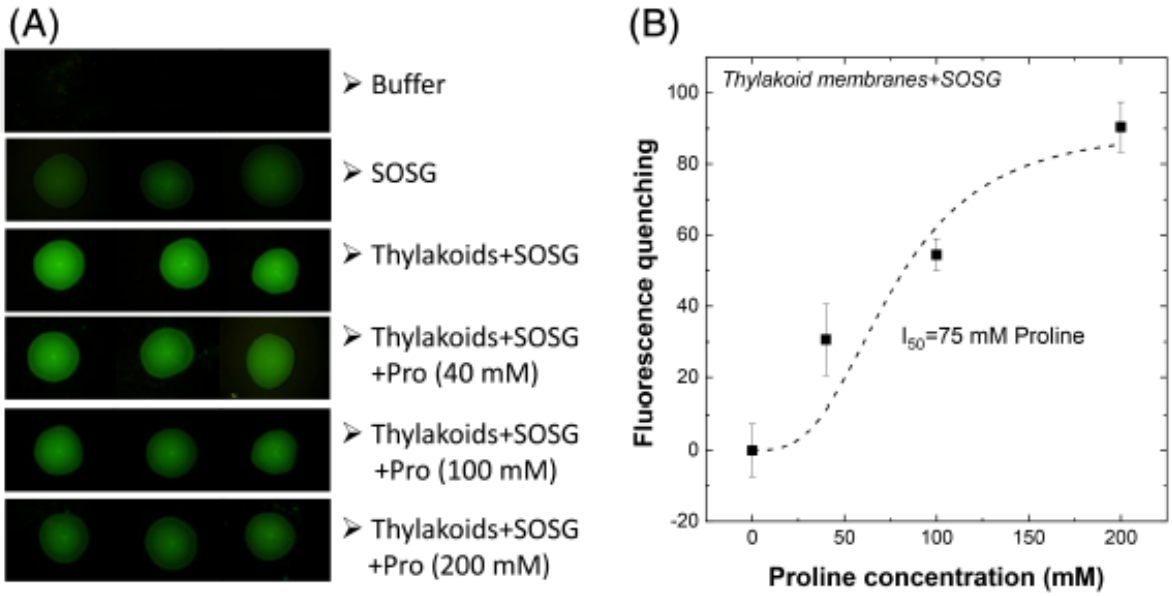

Fig. 4.20. $^1O_2$-scavenging effect of proline in isolated thylakoids detected by the fluorescent probe singlet oxygen sensor green (SOSG). (A) SOSG fluorescence was detected by fluorescence stereo microscopy using 2 µL droplets containing only thylakoid dilution buffer or thylakoids (25 µg Chl mL^{-1}) with different concentrations of proline. The thylakoid-containing samples were illuminated with 2300 µmole photons m^{-2} s^{-1} intensity visible light to induce $^1O_2$ production. (B) Fluorescence quenching due to proline-induced $^1O_2$ scavenging was

quantified by measuring average fluorescence intensities of SOSG-containing droplets, and the change in fluorescence emission relative to the control sample that contained only SOSG and thylakoids was plotted as a function of proline concentration. The data represent the means of five independent measurements with the indicated standard deviations. The proline concentration which results in 50% quenching of the SOSG signal is also shown.

Table 1 summarizes the data regarding the concentrations of Pro, Asc, α-tocopherol and superoxide dismutase in leaves of WT *Arabidopsis*, their $^1O_2$-scavenging rate constants, and their estimated $^1O_2$-detoxifying capacities (obtained as the product of concentration and rate constant). From these data, it follows that in osmotic or salt-stressed *Arabidopsis* leaves the $^1O_2$-scavenging capacity of Pro can reach up to two third of that of α-tocopherol and one fourth or more of that of Asc.

	Concentration ($\mu M\ g^{-1}$ FW)	$^1O_2$ scavenging rate ($10^7\ M^{-1}\ s^{-1}$)	$^1O_2$ scavenging capacity ($10^7\ g^{-1}$ FW $s^{-1)}$)
Proline	50[1]	0.15–0.4[4]	7.5–20
Ascorbate	3[2]	0.8–30[5]	2.4–90
α-tocopherol	0.95[3]	33[6]	31
Superoxide dismutase	NA	NA	NA

Table 1. Rate constants of $^1O_2$ removal and total ROS-detoxifying capacities of proline in comparison to other antioxidants. The concentration values were obtained from the literature for osmotic or salt-stressed wild-type Arabidopsis. The total ROS-scavenging capacities were calculated by multiplying the concentration values and the respective rate constants. [1](Verslues & Sharma, 2010), [2](Tóth *et al.*, 2011), [3](Ellouzi *et al.*, 2011), [4]((Rehman *et al.*, 2021)), [5](Chou & Khan, 1983; Kramarenko *et al.*, 2006; Jung & Min, 2009), [6](Park *et al.*, 2014)

4.3. Singlet oxygen mediated photodamage to PSII in isolated thylakoid membranes and *Chlorella sorokiniana*

4.3.1 Externally produced $^1O_2$ accelerates photodamage of PSII in isolated thylakoid membranes

In order to investigate the effect of externally generated $^1O_2$ on photosynthetic activity of isolated thylakoid membranes, samples were illuminated in the presence of various concentrations of RB in 24-well plate and PSII activity was quantified by determining the F_v/F_m values in each well using variable Chl fluorescence imaging. This is a particularly useful approach when PSII activity has to be determined simultaneously in a large number of samples (Schreiber *et al.*, 2007). At the initial time point (t=0), thylakoid membranes imaged in the well plates exhibited homogeneous F_v/F_m values of approx. 0.66-0.74, however, somewhat lower F_v/F_m was observed with increasing RB concentrations (Fig. 4.21a).

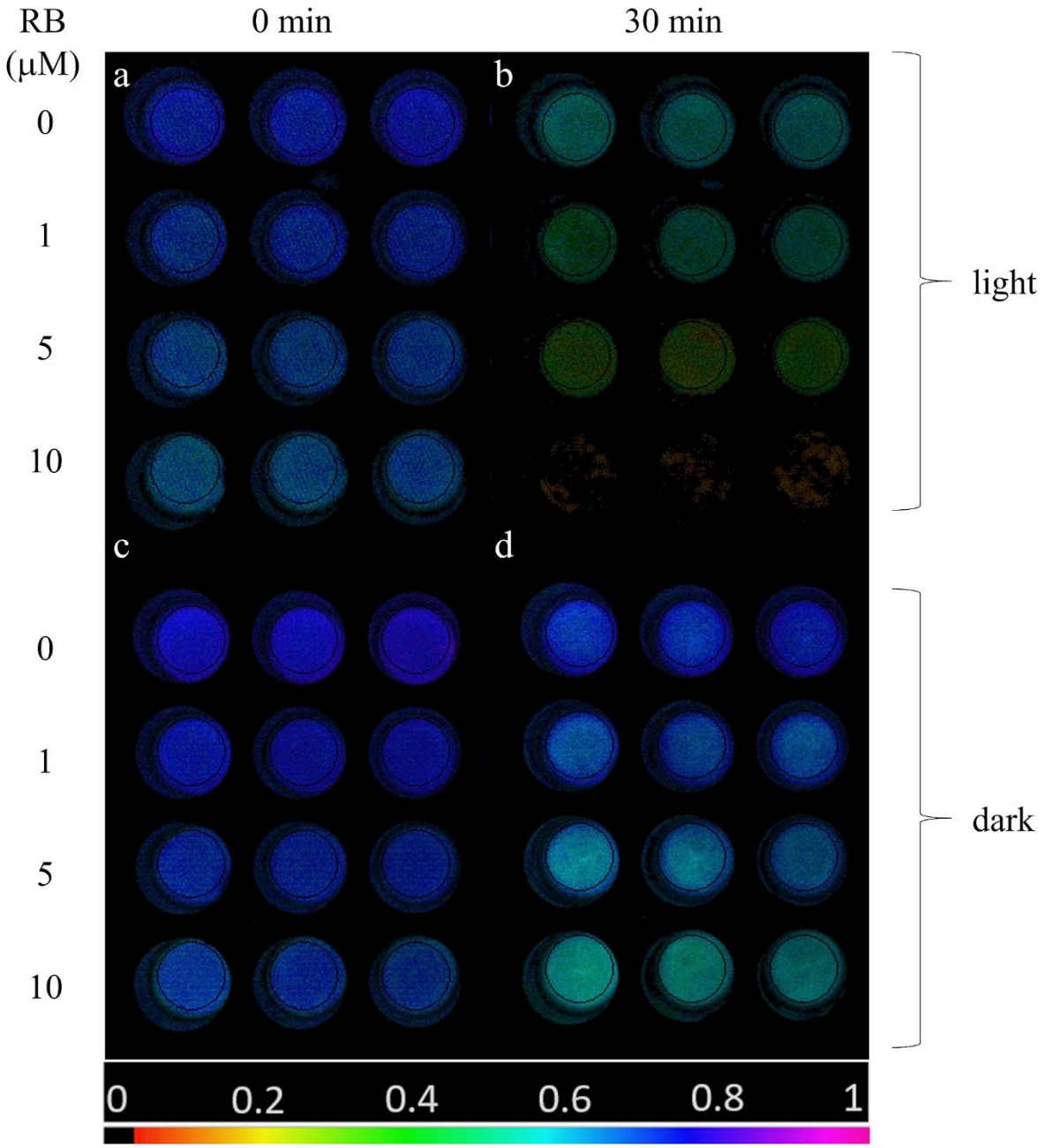

Fig. 4.21. F_v/F_m image of thylakoid membranes illuminated with green+white light (panels a,b) or kept in darkness (c,d) for 0 min (a,c) and 30 min (b,d). In all panels first row represents control (0 µM RB), second row 1 µM RB, third row 5 µM RB, fourth row 10 µM RB (n=3). F_v/F_m values are determined in the selected circular areas of interest. The color bar indicates the relative intensity of F_v/F_m.

F_v/F_m decreased during the light exposure in a RB concentration dependent manner; at 10 µM the F_v/F_m essentially dropped to 0 after 30 min (Fig. 4.21b). The F_v/F_m values also showed some decrease in darkness, which was more pronounced at higher RB concentrations (Fig. 4.21c and 4.21d). These findings demonstrate that illumination of isolated thylakoids in the presence of RB, which induces $^1O_2$ formation in a concentration dependent manner, causes the loss of PSII activity**.**

The detailed time course of F_v/F_m changes show that PSII activity was gradually decreased in the light-exposed thylakoid membranes (Fig. 4.22a). Importantly, this effect showed a strong dependence on RB concentration. While in the absence of RB the thylakoids retained ca. 75% of their initial activity even after 30 min of light exposure, in the presence of 10 µM RB a complete loss of F_v/F_m occurred (Fig. 4.22a). The thylakoids which were treated with 1 and 5 µM RB showed an intermediate behavior. The F_v/F_m values showed some decrease even in darkness. This effect was negligible in the absence of RB up to 30 min (95% of the initial activity remained), but was enhanced when RB was also present (80% remaining activity at 10 µM RB after 30 min) (Fig. 4.22b). In order to compensate for the slow dark inactivation of PSII activity of thylakoids the F_v/F_m data are also shown after normalization of the data obtained in the light to those obtained in the dark (Fig. 4.22c). This representation shows the extent of PSII activity loss, which is actually caused by externally generated $^1O_2$.

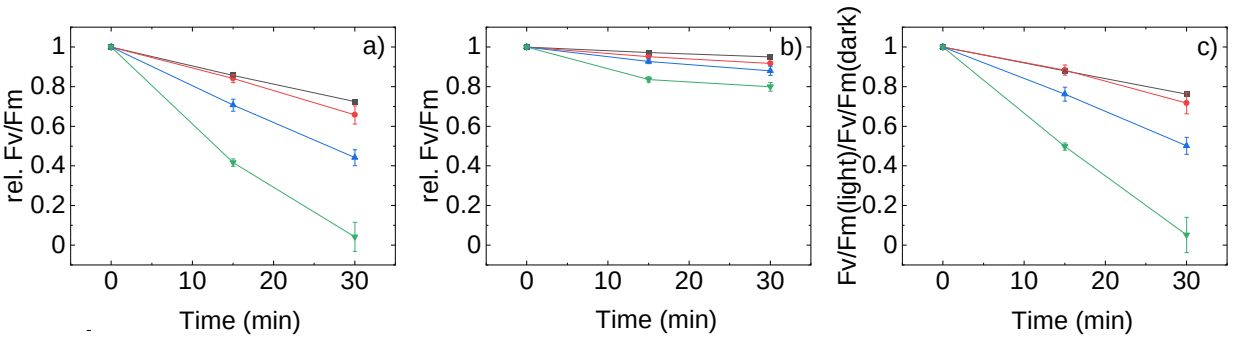

Fig. 4.22. Effect of RB on the maximum quantum efficiency of PSII (Fv/Fm) of thylakoid membranes treated with green-white light (a), or kept in dark (b) for the indicated time periods. Panel c) represents the ratio of Fv/Fm recorded during the light treatment or dark incubation experiment (Fv/Fm values in panel a) were divided by the values on panel b)). Thylakoid membranes were incubated in 0 µM (black), 1 µM (red), 5 µM (blue) or 10 µM (green) RB.

4.3.2 Histidine ameliorates the photodamaging effect of externally produced $^1O_2$ in thylakoids

In order to check if the observed loss of PSII activity by illumination in the presence of RB is indeed related to $^1O_2$-induced damage or not, His was also added to the thylakoid samples. His is a known chemical scavenger of $^1O_2$ (MAtheson, I. B. C.; Lee, 1979; Méndez-Hurtado *et al.*, 2012), which can be used in photosynthetic systems without affecting electron transport (Rehman *et al.*, 2013). The addition of 5 mM His together with 5 µM RB provided a significant protection against the loss of PSII activity when compared to the effect of RB addition alone (Fig. 4.23), confirming the involvement of $^1O_2$ in PSII damage.

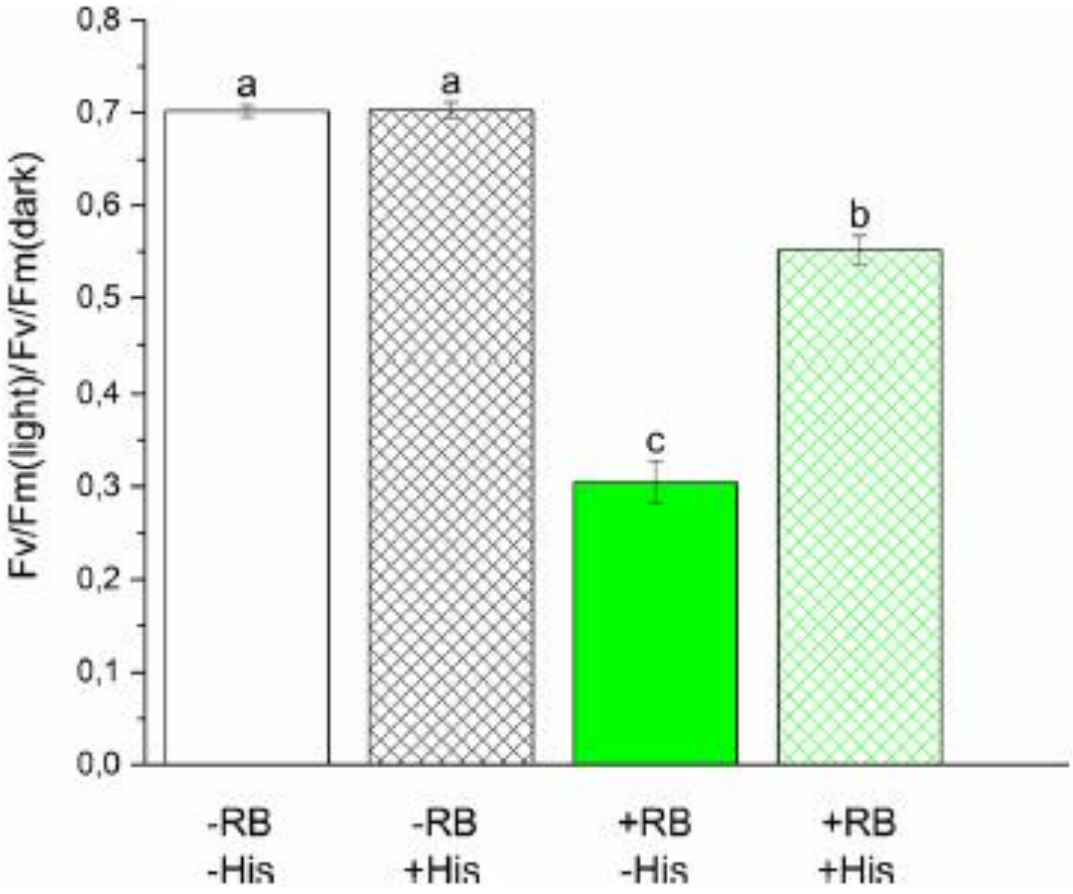

Fig. 4.23. Effect of histidine on RB-induced loss of PSII activity. Thylakoids were illuminated for 60 min in the absence and presence of 5 µM RB as in Fig. 4.20, either without further addition, or in the presence 5 mM histidine. The F_v/F_m values are shown after correction for the change that occurs during dark storage of samples. Different letters above the bars indicate significant differences ($p < 0.05$)

4.3.3. Externally produced $^1O_2$ accelerates photodamage of PSII in intact *Chlorella* cells

In order to assess the effect of externally produced $^1O_2$ in intact cells first we wanted to have an estimation of the $^1O_2$ flux, which is produced by the illumination of RB. This was achieved by using the His-mediated chemical trapping method, which removes dissolved O_2 from the medium as a result of $^1O_2$-induced oxidation of His, which results in easily measurable O_2 uptake (Rehman *et al.*, 2013). By using this approach, we showed that the O_2 evolution rate decreased in *Chlorella* cells in the presence of 5 mM His compared to control cells in which His was absent, showing a ca. 52.8 ± 4.2 μmol O_2 mg Chl^{-1} h^{-1} rate of $^1O_2$ production under the illumination conditions which were applied for the photoinhibition experiments. When *Chlorella* cells were illuminated in the presence of 1 μM RB the O_2 evolution rate was significantly reduced due to chemical trapping of $^1O_2$ by proteins and lipids in the cells. Addition of His together with RB resulted in a large O_2 uptake (Fig. 4.24), which shows a ca. -760.8 ± 195.5 μmol O_2 mg Chl^{-1} h^{-1} rate of $^1O_2$ production in the presence of RB.

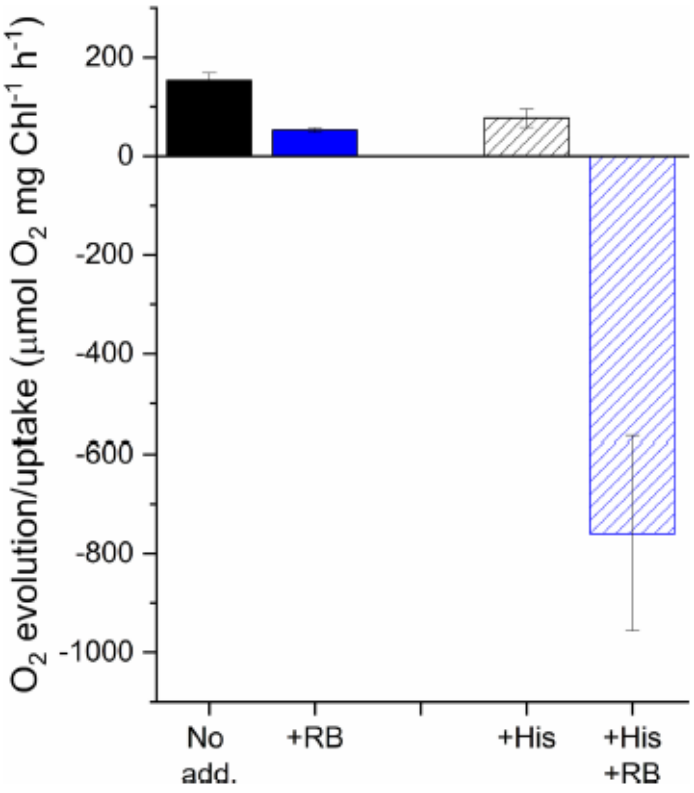

Fig. 4.24. Oxygen evolution/uptake of Chlorella cells. Black, no treatment, blue, 1 μM RB treatment. Closed bars, no His, checked bars, in the presence of 5 mM His.

The $^1O_2$ production rate in the bulk medium is significantly higher than the $^1O_2$ production rate originating from the photosynthetic pigments, i.e. in the absence of RB. However, although RB has been shown to reach chloroplasts in intact leaves (Kovács *et al.*, 2014), its local concentration is most likely lower in the chloroplasts of the *Chlorella* cells than in the bulk medium. Therefore, the $^1O_2$ concentration in the vicinity of PSII is expected to be somewhere between the ambient level, produced by the photosynthetic pigments in the absence of RB, and the bulk level in the culture medium.

In order to clarify the effect of externally generated $^1O_2$ on PSII activity in vivo, intact *Chlorella* cells were incubated in light and in darkness in the presence of different concentrations of RB. In intact systems photodamage and repair of PSII proceeds in parallel. To separate these two processes, the experiments were performed both in the absence and presence of lincomycin, which blocks protein synthesis dependent PSII repair and thus allows the investigation of PSII photodamage without the effect of the ongoing repair. At the beginning of the experiment (t=0 min) the cells exhibited similar F_v/F_m values (0.63-0.65) in the entire plate, indicating that the RB treatment did not affect maximal PSII quantum yield (Fig. 4.25a, 4.25c). After 60 min light treatment, a RB concentration dependent decrease in F_v/F_m could be observed, which was more pronounced in the presence of lincomycin (Fig. 4.24b, well columns 4-6). When the cells were incubated in complete darkness only a minor decrease in F_v/F_m was observed, which was independent of RB concentration (Fig. 4.25d).

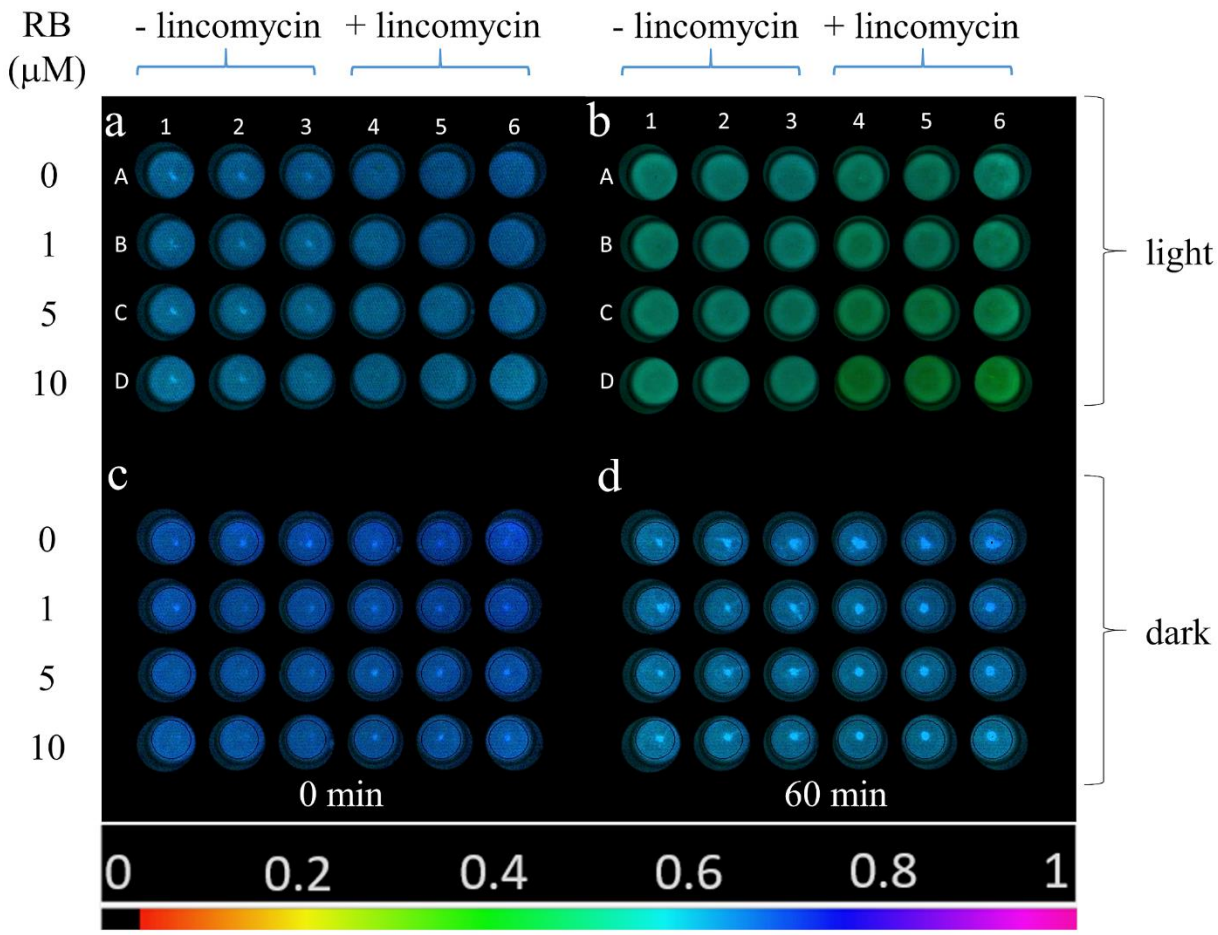

Fig. 4.25. Fv/Fm image of Chlorella sorokiniana cells in the 24 well plates illuminated with green+white light (a,b) or kept in darkness (c,d) at 0 min (a,c) and after 60 min (b,d). Wells A1-3: 0 μM RB, A4-6: 0 μM RB+lincomycin, B1-3: 1 μM RB, B4-6: 1 μM RB+lincomycin, C1-3: 5 μM RB, C4-6: 5 μM RB+lincomycin, D1-3: 10 μM RB, D4-6: 10 μM RB+lincomycin. The color bar indicates the relative intensity of F_v/F_m (black: $F_v/F_m=0$, magenta: $F_v/F_m=1$).

The detailed time course of F_v/F_m values shows that in the absence of lincomycin PSII activity loss showed a tendency to increase after 60 min light exposure in the presence of RB (Fig. 4.26a). However, this effect was statistically significant only after 60 min light exposure (see below, Fig. 4.26). The presence of lincomycin accelerated PSII damage, which became clearly visible already after 30 min (Fig. 4.26). The enhancement of PSII photodamage showed a clear dependence on RB concentration. While 1 μM RB had practically no effect on F_v/F_m, 5 and 10 μM produced significantly larger F_v/F_m loss after 30 min, than 0 or 1 μM RB (Fig. 4.26a).

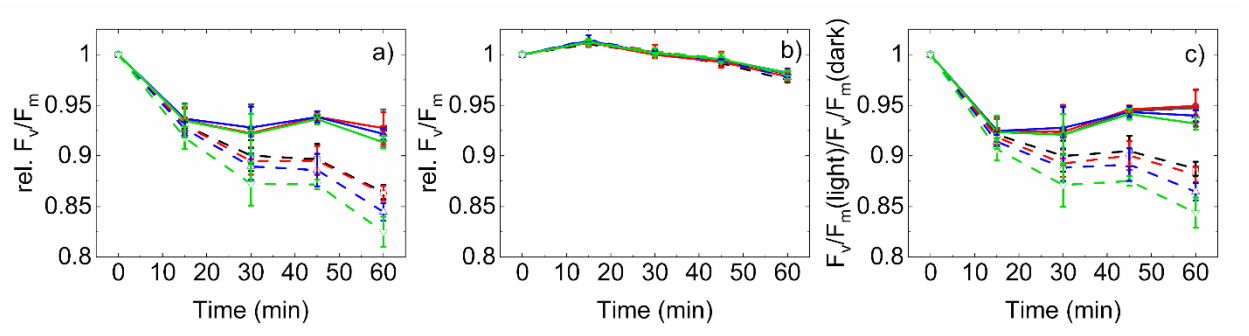

Fig. 4.26. Effect of RB on the maximum quantum efficiency of PSII (F_v/F_m) of Chlorella sorokiniana cells treated with green-white light (240 µmol photons m^{-2} s^{-1}) (a), or kept in dark (b) for the indicated time periods. Panel c) represents the ratio of F_v/F_m recorded during the light treatment and dark incubation experiment (F_v/F_m values in panel a) were divided by the values on panel b). Cells were incubated in the presence of 0 µM (black), 1 µM (red), 5 µM (blue) or 10 µM (green) RB. Solid lines, cells with no lincomycin, dashed lines, cells in the presence of 300 µg/ml lincomycin.

When *Chlorella* cells were kept in the dark, the F_v/F_m values showed a minor increase followed by a small decrease reaching ca. 97.5 % of the initial PSII activity. This effect was independent of the absence or presence of RB after 60 min (Fig. 4.26b). In order to correct for the small changes of PSII activity in the dark the F_v/F_m data are also shown after normalization of the data obtained in the light to those obtained in the dark (Fig. 4.26c).

The changes in F_v/F_m are relatively small in *Chlorella* cells as compared to those obtained in isolated thylakoids, when the same irradiance and timescale of treatment is applied (Fig. 4.26). However, after 60 min light treatment the enhanced decline of F_v/F_m is obvious in the presence of RB, especially in the lincomycin treated cells (Fig. 4.26c). Although Fig. 4.26 clearly shows the tendency of cells experiencing larger PSII activity loss in the presence of higher RB concentrations, the extent of these changes was also analyzed for statistically significant differences. As shown in Fig. 4.27, illumination of the *Chlorella* cells in the absence of RB resulted in a significant loss of the maximal quantum yield of PSII after 60 min even in the absence of lincomycin, showing that despite the relatively low light intensity photoinhibition of PSII has occurred.

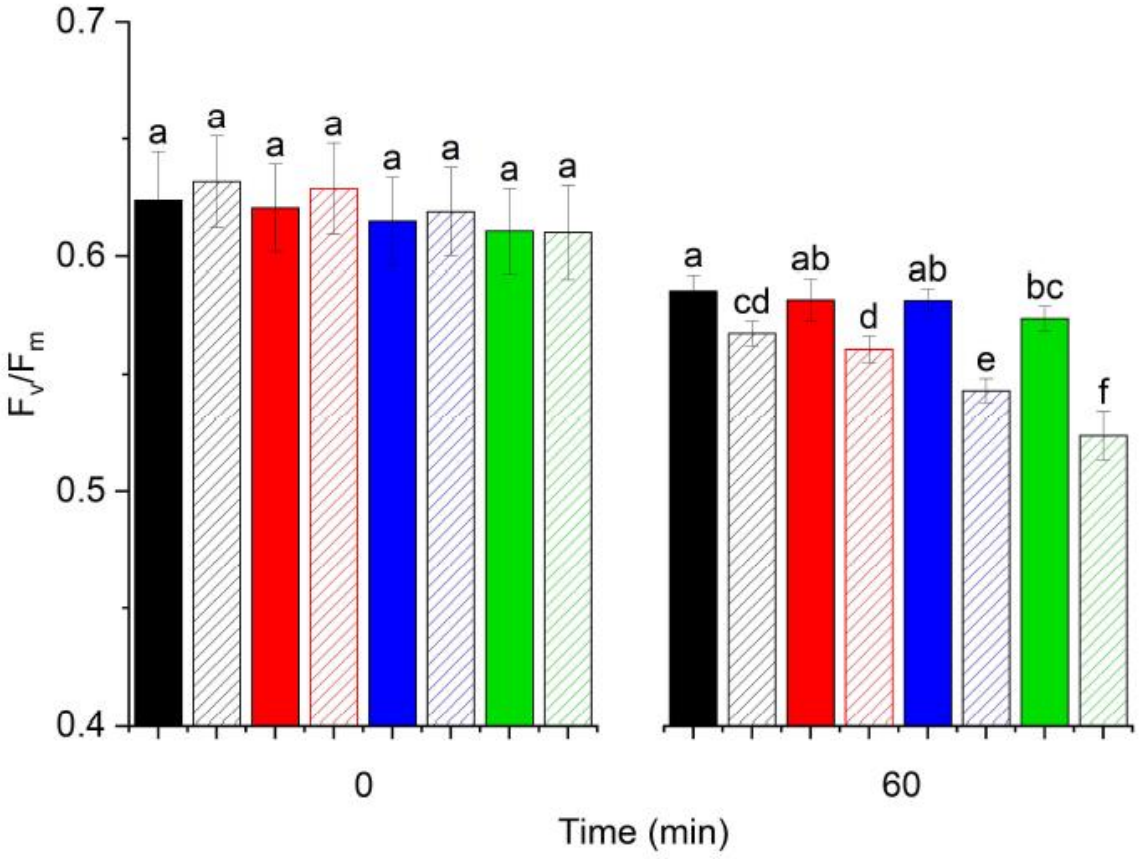

Fig. 4.27. Maximum quantum efficiency of PSII (F_v/F_m) of Chlorella sorokiniana cells treated with green-white light (240 µmol photons m^{-2} s^{-1}) in the presence of 0 µM (black), 1 µM (red), 5 µM (blue) or 10 µM (green) RB for the indicated time periods. Closed bars, cells with no lincomycin, checkered bars, cells in the presence of 300 µg/ml lincomycin. Different letters indicate significant differences ($p<0.05$, $n=9$). Statistical analysis was performed using one-way ANOVA with Tukey's post-hoc multiple comparison tests ($\propto=0.05$). Normality tests were performed using Kolmogorov-Smirnov method and the homogeneity of variance test was performed using Levene's method.

The PSII activity loss was enhanced in the presence of lincomycin due to the lack of protein synthesis dependent repair. This effect was further enhanced when RB was present, as an external source of $^1O_2$, and the extent of PSII activity loss was increasing practically linearly with increasing concentration of RB. In the absence of lincomycin there was a tendency of increased PSII activity loss in the presence of RB, but the effect statistically significant only in case of 10 µM RB.

5. DISCUSSION

5.1. $^1O_2$-mediated photooxidative stress in the symbiotic dinoflagellate *Symbiodinium*

Oxidative stress and oxidative damage have long been implicated as major factors in coral bleaching (Lesser, 1997), recently reviewed in (Szabó, 2020). The mechanism(s) that cause the symbiotic partner to be expelled are not fully understood. However, $^1O_2$ is considered to be one of the most common ROS involved in coral bleaching, which is formed under combined heat and light stress (Rehman *et al.*, 2016b). In order to reveal the impacts of extreme climatic factors on corals, it is very important to understand the mechansim of $^1O_2$ production and its adverse effects in the symbiotic dinoflagellate cells. In the past years, emphasis of investigating the impact of oxidative stress and reactive oxygen species in coral physiology is increasingly based on single cell studies applying multiple fluorescent sensors and single cell photosynthetic activity assays (e.g. (Nielsen *et al.*, 2018; Petrou *et al.*, 2018). Major hindrance of application of fluorophores in intact cells is the impermeability of the fluorescent dye due to the presence of cell wall, which is particularly relevant for the intracellular $^1O_2$ labeling dye Singlet Oxygen Sensor Green (SOSG).

Previous studies and attempts have failed to label intracellular $^1O_2$ in *Symbiodinium*. Rehman et al, found that SOSG did not penetrate the cell wall, therefore intracellular labeling could not be performed although the production of $^1O_2$ could indirectly be measured with the His uptake method and the intensification of extracellular SOSG fluorescence possibly due to the export of $^1O_2$ sensitizing metabolite (Rehman *et al.*, 2016b). Wietheger (2018) reported that some intracellular SOSG staining could be observed in intact *Symbiodinium* cells, however the subcellular localization of SOSG could not be assigned and no optical sectioning was performed to analyze the intracellular distribution of the dye (Wietheger *et al.*, 2018). This was mainly due to the lack of suitable $^1O_2$ detection methods that could be applied for the detection and quantification of $^1O_2$ inside the cells (intracellularly). Therefore, it was a particular importance of the present study to investigate the intracellular $^1O_2$ formation using the SOSG dye, for which preparation of physiologically competent protoplast is essential. Using the advantage of the protoplast preparation method under highly controlled environment, as demonstrated in the sections 3.4 and 3.8, SOSG labeling was applied to image the intracellular distribution of $^1O_2$ in *Symbiodinium.*

In section 4.1.1, first we have shown that protoplast preparation and regeneration protocol can be improved by using the higher concentration of the cellulase (4%) in combination with 1% macerozyme, and this higher enzyme concentration did not impact the

health of cells. Protoplast formation time was reduced to 24 hours compared to the previous study (Levin *et al.*, 2017) where this process completed in 36-48 hours. We then used the optimized protoplast technology to investigate the penetration of $^1O_2$ sensitive fluorescent dyes inside the cells.

Our findings (in section 4.1.4 and 4.1.5) showed that *Symbiodinium* cells undergo changes in the cell size and morphology during the process of protoplast formation. Cell size and morphology is known to vary in *Symbiodinium* as a result of stress conditions (e.g. elevated temperature (Franklin *et al.*, 2004; Petrou *et al.*, 2018), or as more relevant as shown in our results (section 4.1.4), due to the shear stress. However, the characteristic increase and then the equilibrium state of cell area and other morphological parameters during the enzymatic cell wall digestion could be clearly distinguished from other stress-induced cell morphology changes, because heat stress or bleaching conditions typically cause vacuolization, disorganization of chloroplast and other structural degradation of symbionts (Franklin *et al.*, 2004; Petrou *et al.*, 2018), which was not observed during protoplast formation.

In order to test whether protoplast formation process can be made faster with increasing the flow rate in the microfluidic chamber, we tested different flow rates. We observed that with higher flow rate, the protoplast formation process completed in somewhat shorter time (showed in section 4.1.5). However, it has to be noted that higher flow rates, although enable faster protoplast formation process, cause a significant loss in photosynthetic efficiency during enzyme treatment. Therefore, based on the results presented in section 4.1.6, for the optimization of the protoplast isolation procedures it is important to consider that faster protoplast isolation procedure at elevated flow rates might partially compromise photosynthetic activity, which can be particularly important when maintaining physiological competence of protoplasts is a priority.

Our results shown in section 4.1.6 confirmed the previous findings of (Rehman *et al.*, 2016b) that intact cells does not show any SOSG fluorescence intracellularly, fluorescence could only be detected externally. The protoplast were labelled intracellularly and the green fluorescence of SOSG was observed to be co-localized with the red fluorescence of chlorophyll indicating the localization of the SOSG dye in the chloroplast (Fig 4.10). However, in some cases the SOSG dye was evenly distributed in the cytoplasm and it did not show considerable co-localization with chlorophyll autofluorescence (Fig 4.9d). These discrepancies indicate the nature of the photosensitization of the SOSG dye itself, as it cannot be excluded that a significant part of the SOSG fluorescence is originated from the endoperoxide side-products, and therefore the SOSG pattern observed in the current experiments cannot be unequivocally

assigned to $^1O_2$ production (Gollmer *et al.*, 2011). Nevertheless, the results shown in section 4.1.6 demonstrated for the first time that SOSG is penetrated to the protoplasts of *Symbiodinium* and therefore protoplasts are amenable to investigate singlet oxygen signaling in *Symbiodinium*.

The same experiment was performed in microfluidic chambers and SOSG staining was performed in the trapped cells and protoplast. The main advantage of the preparation of protoplasts from trapped *Symbiodinium* cells is that single protoplasts can be retained in a fixed position, therefore the SOSG fluorescence level can be precisely measured before and after illumination with strong light (i.e. signal changes before and after $^1O_2$ production) (Fig 4.13). This is particularly important to consider when semi-quantitative assays of fluorescence changes are required, which is the case for the SOSG dye assay. Furthermore, parallel assays of Chl autofluorescence and SOSG fluorescence was performed on the same trapped protoplast, which enabled the co-localization of the two fluorescence signals (Fig. 4.10) and therefore the site of $^1O_2$ production in relation to chloroplast position can be revealed.

5.2. Proline is a $^1O_2$ quencher both in vitro and in isolated thylakoids

By using three different approaches: EPR spin trapping by TEMPD, the fluorescent reporter dye SOSG and O_2 uptake measurements we could clearly show that Pro does quench $^1O_2$ both in vitro and in photosynthetically active plant thylakoid membranes. When Pro was present in the aqueous buffer containing TEMPD+MB, we observed a significant decrease in the TEMPO-D signal whereas this signal was absent when there was no MB in the mixture due to the lack of $^1O_2$ (showed in Fig. 4.15A). This effect showed the sigmoidal concentration dependency (Fig 4.15C). This effect could be due to following reasons;

(1) Pro competes with TEMPD for $^1O_2$ interaction. With increased Pro concentration, its $^1O_2$ quenching or scavenging activity increases, so TEMPD will catch less $^1O_2$ as indicated by Mohanty and colleagues (Alia *et al.*, 1997, 2001; Matysik *et al.*, 2002).

(2) Instead of quenching or scavenging $^1O_2$, Pro interacts with the TEMPO-D product, lowering its stability, as indicated by Signorelli et al. based on the EPR line shape change observed with TEMPO (Signorelli *et al.*, 2013).

In our experiments, we used a slightly modified version of the spin trap, TEMPD, instead of the TEMP used by Mohanty and coworkers and added an aqueous solution, as used by (Signorelli *et al.*, 2013). The EPR line shape did not change under our conditions (Fig 4.15(B)), indicating no significant interaction between TEMPO-D and Pro. Our findings support the original interpretation by Alia et al. (1997) that the explanation for the decreased

signal of the TEMPO-D product is the removal of $^1O_2$ by Pro, which reduces the likelihood of $^1O_2$ being trapped by TEMPD.

We could also demonstrate that $^1O_2$ quenching by Pro occurs via a physical mechanism, i.e., it does not include a chemical (oxidation) reaction. Physical quenching of $^1O_2$ by Pro most likely proceed via forming a charge transfer complex, due to the low ionization potential of Pro, which relaxes O_2 back to its triplet ground state via inter system crossing (Alia *et al.*, 2001). Our results confirm the original findings of Mohanty and coworkers (Alia *et al.*, 1997, 2001) regarding the $^1O_2$ quenching ability of Pro, which was questioned on the basis of a result, that excluded only the chemical scavenging mechanism (Signorelli *et al.*, 2016), but not the physical quenching of $^1O_2$ by Pro. From the data shown in Fig 4.15, it can be estimated that the half-inhibitory concentration of His-mediated O_2 uptake by NaN_3 is ca. 1 mM, whereas that of Pro is 350 mM. Therefore, the $^1O_2$ quenching efficiency of Pro is ca. 350 times less than that of NaN_3. Since the bimolecular quenching rate constant of NaN_3 is ca. 0.5–1.5 × 10^9 M^{-1} s^{-1} (Musbat *et al.*, 2013), we can estimate that the $^1O_2$- quenching rate constant of Pro is ca. 1.5–4 × 10^6 M^{-1} s^{-1}. The above estimated $^1O_2$-quenching rate constant of Pro is smaller than that of Asc, which ranges from 0.8–1.2 × 10^7 M^{-1} s^{-1} (Chou & Khan, 1983; Jung & Min, 2009), or 3.2 × 10^8 M^{-1} s^{-1} (Kramarenko *et al.*, 2006), and of α-tocopherol (3.3 × 10^8 M^{-1} s^{-1}) (Park *et al.*, 2014) when compared on equal molar basis. However, this can be partly compensated by the significant accumulation of Pro in stress-exposed plants.

The actual efficiency of Pro to contribute to detoxification of $^1O_2$ obviously depends on the concentration of Pro in cell compartments. The main sites of $^1O_2$ production in plants are the chloroplasts, while it is formed both in the chloroplasts and mitochondria. Enzymes mediating Pro biosynthesis are localized in chloroplasts and cytosol, while those of Pro oxidation are located in mitochondria (Szabados & Savouré, 2010). Apart from *Arabidopsis* data, there is only scarce information available about the concentration of Pro, Asc, α-tocopherol, and SOD in plants under comparable conditions. The amount of Pro is below 1 μmol g^{-1} FW in unstressed *Arabidopsis*, but it can increase up to 50 μmol g^{-1} FW under osmotic or salt stress (Verslues & Sharma, 2010). The Asc content of wild-type (WT) *Arabidopsis* is 2 nmol mg^{-1} Chl (Tóth *et al.*, 2011), corresponding to ca. 3 μmol g^{-1} FW (Tóth et al., personal communication, June 8, 2020). The total SOD activity in WT *Arabidopsis* is ca. 10 unit mg^{-1} protein (Holzmeister *et al.*, 2015), which corresponds to ca. 100 unit g^{-1} FW. The α-tocopherol content is ca. 80 and 40 mg g^{-1} DW in unstressed and salt-stressed *Arabidopsis*, respectively (Ellouzi *et al.*, 2011), which corresponds to ca. 1.9 and 0.95 μmol g^{-1} FW. Table 1 summarizes the data regarding the concentrations of Pro, Asc, α-tocopherol and superoxide dismutase in

leaves of WT *Arabidopsis*, their $^1O_2$-scavenging rate constants, and their estimated $^1O_2$-detoxifying capacities (obtained as the product of concentration and rate constant). From these data, it follows that in osmotic or salt-stressed *Arabidopsis* leaves the $^1O_2$-scavenging capacity of Pro can reach up to two third of that of α-tocopherol and one fourth or more of that of Asc. Therefore, the $^1O_2$-quenching potential of Pro can provide physiologically relevant contribution to $^1O_2$ detoxification in stressed plants, in cell compartments having low levels of more efficient antioxidants.

5.3. Externally produced $^1O_2$ is capable of damaging PSII

It is generally accepted that $^1O_2$, as one of the highly reactive ROS forms, is involved in the process of photoinhibition (Krieger-Liszkay, 2005; Nishiyama *et al.*, 2006; Vass, 2011; Tyystjärvi, 2013a). However, the exact action mechanism of $^1O_2$ is debated. The main topic of this debate is whether $^1O_2$ can directly damage the PSII complex, or it can inhibit only the protein synthesis dependent repair of PSII. The idea that $^1O_2$ is an elicitor of PSII photodamage is supported by various lines of experimental evidence. These evidences demonstrate $^1O_2$ production in light exposed isolated (Macpherson *et al.*, 1993; Hideg *et al.*, 1994a) and intact (Hideg *et al.*, 1998; Rehman *et al.*, 2013, 2016b) photosynthetic systems. In addition, the correlation between the rate of photodamage and the rate of $^1O_2$ production has also been clearly shown (Rehman *et al.*, 2013; Bersanini *et al.*, 2014; Hakkila *et al.*, 2014; Sedoud *et al.*, 2014). The findings that higher $^1O_2$ production rates are accompanied in general with higher PSII photodamage rates do not necessarily prove that $^1O_2$ is the cause of PSII damage, since in principle it may happen that photodamaged PSII centers produce more $^1O_2$ than the active ones. However, the effect of mutations that enhance or decrease photodamage in parallel with modifications of $^1O_2$ production pathways in PSII, which suppress or enhance protective charge recombination routes, respectively (Fufezan *et al.*, 2007; Rehman *et al.*, 2013), provide support for the idea that $^1O_2$ is indeed an agent that induces or mediates the damage of PSII. This idea is supported also by the correlation of extreme light tolerance and decreased $^1O_2$ levels in *Chlorella ohadii* (Treves *et al.*, 2016).

The idea that $^1O_2$ is a direct damaging agent of the PSII complex was challenged on the basis experiments, in which no PSII activity loss was observed when *Synechocystis* PCC 6803 cells were illuminated in the presence of RB, as an external $^1O_2$ source, as well as chloramphenicol as protein synthesis inhibitor (Nishiyama *et al.*, 2001, 2004, 2006). In contrast to these findings infiltration of RB into lincomycin treated intact tobacco leaves accelerated the loss of PSII activity and of the D1 protein (Hideg *et al.*, 2007; Kovács *et al.*, 2014) supporting

the idea that external $^1O_2$ can damage the structure and function of PSII. However, the high concentration of RB which was applied in these leaf infiltration studies (1 mM and 100 μM, respectively) raised the possibility of unspecific damage by the high concentration of externally generated $^1O_2$.

Our present data provides evidence that illumination in the presence of RB can indeed damage PSII activity even when relatively low concentrations of RB (1–10 μM) are used, and this damaging effect can be ameliorated in thylakoids by adding His, which is a chemical scavenger of $^1O_2$ (Fig. 4.22). These demonstrate that externally generated $^1O_2$ inactivates PSII and confirm the validity of earlier leaf infiltration studies in which much larger concentrations (100–1000 μM) of RB were used (Hideg *et al.*, 2007; Kovács *et al.*, 2014). The damaging effect is obviously more substantial in the isolated thylakoids (Figs. 4.20 and 4.21) than in the intact *Chlorella* cells (Figs. 4.25–4.27), but even in the latter case the enhancement of PSII activity loss is statistically significant and increases with increasing RB concentrations, especially in the presence of lincomycin, which blocks protein synthesis dependent PSII repair (Fig. 4.26). $^1O_2$ has a very short lifetime and travel distance in a cellular environment (Krasnovsky, 1998; Skovsen *et al.*, 2005), therefore it is unlikely that the $^1O_2$, which is produced outside the cells could reach the thylakoid embedded PSII complexes in the chloroplasts. The ability of RB to penetrate inside the cells and reach chloroplasts has been shown in tobacco leaves (Kovács *et al.*, 2014). RB can also influence intracellular processes in *Synechocystis* 6803 (Nishiyama *et al.*, 2004) and *Chlorella vulgaris* (Dall'Osto *et al.*, 2019) and this is also the case in *Chlorella sorokiniana* used in the present study. The reason for the weaker inhibition of PSII in the intact *Chlorella* cells in comparison to the isolated thylakoids should be related to the lower local RB concentration inside the chloroplasts in the algal cells as compared to the bulk medium, and/or the presence of efficient $^1O_2$ scavenging processes in the intact system. This idea is supported by the observation that even though a large amount of $^1O_2$ was produced at 1 μM RB concentrations in the bulk medium (Fig. 4.23) PSII activity loss was significant only in the higher concentration range of 5–10 μM (Figs. 4.24, 4.25).

Similarly to the case of isolated thylakoids we have attempted to check the protective effect of His also in the *Chlorella* cells. However, the results were not conclusive (not shown) most likely due to the relatively small extent of PSII activity loss, which was observed as a result of illuminating *Chlorella* cells in the presence of RB (Figs. 4.25, 4.26). It is also possible that the penetration of His to the vicinity of PSII complexes inside the *Chlorella* cells, where it could exert its protective action, was limited. However, based on the strong protective effect of

His in thylakoids, we can assume that His would ameliorate PSII activity loss in *Chlorella* as well, provided that it can reach the thylakoids inside the cells.

The loss of PSII activity by externally generated $^1O_2$ is in full agreement with previous studies, which showed the impact of $^1O_2$ in vitro can be related to the fragmentation of D1 protein, i.e. the scission of peptide bonds in the D1 protein (Miyao, 1994; Lupínková & Komenda, 2004), and consequently inactivation of electron transport (Mishra *et al.*, 1994), and also with the degradation of the D1 protein during illumination of RB infiltrated leaves (Hideg *et al.*, 2007; Kovács *et al.*, 2014). In addition, mass spectrometry analysis of photodamaged PSII showed the presence of oxidized amino acid residues both at the acceptor and donor sides of the PSII RC complex, which demonstrates the damage of the D1 and D2 proteins by ROS (Kale *et al.*, 2017; Zhou *et al.*, 2021).

Reasons for disagreement with previous data

Considering the discrepancy between the results of our study regarding the damaging effect of externally produced $^1O_2$ and those of earlier studies by Nishiyama and coworkers, which found no effect of RB induced $^1O_2$ on PSII damage rate (Nishiyama *et al.*, 2004), it is important to figure out what is causing the discrepancy. The experimental conditions in this study differ from those in the previous study (Nishiyama *et al.*, 2004) in four ways:
(i) we used isolated spinach thylakoids and *Chlorella sorokiniana* cells while previous study was done on the cyanobacterium *Synechocystis* PCC 6803, (ii) we used relatively weak green dominated light (240 mol photons m^{-2} s^{-1}) without considerable excitation of Chl as compared to previous study where strong white light (1500 mol photons m^{-2} s^{-1}) illumination was used, (iii) we used lincomycin as protein synthesis inhibitor while previous study used the chloramphenicol, (iv) we measured PSII activity by using Chl fluorescence imaging to calculate Fv/Fm vs. O_2 evolution data using a Clark type oxygen electrode in the previous study (Nishiyama *et al.*, 2004). The significance of these changes is discussed one by one in detail.

In order to examine the effect of externally produced $^1O_2$, it must be ensured that the added photosensitizer, in this case RB, can reach the area of the target, i.e. the PSII complex. In the aqueous suspension of isolated thylakoid membranes, this is simple to achieve. Therefore, isolated thylakoid membranes were applied as one of our experimental objects. The previous study (Nishiyama *et al.*, 2004) used the cyanobacterium *Synechocystis* 6803, which is unquestionably a useful and extensively used model organism for photosynthesis and photoinhibition research. However, it is possible that the lack of RB-induced PSII damage was

due to RB restricted penetration inside *Synechocystis* cells, limiting the quantity of $^1O_2$ near the thylakoid membranes. Since RB penetration into *Chlorella* cells has been reported in the closely related *Chlorella vulgaris* species (Dall'Osto *et al.*, 2019), we choose the green alga *Chlorella sorokiniana*. Since the damaging effect of RB-mediated $^1O_2$ production was clearly visible in both isolated thylakoids (Figs. 4.20–4.22) and *Chlorella* cells (Figs. 4.24–4.26), one factor in the lack of detection of PSII activity loss in *Synechocystis* (Nishiyama *et al.*, 2004) is likely the limited reach of RB into the vicinity of the thylakoid embedded PSII complexes in this cyanobacterium. It is worth noting that illumination of RB in *Synechocystis* cells produced some $^1O_2$, as seen by the reduction of psbA mRNA elongation, which is a vital step in the D1 protein synthesis dependent PSII repair (Nishiyama *et al.*, 2004). However, because RB is much more soluble in water than in organic solvents, RB sensitized $^1O_2$ can more easily reach the site of D1 synthesis, which occurs in ribosomes attached to the cytosolic surface of the thylakoid membrane (Tyystjärvi *et al.*, 2001), rather than the hydrophobic inner parts of the thylakoids, where the majority of the functional components of PSII complex are located.

We employed a low-intensity light (240 mol photons m^{-2} s^{-1}) with a significant contribution in the green spectral range, which excites RB particularly without driving photosynthetic electron transport. As a result, we were able to avoid strong photoinhibition by photosynthetically active light, and the harmful effect on PSII was mostly caused by the $^1O_2$ produced by the RB. In contrast, Nishiyama et al. (Nishiyama *et al.*, 2004) used very strong (1500 mol photons m^{-2} s^{-1}) visible light with RB, which caused substantial photodamage of PSII itself. As a result, the effect of RB addition on photodamage rate was most likely negligible, allowing it to go unnoticed. Green light, which preferentially excites RB, was also employed in Nishiyama et al. (Nishiyama *et al.*, 2004), but merely to examine the influence of $^1O_2$ on the repair process (i.e. in the absence of protein synthesis inhibitor). It remains unclear why this simple method was not employed to test the influence of $^1O_2$ on photodamage rate (in the presence of a protein synthesis inhibitor).

Intact cells must be treated with a protein synthesis inhibitor to distinguish the photodamage and repair processes in PSII. Lincomycin and chloramphenicol are the most commonly used protein synthesis inhibitors in photoinhibition research (Kodru *et al.*, 2020). They are used with the idea that they will not interfere with photosynthetic electron transport mechanisms. Unfortunately, chloramphenicol cannot be used in this case as it behave as an electron acceptor in PSI and produces reactive superoxide upon oxygen reduction (Okada *et al.*, 1991). More recently, it was discovered that chloramphenicol accepts electrons not only from PSI but also from PSII (Rehman *et al.*, 2016a) and that this effect artificially increases

PSII photodamage via superoxide production in intact *Synechocystis* cells if chloramphenicol is applied at a concentration greater than 100 μg mL^{-1} (Kodru *et al.*, 2020). Therefore, lincomycin was employed in this investigation, as opposed to Nishiyama et al. work, which employed 200 μg mL^{-1} chloramphenicol (Nishiyama *et al.*, 2004). In a previous study (Nishiyama *et al.*, 2004), the presence of a high chloramphenicol concentration could increase the photodamage rate, reducing the possibility of detecting the RB effect.

When RB treated samples are illuminated, a considerable amount of $^1O_2$ is produced which can react chemically and oxidize proteins, lipids and other organic material in their environment. This oxidation causes O_2 uptake, which lowers the apparent O_2 evolution rate when recorded by the Clark type electrode (see Fig. 4.25 showing reduced O_2 rate in the presence of 1 μM RB). Since in the previous study on *Synechocystis* (Nishiyama *et al.*, 2004) 2 and 10 μM RB was used, the modification of the O_2 evolution rate must have been much larger than that we observed here, unless RB was washed out from the cells before the O_2 evolution assay. Despite the fact that Nishiyama et al. makes no mention of such a precaution, this was most likely the case; otherwise, the O_2 evolution rate must have been very low even in non-photoinhibited cells, which is not mentioned in the work. The use of Chl fluorescence imaging in our current investigation was primarily employed based on the fact that it allowed all treatments and PSII activity measurements to be carried out under identical experimental conditions. Furthermore, the Chl fluorescence imaging approach is not affected at all by the $^1O_2$ induced O_2 uptake problem. Consequently, using Chl fluorescence imaging vs. O_2 evolution measurements does not seem to be a crucial factor in the contrasting results.

Based on the above comparison of experimental conditions, we conclude that the failure of previous study to identify the RB-induced increase in PSII photodamage rate (Nishiyama *et al.*, 2004) was most likely due to numerous effects: (i) Since the $^1O_2$ produced by the RB could not reach the thylakoid-embedded functional components of PSII, it lowered the possibility of detecting the PSII activity loss. (ii) Using strong visible light instead of selective excitation of RB for photodamage studies, together with a high chloramphenicol concentration enhanced the photodamage rate, which could easily mask the relatively small enhancement of $^1O_2$-induced PSII damage. These technical issues were solved in our study by selective excitation of RB and the use of lincomycin as a protein synthesis inhibitor that does not interfere with PSII electron transport, allowing to detect $^1O_2$-induced PSII activity loss not only in isolated thylakoids but also in intact *Chlorella* cells.

6. CONCLUSIONS

$^1O_2$ is an important ROS, produced in the photosynthetic organisms under stress conditions. Apart from its role as a signaling molecule, it also plays a destructive role in the cells by destroying proteins and lipids in the photosynthetic organisms. For this reason, the current thesis is based on the investigation of $^1O_2$, specifically its detection methods intracellularly, the photodamage caused by it in the photosynthetic apparatus, and finally the elimination or scavenging of $^1O_2$ to protect the cells from its harmful effects.

In the first part of the project (Aim 1), we established a method for the investigation of $^1O_2$ intracellularly by using the fluorescent probes via protoplast technology. Protoplasts were successfully isolated from *Symbiodinium* in a microfluific system, with trapping and morphometric analysis of single cells throughout the whole protoplast formation and regeneration time. With the presented method, we showed that the protoplast formation process and its associated morphological parameters could be monitored on single cell level, with high time resolution, which is also essential for further biotechnological and environmental applications. The trapped cells also retained physiological activity and photosynthetic competence. The microfluidic method also allowed the localization of $^1O_2$ inside *Symbiodinium* protoplasts using the $^1O_2$ sensitive dye SOSG, creating therefore several possibilities for the investigation of $^1O_2$-mediated signaling pathways and oxidative stress impacts. In this manner, various physiological processes can be investigated with fluorescent dyes whose applicability is otherwise limited due to their impermeability through the cell wall, under various stress scenarios that are relevant for coral bleaching (e.g. heat and light stress).

In the second part of the project (Aim 2), we investigated the role of proline as $^1O_2$ scavenger. Our results showed that proline is an efficient quencher of $^1O_2$. By using various methods (EPR, spin trapping, fluorescence probing by singlet oxygen sensor green and oxygen uptake by chemical trapping), we demonstrated that proline is the quencher of $^1O_2$ in vitro and in isolated thylakoids. While investigating the mechanism of quenching, we compared the effects of chemical scavengers and physical quenchers and our results showed that proline eliminates singlet oxygen via physical mechanism. The scavenging efficiency of proline is relatively small on a molar basis, but considering its presence in high amounts in plant cells under stress conditions it may provide a physiologically relevant contribution to ROS scavenging, supplementing other nonenzymatic ROS scavengers of plant cells.

In the third part of the project (Aim 3), we investigated the effect of $^1O_2$ in damaging the photosystem II of plants and microalgae. We provided a clear experimental evidence that

$^1O_2$ when generated by the externally added photosensitizer RB induces the loss of PSII activity both in isolated thylakoids and intact *Chlorella* cells, which are incapable of PSII repair. These data provide strong support for the idea that the harmful effect of $^1O_2$ is not restricted to the inhibition of the PSII repair, instead $^1O_2$ is capable of direct inactivation of PSII and can act as a mediator in photooxidative damage of the photosynthetic apparatus.

REFERENCES

Ainsworth TD, Heron SF, Ortiz JC, Mumby PJ, Grech A, Ogawa D, Eakin CM, Leggat W. **2016**. Climate change disables coral bleaching protection on the Great Barrier Reef. *Science* **352**: 338–342.

Akhter Banu MN, Hoque MA, Watanabe-Sugimoto M, Islam MM, Uraji M, Matsuoka K, Nakamura Y, Murata Y. **2010**. Proline and glycinebetaine ameliorated NaCl stress via scavenging of hydrogen peroxide and methylglyoxal but not superoxide or nitric oxide in tobacco cultured cells. *Bioscience, Biotechnology and Biochemistry* **74**: 2043–2049.

Albertsson PÅ. **2001**. A quantitative model of the domain structure of the photosynthetic membrane. *Trends in Plant Science* **6**: 349–354.

Alfonso M, Montoya G, Cases R, Rodriguez R, Picorel R. **1994**. Core Antenna Complexes, CP43 and CP47, of Higher Plant Photosystem II. Spectral Properties, Pigment Stoichiometry, and Amino Acid Composition. *Biochemistry* **33**: 10494–10500.

Alia, Mohanty P, Matysik J. **2001**. Effect of proline on the production of singlet oxygen. *Amino Acids* **21**: 195–200.

Alia, Saradhi PP, Mohanty P. **1997**. Involvement of proline in protecting thylakoid membranes against free radical-induced photodamage. *Journal of Photochemistry and Photobiology B: Biology* **38**: 253–257.

Allahverdiyeva Y, Mustila H, Ermakova M, Bersanini L, Richaud P, Ajlani G, Battchikova N, Cournac L, Aro EM. **2013**. Flavodiiron proteins Flv1 and Flv3 enable cyanobacterial growth and photosynthesis under fluctuating light. *Proceedings of the National Academy of Sciences of the United States of America* **110**: 4111–4116.

Allen JF. **1995**. Origins of Photosynthesis. *Nature* **376**: 26.

Allen JF, Forsberg J. **2001**. Molecular recognition in thylakoid structure and function. *Trends in Plant Science* **6**: 317–326.

Anderson JM. **1981**. Consequences of spatial separation of photosystem 1 and 2 in thylakoid membranes of higher plant chloroplasts. *FEBS Letters* **124**: 1–10.

Anderson JM, Chow WS. **2002**. Structural and functional dynamics of plant photosystem II. *Philosophical Transactions of the Royal Society B: Biological Sciences* **357**: 1421–1430.

Andersson B, Anderson JM. **1980**. Lateral heterogeneity in the distribution of chlorophyll-

protein complexes of the thylakoid membranes of spinach chloroplasts. *BBA - Bioenergetics* **593**: 427–440.

Apel K, Hirt H. **2004**. Reactive oxygen species: Metabolism, oxidative stress, and signal transduction. *Annual Review of Plant Biology* **55**: 373–399.

Aranda M, Li Y, Liew YJ, Baumgarten S, Simakov O, Wilson MC, Piel J, Ashoor H, Bougouffa S, Bajic VB, *et al.* 2016. Genomes of coral dinoflagellate symbionts highlight evolutionary adaptations conducive to a symbiotic lifestyle. *Scientific Reports* **6**: 1–15.

Aro EM, McCaffery S, Anderson JM. **1994**. Recovery from Photoinhibition in Peas (Pisum sativum L.) Acclimated to Varying Growth Irradiances (Role of D1 Protein Turnover). *Plant Physiology* **104**: 1033 LP – 1041.

Aro EM, Virgin I, Andersson B. **1993**. Photoinhibition of Photosystem II. Inactivation, protein damage and turnover. *BBA - Bioenergetics* **1143**: 113–134.

Asada K. **1999**. The water-water cycle in chloroplasts: Scavenging of active oxygens and dissipation of excess photons. *Annual Review of Plant Biology* **50**: 601–639.

Asada K. **2006**. Production and scavenging of reactive oxygen species in chloroplasts and their functions. *Plant Physiology* **141**: 391–396.

Baker AC, Glynn PW, Riegl B. **2008**. Climate change and coral reef bleaching: An ecological assessment of long-term impacts, recovery trends and future outlook. *Estuarine, coastal and shelf science* **80**: 435–471.

Barber J. **2007**. Biological solar energy. *Philosophical Transactions of the Royal Society A: Mathematical, Physical and Engineering Sciences* **365**: 1007–1023.

Barber J, Andersson B. **1992**. Too much of a good thing: light can be bad for photosynthesis. *Trends in Biochemical Sciences* **17**: 61–66.

Behrendt L, Mehdi Salek M, Trampe EL, Fernandez VI, Lee KS, Kühl M, Stocker R. **2020**. PhenoChip: A single-cell phenomic platform for highthroughput photophysiological analyses of microalgae. *Science Advances* **6**: 1–14.

Benger G, Govindjee. **1985**. The mechanism of photosynthetic water oxidation. *Photosynthesis Research* **6**: 33–55.

Bersanini L, Battchikova N, Jokel M, Rehman A, Vass I, Allahverdiyeva Y, Aro EM. **2014**. Flavodiiron protein Flv2/Flv4-related photoprotective mechanism dissipates excitation pressure of PSII in cooperation with phycobilisomes in cyanobacteria. *Plant Physiology* **164**:

805–818.

Bertucci A, Moya A, Tambutté S, Allemand D, Supuran CT, Zoccola D. **2013**. Carbonic anhydrases in anthozoan corals - A review. *Bioorganic and Medicinal Chemistry* **21**: 1437–1450.

Bodannes RS, Chan PC. **1979**. Ascorbic acid as a scavenger of singlet oxygen. *FEBS Letters* **105**: 195–196.

Bricheux G, Mahoney DG, Gibbs SP. **1992**. Development of the pellicle and thecal plates following ecdysis in the dinoflagellate Glenodinium foliaceum. *Protoplasma* **168**: 159–171.

Brown BE. **1997**. Coral bleaching: Causes and consequences. *Coral Reefs* **16**: 129–138.

Brown BE, Downs CA, Dunne RP, Gibb SW. **2002**. Exploring the basis of thermotolerance in the reef coral Goniastrea aspera. *Marine Ecology Progress Series* **242**: 119–129.

Carlson PS. **1973**. The Use of Protoplasts for Genetic Research. *Proceedings of the National Academy of Sciences* **70**: 598–602.

Castaldello C, Sforza E, Cimetta E, Morosinotto T, Bezzo F. **2019**. Microfluidic Platform for Microalgae Cultivation under Non-limiting CO2 Conditions. *Industrial & Engineering Chemistry Research* **58**: 18036–18045.

Chen C, Dickman MB. **2005**. Proline suppresses apoptosis in the fungal pathogen Colletotrichum trifolii. *Proceedings of the National Academy of Sciences of the United States of America* **102**: 3459–3464.

Chen MB, Whisler JA, Fröse J, Yu C, Shin Y, Kamm RD. **2017**. On-chip human microvasculature assay for visualization and quantitation of tumor cell extravasation dynamics HHS Public Access dynamics to be observed in high detail with a moderate number of data points. This Protocol Extension describes an adaptation of. *Nat Protoc* **12**: 865–880.

Chou P-T, Khan AU. **1983**. L-ascorbic acid quenching of singlet delta molecular oxygen in aqueous media: Generalized antioxidant property of vitamin C. *Biochemical and Biophysical Research Communications* **115**: 932–937.

Csonka LN, Hanson AD. **1991**. PROKARYOTIC OSMOREGULATION: Genetics and Physiology. *Annual Review of Microbiology* **45**: 569–606.

Dall'Osto L, Cazzaniga S, Guardini Z, Barera S, Benedetti M, Mannino G, Maffei ME, Bassi R. **2019**. Combined resistance to oxidative stress and reduced antenna size enhance light-to-biomass conversion efficiency in Chlorella vulgaris cultures. *Biotechnology for Biofuels* **12**:

1–17.

Dekker JP, Boekema EJ. **2005**. Supramolecular organization of thylakoid membrane proteins in green plants. *Biochimica et Biophysica Acta - Bioenergetics* **1706**: 12–39.

Demmig-Adams B, Adams WW. **1996**. The role of xanthophyll cycle carotenoids in the protection of photosynthesis. *Trends in Plant Science* **1**: 21–26.

Dobáková M, Tichý M, Komenda J. **2007**. Role of the PsbI protein in photosystem II assembly and repair in the cyanobacterium Synechocystis sp. PCC 6803. *Plant Physiology* **145**: 1681–1691.

Downs CA, Fauth JE, Halas JC, Dustan P, Bemiss J, Woodley CM. **2002**. Oxidative stress and seasonal coral bleaching. *Free Radical Biology and Medicine* **33**: 533–543.

Driever SM, Fryer MJ, Mullineaux PM, Baker NR. **2009**. Imaging of reactive oxygen species in vivo. In: Plant signal transduction. Springer, 109–116.

Edge R, McGarvey DJ, Truscott TG. **1997**. The carotenoids as anti-oxidants — a review. *Journal of Photochemistry and Photobiology B: Biology* **41**: 189–200.

Ellouzi H, Ben Hamed K, Cela J, Munné-Bosch S, Abdelly C. **2011**. Early effects of salt stress on the physiological and oxidative status of Cakile maritima (halophyte) and Arabidopsis thaliana (glycophyte). *Physiologia Plantarum* **142**: 128–143.

Erbas-Cakmak S, Akkaya EU. **2014**. Toward singlet oxygen delivery at a measured rate: A self-reporting photosensitizer. *Organic Letters* **16**: 2946–2949.

Fischer BB, Eggen RIL, Trebst A, Krieger-Liszkay A. **2006**. The glutathione peroxidase homologous gene Gpxh in Chlamydomonas reinhardtii is upregulated by singlet oxygen produced in photosystem II. *Planta* **223**: 583–590.

Fischer BB, Hideg É, Krieger-Liszkay A. **2013**. Production, Detection, and Signaling of Singlet Oxygen in Photosynthetic Organisms. *Antioxidants & Redox Signaling* **18**: 2145–2162.

Fischer BB, Krieger-Liszkay A, Eggen RIL. **2004**. Photosensitizers Neutral Red (Type I) and Rose Bengal (Type II) Cause Light-Dependent Toxicity in Chlamydomonas reinhardtii and Induce the Gpxh Gene via Increased Singlet Oxygen Formation. *Environmental Science & Technology* **38**: 6307–6313.

Flors C, Fryer MJ, Waring J, Reeder B, Bechtold U, Mullineaux PM, Nonell S, Wilson MT, Baker NR. **2006**. Imaging the production of singlet oxygen in vivo using a new fluorescent sensor, Singlet Oxygen Sensor Green®. *Journal of Experimental Botany* **57**: 1725–

1734.

Forti G, Furia A, Bombelli P, Finazzi G. **2003**. In vivo changes of the oxidation-reduction state of NADP and of the ATP/ADP cellular ratio linked to the photosynthetic activity in Chlamydomonas reinhardtii. *Plant Physiology* **132**: 1464–1474.

Foudeh AM, Fatanat Didar T, Veres T, Tabrizian M. **2012**. Microfluidic designs and techniques using lab-on-a-chip devices for pathogen detection for point-of-care diagnostics. *Lab on a Chip* **12**: 3249–3266.

Frank HA, Cogdell RJ. **1996**. Carotenoids in photosynthesis. *Photochemistry and Photobiology* **63**: 257–264.

Franklin DJ, Hoegh-Guldberg O, Jones RJ, Berges JA. **2004**. Cell death and degeneration in the symbiotic dinoflagellates of the coral Stylophora pistillata during bleaching. *Marine Ecology Progress Series* **272**: 117–130.

Frausto F, Thomas SW. **2017**. Ratiometric Singlet Oxygen Detection in Water Using Acene-Doped Conjugated Polymer Nanoparticles. *ACS Applied Materials & Interfaces* **9**: 15768–15775.

Fufezan C, Gross CM, Sjödin M, Rutherford AW, Krieger-Liszkay A, Kirilovsky D. **2007**. Influence of the redox potential of the primary quinone electron acceptor on photoinhibition in photosystem II. *Journal of Biological Chemistry* **282**: 12492–12502.

Fujise L, Nitschke MR, Frommlet JC, Serôdio J, Woodcock S, Ralph PJ, Suggett DJ. **2018**. Cell Cycle Dynamics of Cultured Coral Endosymbiotic Microalgae (Symbiodinium) Across Different Types (Species) Under Alternate Light and Temperature Conditions. *Journal of Eukaryotic Microbiology* **65**: 505–517.

Gibbin E, Gavish A, Domart-Coulon I, Kramarsky-Winter E, Shapiro O, Meibom A, Vardi A. **2018**. Using NanoSIMS coupled with microfluidics to visualize the early stages of coral infection by Vibrio coralliilyticus. *BMC Microbiology* **18**: 1–10.

Glazer AN. **1984**. Phycobilisome a macromolecular complex optimized for light energy transfer. *Biochimica et Biophysica Acta (BBA) - Reviews on Bioenergetics* **768**: 29–51.

Gollmer A, Arnbjerg J, Blaikie FH, Pedersen BW, Breitenbach T, Daasbjerg K, Glasius M, Ogilby PR. **2011**. Singlet oxygen sensor green®: Photochemical behavior in solution and in a mammalian cell. *Photochemistry and Photobiology* **87**: 671–679.

Govindjee. **2004**. Chlorophyll a Fluorescence: A Bit of Basics and History BT - Chlorophyll

a Fluorescence: A Signature of Photosynthesis. In: Papageorgiou GC, Govindjee, eds. Dordrecht: Springer Netherlands, 1–41.

van Grondelle R, Zuber H. **1992**. The light reactions of photosynthesis.

Grossman AR, Schaefer MR, Chiang GG, Collier JL. **1993**. The phycobilisome, a light-harvesting complex responsive to environmental conditions. *Microbiological Reviews* **57**: 725–749.

Hakkila K, Antal T, Rehman AU, Kurkela J, Wada H, Vass I, Tyystjärvi E, Tyystjärvi T. **2014**. Oxidative stress and photoinhibition can be separated in the cyanobacterium Synechocystis sp. PCC 6803. *Biochimica et Biophysica Acta - Bioenergetics* **1837**: 217–225.

Hall RD, Chignell CF. **1987**. Steady-State Near-Infrared Detection of Singlet Molecular Oxygen: a Stern-Volmer Quenching Experiment With Sodium Azide. *Photochemistry and Photobiology* **45**: 459–464.

Hankamer B, Barber J, Boekema EJ. **1997**. ORGANlZ4TION OF PHOTOSYSTEM 1. *In Vivo*.

Hansen G, Daugbjerg N. **2009**. Symbiodinium natans sp. Nov.: a “free-living” dinoflagellate from tenerife (northeast-atlantic ocean) 1. *Journal of Phycology* **45**: 251–263.

Hare PD, Cress WA. **1997**. Metabolic implications of stress-induced proline accumulation in plants. *Plant growth regulation* **21**: 79–102.

Havaux M, Bonfils JP, Lutz C, Niyogi KK. **2000**. Photodamage of the photosynthetic apparatus and its dependence on the leaf developmental stage in the npq1 Arabidopsis mutant deficient in the xanthophyll cycle enzyme violaxanthin de-epoxidase. *Plant Physiology* **124**: 273–284.

Hawkins TD, Krueger T, Wilkinson SP, Fisher PL, Davy SK. **2015**. Antioxidant responses to heat and light stress differ with habitat in a common reef coral. *Coral Reefs* **34**: 1229–1241.

Hendrickson L, Förster B, Pogson BJ, Wah SC. **2005**. A simple chlorophyll fluorescence parameter that correlates with the rate coefficient of photoinactivation of Photosystem II. *Photosynthesis Research* **84**: 43–49.

Hendrickson L, Furbank RT, Chow WS. **2004**. A simple alternative approach to assessing the fate of absorbed light energy using chlorophyll fluorescence. *Photosynthesis Research* **82**: 73–81.

Hideg É. **2008**. A comparative study of fluorescent singlet oxygen probes in plant leaves.

Central European Journal of Biology **3**: 273–284.

Hideg É, Deák Z, Hakala-Yatkin M, Karonen M, Rutherford AW, Tyystjärvi E, Vass I, Krieger-Liszkay A. **2011**. Pure forms of the singlet oxygen sensors TEMP and TEMPD do not inhibit Photosystem II. *Biochimica et Biophysica Acta - Bioenergetics* **1807**: 1658–1661.

Hideg É, Kálai T, Hideg K, Vass I. **1998**. Photoinhibition of photosynthesis in vivo results in singlet oxygen production detection via nitroxide-induced fluorescence quenching in broad bean leaves. *Biochemistry* **37**: 11405–11411.

Hideg É, Kálai T, Kós PB, Asada K, Hideg K. **2006**. Singlet Oxygen in Plants—Its Significance and Possible Detection with Double (Fluorescent and Spin) Indicator Reagents. *Photochemistry and Photobiology* **82**: 1211.

Hideg É, Kós PB, Vass I. **2007**. Photosystem II damage induced by chemically generated singlet oxygen in tobacco leaves. *Physiologia Plantarum* **131**: 33–40.

Hideg É, Ogawa K, Kálai T, Hideg K. **2001**. Singlet oxygen imaging in a Arabidopsis thaliana leaves under photoinhibition by excess photosynthetically active radiation. *Physiologia Plantarum* **112**: 10–14.

Hideg É, Schreiber U. **2007**. Parallel assessment of ROS formation and photosynthesis in leaves by fluorescence imaging. *Photosynthesis Research* **92**: 103–108.

Hideg É, Spetea C, Vass I. **1994a**. Singlet oxygen production in thylakoid membranes during photoinhibition as detected by EPR spectroscopy. *Photosynthesis Research* **39**: 191–199.

Hideg É, Spetea C, Vass I. **1994b**. Singlet oxygen and free radical production during acceptor- and donor-side-induced photoinhibition. Studies with spin trapping EPR spectroscopy. *BBA - Bioenergetics* **1186**: 143–152.

Hirakawa K, Hirano T, Nishimura Y, Arai T, Nosaka Y. **2011**. Control of singlet oxygen generation photosensitized by meso-anthrylporphyrin through interaction with dna. *Photochemistry and Photobiology* **87**: 833–839.

Holzmeister C, Gaupels F, Geerlof A, Sarioglu H, Sattler M, Durner J, Lindermayr C. **2015**. Differential inhibition of Arabidopsis superoxide dismutases by peroxynitrite-mediated tyrosine nitration. *Journal of Experimental Botany* **66**: 989–999.

Howells EJ, Beltran VH, Larsen NW, Bay LK, Willis BL, van Oppen MJH. **2012**. Coral thermal tolerance shaped by local adaptation of photosymbionts. *Nature Climate Change* **2**: 116–120.

Huang WY, Chou ST, Chen CH, Chou SY, Wu JH, Chen YC, Lee G Bin. **2018**. An automatic integrated microfluidic system for allergy microarray chips. *Analyst* **143**: 2285–2292.

Hung M-S, Chang J-H. **2012**. Developing microfluidics for rapid protoplasts collection and lysis from plant leaf. *Proceedings of the Institution of Mechanical Engineers, Part N: Journal of Nanoengineering and Nanosystems* **226**: 15–22.

Ivanov B, Mubarakshina M, Khorobrykh S. **2007**. Kinetics of the plastoquinone pool oxidation following illumination. Oxygen incorporation into photosynthetic electron transport chain. *FEBS Letters* **581**: 1342–1346.

Jakob B, Heber U. **1996**. Photoproduction and detoxification of hydroxyl radicals in chloroplasts and leaves and relation to photoinactivation of photosystems I and II. *Plant and Cell Physiology* **37**: 629–635.

Jeong HJ, Lee SY, Kang NS, Yoo Y Du, Lim AS, Lee MJ, Kim HS, Yih W, Yamashita H, LaJeunesse TC. **2014**. Genetics and morphology characterize the dinoflagellate Symbiodinium voratum, n. sp.,(Dinophyceae) as the sole representative of Symbiodinium clade E. *Journal of Eukaryotic Microbiology* **61**: 75–94.

Jones LW, Kok B. **1966**. Photoinhibition of Chloroplast Reactions. I. Kinetics and Action Spectra. *Plant Physiology* **41**: 1037 LP – 1043.

Juang Y-J, Chang J-S. **2016**. Applications of microfluidics in microalgae biotechnology: A review. *Biotechnology Journal* **11**: 327–335.

Jung MY, Min DB. **2009**. ESR study of the singlet oxygen quenching and protective activity of trolox on the photodecomposition of riboflavin and lumiflavin in aqueous buffer solutions. *Journal of Food Science* **74**.

Kálai T, Hideg É, Vass I, Hideg K. **1998**. Original Contribution DOUBLE (FLUORESCENT AND SPIN) SENSORS FOR DETECTION OF. *Free Radical Biology and Medicine* **24**: 649–652.

Kale R, Hebert AE, Frankel LK, Sallans L, Bricker TM, Pospíšil P. **2017**. Amino acid oxidation of the D1 and D2 proteins by oxygen radicals during photoinhibition of Photosystem II. *Proceedings of the National Academy of Sciences of the United States of America* **114**: 2988–2993.

Kamennaya NA, Ajo-Franklin CM, Northen T, Jansson C. **2012**. Cyanobacteria as biocatalysts for carbonate mineralization. *Minerals* **2**: 338–364.

Kato Y, Ozawa SI, Takahashi Y, Sakamoto W. **2015**. D1 fragmentation in photosystem II repair caused by photo-damage of a two-step model. *Photosynthesis Research* **126**: 409–416.

Keren N, Berg A, Van Kan PJM, Levanon H, Ohad I. **1997**. Mechanism of photosystem II photoinactivation and D1 protein degradation at low light: The role of back electron flow. *Proceedings of the National Academy of Sciences of the United States of America* **94**: 1579–1584.

Kerfeld CA, Kirilovsky D. **2013**. Chapter One - Structural, Mechanistic and Genomic Insights into OCP-Mediated Photoprotection. In: Chauvat F, Cassier-Chauvat CBT-A in BR, eds. Genomics of Cyanobacteria. Academic Press, 1–26.

Kessler F, Schnell DJ. **2006**. The function and diversity of plastid protein import pathways: A multilane GTPase highway into plastids. *Traffic* **7**: 248–257.

Kim S, Fujitsuka M, Majima T. **2013**. Photochemistry of Singlet Oxygen Sensor Green. *The Journal of Physical Chemistry B* **117**: 13985–13992.

Kim MJ, Youn JR, Song YS. **2018**. Focusing manipulation of microalgae in a microfluidic device using self-produced macromolecules. *Lab on a Chip* **18**: 1017–1025.

Kirilovsky D, Rutherford AW, Etienne AL. **1994**. Influence of DCMU and ferricyanide on photodamage in photosystem II. *Biochemistry* **33**: 3087–3095.

Kishor PBK, Sangam S, Amrutha RN, Laxmi PS, Naidu KR, Rao KRSS, Rao S, Reddy KJ, Theriappan P, Sreenivasulu N. **2005**. Regulation of proline biosynthesis, degradation, uptake and transport in higher plants: its implications in plant growth and abiotic stress tolerance. *Current science*: 424–438.

Kodru S, ur Rehman A, Vass I. **2020**. Chloramphenicol enhances Photosystem II photodamage in intact cells of the cyanobacterium Synechocystis PCC 6803. *Photosynthesis Research* **145**: 227–235.

Komenda J, Dobakova M, Tichy M. **2007**. Advances in understanding mechanisms underlying photosystem II assembly and repair in cyanobacteria. In: PHOTOSYNTHESIS RESEARCH. SPRINGER VAN GODEWIJCKSTRAAT 30, 3311 GZ DORDRECHT, NETHERLANDS, 202.

Komenda J, Sobotka R, Nixon PJ. **2012**. Assembling and maintaining the Photosystem II complex in chloroplasts and cyanobacteria. *Current Opinion in Plant Biology* **15**: 245–251.

Kou J, Oguchi R, Fan DY, Chow WS. **2012**. The time course of photoinactivation of

photosystem II in leaves revisited. *Photosynthesis Research* **113**: 157–164.

Kovács L, Ayaydin F, Kálai T, Tandori J, Kós PB, Hideg É. **2014**. Assessing the applicability of singlet oxygen photosensitizers in leaf studies. *Photochemistry and Photobiology* **90**: 129–136.

Kramarenko GG, Hummel SG, Martin SM, Buettner GR. **2006**. Ascorbate Reacts with Singlet Oxygen to Produce Hydrogen Peroxide. *Photochemistry and Photobiology* **82**: 1634.

Krasnovsky AAJ. **1998**. Singlet molecular oxygen in photobiochemical systems: IR phosphorescence studies. *Membrane & cell biology* **12**: 665–690.

Krieger-Liszkay A. **2005**. Singlet oxygen production in photosynthesis. *Journal of Experimental Botany* **56**: 337–346.

Krieger-Liszkay A, Fufezan C, Trebst A. **2008**. Singlet oxygen production in photosystem II and related protection mechanism. *Photosynthesis Research* **98**: 551–564.

Krishnan N, Dickman MB, Becker DF. **2008**. Proline modulates the intracellular redox environment and protects mammalian cells against oxidative stress. *Free Radical Biology and Medicine* **44**: 671–681.

LaJeunesse TC, Wiedenmann J, Casado-Amezúa P, D'ambra I, Turnham KE, Nitschke MR, Oakley CA, Goffredo S, Spano CA, Cubillos VM. **2021**. Revival of Philozoon Geddes for host-specialized dinoflagellates,'zooxanthellae', in animals from coastal temperate zones of northern and southern hemispheres. *European Journal of Phycology*: 1–15.

Laloi C, Havaux M. **2015**. Key players of singlet oxygen-induced cell death in plants. *Frontiers in Plant Science* **6**.

Larkum AWD. **2003**. Light-harvesting systems in algae. In: Photosynthesis in algae. Springer, 277–304.

Larkum AWD, Vesk M. **2003**. Algal Plastids: Their Fine Structure and Properties BT - Photosynthesis in Algae. In: Larkum AWD, Douglas SE, Raven JA, eds. Dordrecht: Springer Netherlands, 11–28.

De Las Rivas J, Barber J. **2004**. Analysis of the structure of the PsbO protein and its implications. *Photosynthesis Research* **81**: 329–343.

De Las Rivas J, Heredia P, Roman A. **2007**. Oxygen-evolving extrinsic proteins (PsbO,P,Q,R): Bioinformatic and functional analysis. *Biochimica et Biophysica Acta - Bioenergetics* **1767**: 575–582.

Lee SY, Jeong HJ, Kang NS, Jang TY, Jang SH, Lajeunesse TC. **2015**. Symbiodinium tridacnidorum sp. nov., a dinoflagellate common to Indo-Pacific giant clams, and a revised morphological description of Symbiodinium microadriaticum Freudenthal, emended Trench & Blank. *European Journal of Phycology* **50**: 155–172.

Leisinger U, Rüfenacht K, Fischer B, Pesaro M, Spengler A, Zehnder AJB, Eggen RIL. **2001**. The glutathione peroxidase homologous gene from Chlamydomonas reinhardtii is transcriptionally up-regulated by singlet oxygen. *Plant Molecular Biology* **46**: 395–408.

Lesser MP. **1996**. Elevated temperatures and ultraviolet radiation cause oxidative stress and inhibit photosynthesis in symbiotic dinoflagellates. *Limnology and Oceanography* **41**: 271–283.

Lesser MP. **1997**. Oxidative stress causes coral bleaching during exposure to elevated temperatures. *Coral Reefs* **16**: 187–192.

Lesser MP, Stochaj WR, Tapley DW, Shick JM. **1990**. Coral Reefs effects of irradiance , ultraviolet radiation , and temperature. *Coral Reefs* **8**: 225–232.

Levin RA, Beltran VH, Hill R, Kjelleberg S, McDougald D, Steinberg PD, Van Oppen MJH. **2016**. Sex, Scavengers, and Chaperones: Transcriptome Secrets of Divergent Symbiodinium Thermal Tolerances. *Molecular Biology and Evolution* **33**: 2201–2215.

Levin RA, Suggett DJ, Nitschke MR, van Oppen MJH, Steinberg PD. **2017**. Expanding the Symbiodinium (Dinophyceae, Suessiales) Toolkit Through Protoplast Technology. *Journal of Eukaryotic Microbiology* **64**: 588–597.

Li L, Aro EM, Millar AH. **2018**. Mechanisms of Photodamage and Protein Turnover in Photoinhibition. *Trends in Plant Science* **23**: 667–676.

Lichtenthaler HKBT-M in E. **1987**. [34] Chlorophylls and carotenoids: Pigments of photosynthetic biomembranes. In: Plant Cell Membranes. Academic Press, 350–382.

Lima-Melo Y, Alencar VTCB, Lobo AKM, Sousa RHV, Tikkanen M, Aro EM, Silveira JAG, Gollan PJ. **2019**. Photoinhibition of photosystem i provides oxidative protection during imbalanced photosynthetic electron transport in Arabidopsis thaliana. *Frontiers in Plant Science* **10**: 1–13.

Lingvay M, Akhtar P, Sebők-Nagy K, Páli T, Lambrev PH. **2020**. Photobleaching of Chlorophyll in Light-Harvesting Complex II Increases in Lipid Environment. *Frontiers in Plant Science* **11**: 1–14.

Lion Y, Gandin E. **1980**. on the Production of Nitroxide Radicals By. **31**.

Liu LN, Chen XL, Zhang YZ, Zhou BC. **2005**. Characterization, structure and function of linker polypeptides in phycobilisomes of cyanobacteria and red algae: An overview. *Biochimica et Biophysica Acta - Bioenergetics* **1708**: 133–142.

Loeblich AR, Sherley JL. **1979**. Observations on the theca of the motile phase of free-living and symbiotic isolates of Zooxanthella microadriatica (Freudenthal) comb. nov. *Journal of the Marine Biological Association of the United Kingdom* **59**: 195–205.

Lupínková L, Komenda J. **2004**. Oxidative Modifications of the Photosystem II D1 Protein by Reactive Oxygen Species: From Isolated Protein to Cyanobacterial Cells¶. *Photochemistry and Photobiology* **79**: 152.

Macpherson AN, Telfer A, Barber J, Truscott TG. **1993**. Direct detection of singlet oxygen from isolated Photosystem II reaction centres. *BBA - Bioenergetics* **1143**: 301–309.

MARKELL D, TRENCH R, IGLESIAS-PRIETO R. **1992**. Macromolecules associated with the cell walls of symbiotic dinoflagellates. *Symbiosis (Philadelphia, PA)* **12**: 19–31.

MAtheson, I. B. C.; Lee J. 1979. Chemical Reaction Rates of Amino Acids. *Photochem. Photobiol.* **29**: 879–881.

Matysik J, Alia, Bhalu B, Mohanty P. **2002**. Molecular mechanisms of quenching of reactive oxygen species by proline under stress in plants. *Current Science* **82**: 525–532.

Meena M, Divyanshu K, Kumar S, Swapnil P, Zehra A, Shukla V, Yadav M, Upadhyay RS. **2019**. Regulation of L-proline biosynthesis, signal transduction, transport, accumulation and its vital role in plants during variable environmental conditions. *Heliyon* **5**: e02952.

Mehta SK, Gaur JP. **1999**. Heavy-metal-induced proline accumulation and its role in ameliorating metal toxicity in Chlorella vulgaris. *New Phytologist* **143**: 253–259.

Méndez-Hurtado J, Lõpez R, Suárez D, Menéndez MI. **2012**. Theoretical study of the oxidation of histidine by singlet oxygen. *Chemistry - A European Journal* **18**: 8437–8447.

Menke W. **1962**. Structure and Chemistry of Plastids. *Annual Review of Plant Physiology* **13**: 27–44.

Menke W. **1990**. Retrospective of a botanist. *Photosynthesis Research* **25**: 77–82.

Mishra NP, Francke C, van Gorkom HJ, Ghanotakis DF. **1994**. Destructive role of singlet oxygen during aerobic illumination of the Photosystem II core complex. *BBA - Bioenergetics*

1186: 81–90.

Miskiewicz E, Ivanov AG, Huner NPA. **2002**. Stoichiometry of the photosynthetic apparatus and phycobilisome structure of the cyanobacterium Plectonema boryanum UTEX 485 are regulated by both light and temperature. *Plant Physiology* **130**: 1414–1425.

Miyao M. **1994**. Involvement of Active Oxygen Species in Degradation of the D1 Protein under Strong Illumination in Isolated Subcomplexes of Photosystem II. *Biochemistry* **33**: 9722–9730.

Mor A, Koh E, Weiner L, Rosenwasser S, Sibony-Benyamini H, Fluhr R. **2014**. Singlet oxygen signatures are detected independent of light or chloroplasts in response to multiple stresses. *Plant Physiology* **165**: 249–261.

Mori H, Yamamoto Y. **1992**. Deletion of antenna chlorophyll-a-binding proteins CP43 and CP47 by Tris-treatment of PS II membranes in weak light: Evidence for a photo-degradative effect on the PS II components other than the reaction center-binding proteins. *Biochimica et Biophysica Acta (BBA)/Protein Structure and Molecular* **1100**: 293–298.

Morrill LC, Loeblich III AR. **1981**. A survey for body scales in dinoflagellates and a revision of Cachonina and Heterocapsa (Pyrrhophyta). *Journal of Plankton Research* **3**: 53–65.

Murata N, Allakhverdiev SI, Nishiyama Y. **2012**. The mechanism of photoinhibition in vivo: Re-evaluation of the roles of catalase, α-tocopherol, non-photochemical quenching, and electron transport. *Biochimica et Biophysica Acta - Bioenergetics* **1817**: 1127–1133.

Murata N, Nishiyama Y. **2018**. ATP is a driving force in the repair of photosystem II during photoinhibition. *Plant Cell and Environment* **41**: 285–299.

Murray SA, Suggett DJ, Doblin MA, Kohli GS, Seymour JR, Fabris M, Ralph PJ. **2016**. Unravelling the functional genetics of dinoflagellates: a review of approaches and opportunities. *Perspectives in Phycology* **3**: 37–52.

Musbat L, Weitman H, Ehrenberg B. **2013**. Azide Quenching of Singlet Oxygen in Suspensions of Microenvironments of Neutral and Surface Charged Liposomes and Micelles. *Photochemistry and Photobiology* **89**: 253–258.

Muscatine L. **1990**. The role of symbiotic algae in carbon and energy flux in reef corals. *Ecosystems of the world* **25**: 75–87.

Muscatine L, Porter JW. **1977**. Reef Corals: Mutualistic Symbioses Adapted to Nutrient-Poor Environments. *BioScience* **27**: 454–460.

Mustárdy L, Garab G. **2003**. Granum revisited. A three-dimensional model - Where things

fall into place. *Trends in Plant Science* **8**: 117–122.

Nelson N, Yocum CF. **2006**. Structure and function of photosystems I and II. *Annual Review of Plant Biology* **57**: 521–565.

Nield J, Barber J. **2006**. Refinement of the structural model for the Photosystem II supercomplex of higher plants. *Biochimica et Biophysica Acta - Bioenergetics* **1757**: 353–361.

Nielsen DA, Petrou K, Gates RD. **2018**. Coral bleaching from a single cell perspective. *ISME Journal* **12**: 1558–1567.

Nimmo IC, Barbrook AC, Lassadi I, Chen JE, Geisler K, Smith AG, Aranda M, Purton S, Waller RF, Nisbet RER, *et al.* 2019. Genetic transformation of the dinoflagellate chloroplast. *eLife* **8**: 1–15.

Nishiyama Y, Allakhverdiev SI, Murata N. **2006**. A new paradigm for the action of reactive oxygen species in the photoinhibition of photosystem II. *Biochimica et Biophysica Acta - Bioenergetics* **1757**: 742–749.

Nishiyama Y, Allakhverdiev SI, Yamamoto H, Hayashi H, Murata N. **2004**. Singlet oxygen inhibits the repair of photosystem II by suppressing the translation elongation of the D1 protein in Synechocystis sp. PCC 6803. *Biochemistry* **43**: 11321–11330.

Nishiyama Y, Yamamoto H, Allakhverdiev SI, Inaba M, Yokota A, Murata N. **2001**. Oxidative stress inhibits the repair of photodamage to the photosynthetic machinery. *EMBO Journal* **20**: 5587–5594.

Nixon PJ, Michoux F, Yu J, Boehm M, Komenda J. **2010**. Recent advances in understanding the assembly and repair of photosystem II. *Annals of Botany* **106**: 1–16.

Noda J, Mühlroth A, Bučinská L, Dean J, Bones AM, Sobotka R. **2017**. Tools for biotechnological studies of the freshwater alga Nannochloropsis limnetica: antibiotic resistance and protoplast production. *Journal of Applied Phycology* **29**: 853–863.

Ogilby PR. **2010**. Singlet oxygen: There is indeed something new under the sun. *Chemical Society Reviews* **39**: 3181–3209.

Oguchi R, Terashima I, Chow WS. **2009**. The involvement of dual mechanisms of photoinactivation of photosystem II in capsicum annuum L. plants. *Plant and Cell Physiology* **50**: 1815–1825.

Ohad I, Kyle DJ, Arntzen CJ. **1984**. Membrane protein damage and repair: removal and replacement of inactivated 32-kilodalton polypeptides in chloroplast membranes. *The Journal*

of cell biology **99**: 481–485.

Okada K, Ikeuchi M, Yamamoto N, Ono TA, Miyao M. **1996**. Selective and specific cleavage of the D1 and D2 proteins of Photosystem II by exposure to singlet oxygen: Factors responsible for the susceptibility to cleavage of the proteins. *Biochimica et Biophysica Acta - Bioenergetics* **1274**: 73–79.

Okada K, Satoh K, Katoh S. **1991**. Chloramphenicol is an inhibitor of photosynthesis. *FEBS Letters* **295**: 155–158.

Olson JM. **2006**. Photosynthesis in the Archean era. *Photosynthesis Research* **88**: 109–117.

Pandolfi JM, Connolly SR, Marshall DJ, Cohen AL. **2011**. Projecting coral reef futures under global warming and ocean acidification. *Science* **333**: 418–422.

Park SN, Won DH, Hwang JP, Han SB. **2014**. Cellular protective effects of dehydroeffusol isolated from Juncus effusus L. and the mechanisms underlying these effects. *Journal of Industrial and Engineering Chemistry* **20**: 3046–3052.

Pedersen SK, Holmehave J, Blaikie FH, Gollmer A, Breitenbach T, Jensen HH, Ogilby PR. **2014**. Aarhus sensor green: A fluorescent probe for singlet oxygen. *Journal of Organic Chemistry* **79**: 3079–3087.

Petrou K, Nielsen DA, Heraud P. **2018**. Single-cell biomolecular analysis of coral algal symbionts reveals opposing metabolic responses to heat stress and expulsion. *Frontiers in Marine Science* **5**: 1–12.

Pfeil BE, Schoefs B, Spetea C. **2014**. Function and evolution of channels and transporters in photosynthetic membranes. *Cellular and Molecular Life Sciences* **71**: 979–998.

Pochon X, Gates RD. **2010**. A new Symbiodinium clade (Dinophyceae) from soritid foraminifera in Hawai'i. *Molecular Phylogenetics and Evolution* **56**: 492–497.

Pospíšil P. **2016**. Production of Reactive Oxygen Species by Photosystem II as a Response to Light and Temperature Stress . *Frontiers in Plant Science* **7**: 1950.

Pozdnyakov I, Skarlato S. **2012**. Dinoflagellate amphiesma at different stages of the life cycle. *Protistology* **7**: 108–115.

Prasad A, Balukova A, Pospíšil P. **2018a**. Triplet excited carbonyls and singlet oxygen formation during oxidative radical reaction in skin. *Frontiers in Physiology* **9**: 1–9.

Prasad A, Sedlářová M, Pospíšil P. **2018b**. Singlet oxygen imaging using fluorescent probe

Singlet Oxygen Sensor Green in photosynthetic organisms. *Scientific Reports* **8**: 1–13.

Pribil M, Sandoval-Ibáñez O, Xu W, Sharma A, Labs M, Liu Q, Galgenmüller C, Schneider T, Wessels M, Matsubara S, *et al.* 2018. Fine-tuning of photosynthesis requires CURVATURE THYLAKOID1-mediated thylakoid plasticity. *Plant Physiology* **176**: 2351–2364.

Qin D, Xia Y, Whitesides GM. **2010**. Soft lithography for micro- and nanoscale patterning. *Nature Protocols* **5**: 491–502.

Ragàs X, Jiménez-Banzo A, Sánchez-García D, Batllori X, Nonell S. **2009**. Singlet oxygen photosensitisation by the fluorescent probe Singlet Oxygen Sensor Green®. *Chemical Communications*: 2920–2922.

Ramel F, Birtic S, Cuiné S, Triantaphylidès C, Ravanat JL, Havaux M. **2012**. Chemical quenching of singlet oxygen by carotenoids in plants. *Plant Physiology* **158**: 1267–1278.

Rast A, Heinz S, Nickelsen J. **2015**. Biogenesis of thylakoid membranes. *Biochimica et Biophysica Acta - Bioenergetics* **1847**: 821–830.

Rehman AU, Bashir F, Ayaydin F, Kóta Z, Páli T, Vass I. **2021**. Proline is a quencher of singlet oxygen and superoxide both in in vitro systems and isolated thylakoids. *Physiologia Plantarum* **172**: 7–18.

Rehman AU, Cser K, Sass L, Vass I. **2013**. Characterization of singlet oxygen production and its involvement in photodamage of Photosystem II in the cyanobacterium Synechocystis PCC 6803 by histidine-mediated chemical trapping. *Biochimica et Biophysica Acta - Bioenergetics* **1827**: 689–698.

Rehman AU, Kodru S, Vass I. **2016a**. Chloramphenicol mediates superoxide production in photosystem II and enhances its photodamage in isolated membrane particles. *Frontiers in Plant Science* **7**: 1–5.

Rehman AU, Szabó M, Deák Z, Sass L, Larkum A, Ralph P, Vass I. **2016b**. Symbiodinium sp. cells produce light-induced intra- and extracellular singlet oxygen, which mediates photodamage of the photosynthetic apparatus and has the potential to interact with the animal host in coral symbiosis. *New Phytologist* **212**: 472–484.

Renger G. **2010**. The light reactions of photosynthesis. *Current Science* **98**: 1305–1319.

Richier S, Furla P, Plantivaux A, Merle PL, Allemand D. **2005**. Symbiosis-induced adaptation to oxidative stress. *Journal of Experimental Biology* **208**: 277–285.

Rinalducci S, Pedersen JZ, Zolla L. **2004**. Formation of radicals from singlet oxygen produced during photoinhibition of isolated light-harvesting proteins of photosystem II. *Biochimica et Biophysica Acta - Bioenergetics* **1608**: 63–73.

Rinalducci S, Pedersen JZ, Zolla L. **2008**. Generation of reactive oxygen species upon strong visible light irradiation of isolated phycobilisomes from Synechocystis PCC 6803. *Biochimica et Biophysica Acta - Bioenergetics* **1777**: 417–424.

Roth MS. **2014**. The engine of the reef: Photobiology of the coral-algal symbiosis. *Frontiers in Microbiology* **5**: 1–22.

Ruban A V., Berera R, Ilioaia C, Van Stokkum IHM, Kennis JTM, Pascal AA, Van Amerongen H, Robert B, Horton P, Van Grondelle R. **2007**. Identification of a mechanism of photoprotective energy dissipation in higher plants. *Nature* **450**: 575–578.

Rutherford AW. **1989**. Photosystem II, the water-splitting enzyme. *Trends in biochemical sciences* **14**: 227–232.

Sakai K, Charlot F, Saux T Le, Bonhomme S, Nogué F, Palauqui JC, Fattaccioli J. **2019**. Design of a comprehensive microfluidic and microscopic toolbox for the ultra-wide spatio-temporal study of plant protoplasts development and physiology. *Plant Methods* **15**: 1–12.

Schreiber U, Quayle P, Schmidt S, Escher BI, Mueller JF. **2007**. Methodology and evaluation of a highly sensitive algae toxicity test based on multiwell chlorophyll fluorescence imaging. *Biosensors and Bioelectronics* **22**: 2554–2563.

Sedoud A, López-Igual R, Rehman AU, Wilson A, Perreau F, Boulay C, Vass I, Krieger-Liszkay A, Kirilovsky D. **2014**. The cyanobacterial photoactive orange carotenoid protein is an excellent singlet oxygen quencher. *Plant Cell* **26**: 1781–1791.

Seibert M, DeWit M, Staehelin LA. **1987**. Structural localization of the O2-evolving apparatus to multimeric (tetrameric) particles on the luminal surface of freeze-etched photosynthetic membranes. *Journal of Cell Biology* **105**: 2257–2265.

Seidler A. **1996**. The extrinsic polypeptides of photosystem II. *Biochimica et Biophysica Acta - Bioenergetics* **1277**: 35–60.

Seymour JR, Ahmed T, Marcos, Stocker R. **2008**. A microfluidic chemotaxis assay to study microbial behavior in diffusing nutrient patches. *Limnology and Oceanography: Methods* **6**: 477–488.

Shoaf WT, Lium BW. **1976**. Improved extraction of chlorophyll a and b from algae using

dimethyl sulfoxide. *Limnology and Oceanography* **21**: 926–928.

Signorelli S, Arellano JB, Melø TB, Borsani O, Monza J. **2013**. Proline does not quench singlet oxygen: Evidence to reconsider its protective role in plants. *Plant Physiology and Biochemistry* **64**: 80–83.

Signorelli S, Imparatta C, Rodríguez-Ruiz M, Borsani O, Corpas FJ, Monza J. **2016**. *In vivo* and *in vitro* approaches demonstrate proline is not directly involved in the protection against superoxide, nitric oxide, nitrogen dioxide and peroxynitrite. *Functional Plant Biology* **43**: 870–879.

Sinha RK, Komenda J, Knoppová J, Sedlářová M, Pospíšil P. **2012**. Small CAB-like proteins prevent formation of singlet oxygen in the damaged photosystem II complex of the cyanobacterium Synechocystis sp. PCC 6803. *Plant, Cell and Environment* **35**: 806–818.

Skovsen E, Snyder JW, Lambert JDC, Ogilby PR. **2005**. Lifetime and diffusion of singlet oxygen in a cell. *Journal of Physical Chemistry B* **109**: 8570–8573.

Smirnoff N, Cumbes QJ. **1989**. Hydroxyl radical scavenging activity of compatible solutes. *Phytochemistry* **28**: 1057–1060.

Sonoike K, Terashima I. **1994**. Mechanism of photosystem-I photoinhibition in leaves of Cucumis sativus L. *Planta* **194**: 287–293.

Sonoike K, Terashima I, Iwaki M, Itoh S. **1995**. Destruction of photosystem I iron-sulfur centers in leaves of Cucumis sativus L. by weak illumination at chilling temperatures. *FEBS Letters* **362**: 235–238.

Staehelin LA. **1975**. Chloroplast membrane structure. *Biochimica et biophysica acta* **408**: 1–11.

Staehelin LA, van der Staay GWM. **1996**. Structure, Composition, Functional Organization and Dynamic Properties of Thylakoid Membranes. : 11–30.

Steele RE, David CN, Technau U. **2011**. A genomic view of 500 million years of cnidarian evolution. *Trends in Genetics* **27**: 7–13.

Suorsa M, Aro EM. **2007**. Expression, assembly and auxiliary functions of photosystem II oxygen-evolving proteins in higher plants. *Photosynthesis Research* **93**: 89–100.

Szabados L, Savouré A. **2010**. Proline: a multifunctional amino acid. *Trends in Plant Science* **15**: 89–97.

Szabó M. **2020**. No Title. In: Photosynthesis in Algae: Biochemical and Physiological Mechanisms,. 459–488.

Tanaka A, Makino A. **2009**. Photosynthetic research in plant science. *Plant and Cell Physiology* **50**: 681–683.

Tandeau De Marsac N. **2003**. Phycobiliproteins and phycobilisomes: The early observations. *Photosynthesis Research* **76**: 193–205.

Tang CY, Wu FY, Yang MK, Guo YM, Lu GH, Yang YH. **2016**. A classic near-infrared probe indocyanine green for detecting singlet oxygen. *International Journal of Molecular Sciences* **17**: 1–8.

Telfer A, Bishop SM, Phillips D, Barber J. **1994**. Isolated photosynthetic reaction center of photosystem II as a sensitizer for the formation of singlet oxygen. Detection and quantum yield determination using a chemical trapping technique. *Journal of Biological Chemistry* **269**: 13244–13253.

Telfer A, Oldham TC, Phillips D, Barber J. **1999**. Singlet oxygen formation detected by near-infrared emission from isolated photosystem II reaction centres: Direct correlation between P680 triplet decay and luminescence rise kinetics and its consequences for photoinhibition. *Journal of Photochemistry and Photobiology B: Biology* **48**: 89–96.

Tiwari A, Mamedov F, Grieco M, Suorsa M, Jajoo A, Styring S, Tikkanen M, Aro EM. **2016**. Photodamage of iron-sulphur clusters in photosystem i induces non-photochemical energy dissipation. *Nature Plants* **2**.

Tóth SZ, Nagy V, Puthur JT, Kovács L, Garab G. **2011**. The physiological role of ascorbate as photosystem II electron donor: Protection against photoinactivation in heat-stressed leaves. *Plant Physiology* **156**: 382–392.

Trench RK, Blank RJ. **1987**. Symbiodinium Microadriaticum Freudenthal, S. Goreauii Sp. Nov., S. Kawagutii Sp. Nov. and S. Pilosum Sp. Nov.: Gymnodinioid Dinoflagellate Symbionts of Marine Invertebrates. *Journal of Phycology* **23**: 469–481.

Treves H, Raanan H, Kedem I, Murik O, Keren N, Zer H, Berkowicz SM, Giordano M, Norici A, Shotland Y, *et al.* 2016. The mechanisms whereby the green alga Chlorella ohadii, isolated from desert soil crust, exhibits unparalleled photodamage resistance. *New Phytologist* **210**: 1229–1243.

Triantaphylidès C, Havaux M. **2009**. Singlet oxygen in plants: production, detoxification and

signaling. *Trends in Plant Science* **14**: 219–228.

Triantaphylidès C, Krischke M, Hoeberichts FA, Ksas B, Gresser G, Havaux M, Van Breusegem F, Mueller MJ. **2008**. Singlet oxygen is the major reactive oxygen species involved in photooxidative damage to plants. *Plant Physiology* **148**: 960–968.

Tyystjärvi E. **2013a**. Chapter Seven - Photoinhibition of Photosystem II∗. In: Jeon KWBT-IR of C and MB, ed. International Review of Cell and Molecular Biology. Academic Press, 243–303.

Tyystjärvi E. **2013b**. *Photoinhibition of Photosystem II**.

Tyystjärvi E, Aro EM. **1996**. The rate constant of photoinhibition, measured in lincomycin-treated leaves, is directly proportional to light intensity. *Proceedings of the National Academy of Sciences of the United States of America* **93**: 2213–2218.

Tyystjärvi T, Herranen M, Aro EM. **2001**. Regulation of translation elongation in cyanobacteria: Membrane targeting of the ribosome nascent-chain complexes controls the synthesis of D1 protein. *Molecular Microbiology* **40**: 476–484.

Vass I. **2011**. Role of charge recombination processes in photodamage and photoprotection of the photosystem II complex. *Physiologia Plantarum* **142**: 6–16.

Vass I. **2012**. Molecular mechanisms of photodamage in the Photosystem II complex. *Biochimica et Biophysica Acta - Bioenergetics* **1817**: 209–217.

Vass I, Aro E-M. **2008**. Chapter 10 Photoinhibition of Photosynthetic Electron Transport. In: Primary Processes of Photosynthesis, Part 1: Principles and Apparatus. The Royal Society of Chemistry, 393–425.

Vass I, Cser K. **2009**. Janus-faced charge recombinations in photosystem II photoinhibition. *Trends in Plant Science* **14**: 200–205.

Verslues PE, Sharma S. **2010**. Proline Metabolism and Its Implications for Plant- Environment Interaction Authors : Verslues , Paul E ., and Sharma , Sandeep Published By : The American Society of Plant Biologists Proline Metabolism and Its Implications for Plant-Environment Interactio. **2010**.

Virtanen O, Khorobrykh S, Tyystjärvi E. **2021**. Acclimation of Chlamydomonas reinhardtii to extremely strong light. *Photosynthesis Research* **147**: 91–106.

Vogelmann TC, Han T. **2000**. Measurement of gradients of absorbed light in spinach leaves from chlorophyll fluorescence profiles. *Plant, Cell and Environment* **23**: 1303–1311.

Wakefield TS, Farmer MA, Kempf SC. **2000**. Revised description of the fine structure of in situ ‘zooxanthellae’ genus Symbiodinium. *The Biological Bulletin* **199**: 76–84.

Wang LH, Liu YH, Ju YM, Hsiao YY, Fang LS, Chen CS. **2008**. Cell cycle propagation is driven by light-dark stimulation in a cultured symbiotic dinoflagellate isolated from corals. *Coral Reefs* **27**: 823–835.

Wang F, Zeng B, Sun Z, Zhu C. **2009**. Relationship between proline and Hg 2+-induced oxidative stress in a tolerant rice mutant. *Archives of environmental contamination and toxicology* **56**: 723–731.

Weis VM. **2008**. Cellular mechanisms of Cnidarian bleaching: Stress causes the collapse of symbiosis. *Journal of Experimental Biology* **211**: 3059–3066.

Westerwalbesloh C, Brehl C, Weber S, Probst C, Widzgowski J, Grünberger A, Pfaff C, Nedbal L, Kohlheyer D. **2019**. A microfluidic photobioreactor for simultaneous observation and cultivation of single microalgal cells or cell aggregates. *PLoS ONE* **14**: 1–13.

Whitmarsh J, Govindjee. **1999**. The Photosynthetic Process BT - Concepts in Photobiology: Photosynthesis and Photomorphogenesis. In: Singhal GS, Renger G, Sopory SK, Irrgang K-D, Govindjee, eds. Dordrecht: Springer Netherlands, 11–51.

Wietheger A, Starzak DE, Gould KS, Davy SK. **2018**. Differential ROS generation in response to stress in Symbiodinium spp. *Biological Bulletin* **234**: 11–21.

Yao J, Kim HS, Kim JY, Choi Y-E, Park J. **2020**. Mechanical stress induced astaxanthin accumulation of H. pluvialis on a chip. *Lab on a Chip* **20**: 647–654.

Yellowlees D, Rees TA V., Leggat W. **2008**. Metabolic interactions between algal symbionts and invertebrate hosts. *Plant, Cell and Environment* **31**: 679–694.

Yuyama I, Harii S, Hidaka M. **2012**. Algal symbiont type affects gene expression in juveniles of the coral Acropora tenuis exposed to thermal stress. *Marine Environmental Research* **76**: 41–47.

Zavafer A, Iermak I, Cheah MH, Chow WS. **2019**. Two Quenchers Formed During Photodamage of Phostosystem II and The Role of One Quencher in Preemptive Photoprotection. *Scientific Reports* **9**: 1–9.

Zavafer A, Koinuma W, Chow WS, Cheah MH, Mino H. **2017**. Mechanism of photodamage of the oxygen evolving Mn Cluster of Photosystem II by excessive light energy. *Scientific Reports* **7**: 11–14.

Zhou Y, Liu Z, Yao M, Chen J, Xiao Y, Han G, Shen J-R, Wang F. **2021**. Elucidating the Molecular Mechanism of Dynamic Photodamage of Photosystem II Membrane Protein Complex by Integrated Proteomics Strategy. *CCS Chemistry*: 443–454.

Zolla L, Rinalducci S. **2002**. Involvement of active oxygen species in degradation of light-harvesting proteins under light stresses. *Biochemistry* **41**: 14391–14402.

SUMMARY

Singlet oxygen ($^1O_2$) is an important ROS, produced in photosynthetic organisms under stress conditions. Apart from its role as a signaling molecule, it also plays a destructive role in the cells by damaging proteins and lipids in photosynthetic organisms. Despite intensive research, the mechanism of $^1O_2$ mediated photodamage is still unclear, and previous studies failed to investigate the $^1O_2$ produced intracellularly. The mechanism of $^1O_2$ quenching also needs to be investigated in order to understand how $^1O_2$ can be eliminated from the cells. For this reason, the current thesis is based on the study of $^1O_2$, in particular, its intracellular detection method, the photodamage caused by it in the photosynthetic apparatus, and finally the elimination or scavenging of $^1O_2$ to protect the cells from its harmful effects.

Detection of $^1O_2$-mediated photooxidative stress in the symbiotic dinoflagellate Symbiodinium

Previous studies used histidine (His) uptake method and Singlet Oxygen Sensor Green (SOSG) fluorescent probe for the detection of $^1O_2$ in the coral endosymbiont algae, *Symbiodinium* (Symbiodiniaceae) (Rehman *et al.*, 2016b); however, $^1O_2$ could only be detected externally in *Symbiodinium*. We have established a method for the investigation of intracellularly produced $^1O_2$ by using the fluorescent probe (SOSG) via protoplast technology. *Symbiodinium* protoplasts were successfully isolated by using cellulase enzyme in combination with macerozyme. For the real time monitoring of the process of protoplast formation and regeneration, a microfluidic system was employed, with trapping and morphometric analysis of single cells throughout the whole protoplast formation and regeneration time. The area, major and minor axis of the cells increased, until an equilibrium state in these parameters were attained; however, the eccentricity of the cells exhibited a decrease, indicating that the cells became more rounded over time. Our data show that protoplast process can be accelerated with increasing the flow rate in the microfluidic chambers. Control cells at various flow rates does not show any morphological changes; however, protoplast formation process was faster at higher flow rate. The photosynthetic competency of cells was recorded by measuring the the maximum quantum yield of PSII in dark adapted state (F_v/F_m) of the cells. F_v/F_m before the enzyme treatment was not impacted by the applied flow rate; however, during enzyme treatment, higher flow rate resulted in reduced F_v/F_m. F_v/F_m largely (but not fully) recovered in the regeneration phase, indicating that the enzyme digestion procedure did not impair PSII quantum yield. Our results regarding the SOSG labeling of the *Symbiodinium* cells confirmed

the previous findings of (Rehman *et al.*, 2016b) that intact cells does not show any SOSG fluorescence intracellularly, fluorescence could only be detected externally. The protoplasts were labelled intracellularly and the green fluorescence of SOSG was observed to be co-localized with the red fluorescence of chlorophyll indicating the localization of the SOSG dye in the chloroplast. However, in some cases the SOSG dye was evenly distributed in the cytoplasm and it did not show considerable co-localization with chlorophyll autofluorescence. To confirm $^1O_2$ production in the protoplast, SOSG staining was done in combination with His and results showed that SOSG fluorescence was strongly quenched due to the $^1O_2$ uptake by His. Our results demonstrated for the first time that SOSG is penetrated to the protoplasts of *Symbiodinium* and therefore protoplasts are amenable to investigate singlet oxygen signaling in *Symbiodinium*.

Proline is a $^1O_2$ quencher both in vitro and in isolated thylakoids

Proline (Pro) is an essential antioxidant metabolite that accumulates in large amounts in plant cells in response to stress conditions such as water deficiency, salinity, UV radiation, and heavy metals. Pro reduces the levels of various ROS types in intact plant systems and leads to cellular osmotic change as a compatible solute. While there is consensus in the literature that Pro can directly or indirectly remove OH and H_2O_2 in vivo (Akhter Banu *et al.*, 2010), its function in scavenging $^1O_2$ is debated: some studies reported that Pro is an effective $^1O_2$ quencher (Alia *et al.*, 1997; Matysik *et al.*, 2002). In contrary, Signorelli and colleagues presented indicating that Pro did not scavenge $^1O_2$ (Signorelli *et al.*, 2013). The debate over Pro's ability to interact with $^1O_2$ most likely stems from a misunderstanding of the physical and chemical mechanisms of $^1O_2$ removal. By using three different approaches: EPR spin trapping by TEMPD, the fluorescent reporter dye SOSG and O_2 uptake measurements, we could clearly show that Pro does quench $^1O_2$ both in vitro and in photosynthetically active plant thylakoid membranes. In our experiments, we used a slightly modified version of the spin trap, TEMPD (2,2,6,6-tetramethyl-4-piperidone) instead of the TEMP (2,2,6,6-tetramethylpiperidine) used by Mohanty and coworkers. When TEMPD reacts with $^1O_2$, it forms a stable paramagnetic product known as TEMPO-D. The EPR line shape did not change under our conditions, indicating no significant interaction between TEMPO-D and Pro. Our findings support the original interpretation by Alia *et al.*, (1997) that the explanation for the decreased signal of the TEMPO-D product is the removal of $^1O_2$ by Pro, which reduces the likelihood of $^1O_2$ being trapped by TEMPD. We could also demonstrate that $^1O_2$ quenching by Pro occurs via a physical

mechanism, i.e., it does not include a chemical (oxidation) reaction. Physical quenching of $^1O_2$ by Pro most likely proceed via forming a charge transfer complex, due to the low ionization potential of Pro, which relaxes O_2 back to its triplet ground state via inter system crossing (Alia *et al.*, 2001). We compared the rate constants of $^1O_2$ removal and total ROS-detoxifying capacities of Pro and other antioxidants from previous literature of osmotic or salt-stressed wild-type *Arabidopsis*. From these data, it is revealed that $^1O_2$-scavenging capacity of Pro can reach up to two third of that of α-tocopherol and one fourth or more of that of Asc. Therefore, the $^1O_2$-quenching potential of Pro can provide physiologically relevant contribution to $^1O_2$ detoxification in stressed plants, in cell compartments having low levels of more efficient antioxidants. The scavenging efficiency of proline is relatively small on a molar basis, but considering its presence in high amounts in plant cells under stress conditions it may provide a physiologically relevant contribution to ROS scavenging, supplementing other nonenzymatic ROS scavengers of plant cells.

Externally produced $^1O_2$ is capable of damaging PSII in isolated thylakid membranes and Chlorella sorokiniana cells

We provided a clear experimental evidence that $^1O_2$ when generated by the externally added photosensitizer, RB, induces the loss of PSII activity in isolated thylakoids which are incapable of PSII repair. *Chlorella sorokiniana* cells also showed the loss of PSII activity by externally generated $^1O_2$, when the cells were incubated with the protein synthesis inhibitor lincomycin and therefore the PSII repair mechanisms were blocked. These data provide strong support for the idea that the harmful effect of $^1O_2$ is not restricted to the inhibition of the PSII repair, instead $^1O_2$ is capable of direct inactivation of PSII and can act as a mediator in photooxidative damage of the photosynthetic apparatus. Our data show that illumination of thylakoids and intact *Chlorella* cells in the presence of RB can damage PSII activity even when relatively low concentrations of RB (1–10 μM) are used. The loss of PSII activity by externally generated $^1O_2$ is in full agreement with previous studies, which showed the impact of $^1O_2$ in vitro can be related to the fragmentation of D1 protein, i.e. the scission of peptide bonds in the D1 protein (Miyao, 1994; Lupínková & Komenda, 2004), and consequently inactivation of electron transport (Mishra *et al.*, 1994), and also with the degradation of the D1 protein during illumination of RB infiltrated leaves (Hideg *et al.*, 2007; Kovács *et al.*, 2014). The damaging effect is obviously more substantial in the isolated thylakoids than in the intact *Chlorella* cells, but even in the latter case the enhancement of PSII activity loss is statistically significant and

increases with increasing RB concentrations, especially in the presence of lincomycin, which blocks protein synthesis dependent PSII repair. The addition of His together with RB in thylakoids provided a significant protection against the loss of PSII activity when compared to the effect of RB addition alone, confirming the involvement of $^1O_2$ in PSII damage. In the case of *Chlorella* cells, the protective effect of His was not conclusive most likely due to the relatively small extent of PSII activity loss. It is also possible that the penetration of His to the vicinity of PSII complexes inside the *Chlorella* cells, where it could exert its protective action, was limited. However, based on the strong protective effect of His in thylakoids, we can assume that His would ameliorate PSII activity loss in *Chlorella* as well, provided that it can reach the thylakoids inside the cells. Our results contradict with those of earlier studies by Nishiyama and coworkers (Nishiyama *et al.*, 2004) in which no effect of RB induced $^1O_2$ on PSII damage rate was observed. This contradition is due to the differences in the experimental conditions in both studies. Our findings conclude that failure of previous study (Nishiyama *et al.*, 2004) to identify the RB-induced increase in PSII photodamage rate was most likely due to numerous effects: (i) Since the $^1O_2$ produced by the RB could not reach the thylakoid-embedded functional components of PSII, it lowered the possibility of detecting the PSII activity loss. (ii) Using strong visible light instead of selective excitation of RB for photodamage studies, together with a high chloramphenicol concentration enhanced the photodamage rate, which could easily mask the relatively small enhancement of $^1O_2$-induced PSII damage. These technical issues were solved in our study by selective excitation of RB and the use of lincomycin as a protein synthesis inhibitor that does not interfere with PSII electron transport, allowing to detect $^1O_2$-induced PSII activity loss not only in isolated thylakoids but also in intact *Chlorella* cells.

A DOLGOZAT ÖSSZEFOGLALÁSA

A szinglet oxigén ($^1O_2$) egy fontos reaktív oxigénforma, amely a fotoszintetikus szervezetekben képződik stresszkörülmények között. Amellett, hogy fontos szignálmolekula, jelentős károsító hatású a fotoszintetikus szervezetek fehérjéire és a lipidekre. Az intenzív kutatások ellenére a $^1O_2$ általl közvetített fotokémiai károdosás mechanizmusai még nem teljesen tisztázottak, valamint a $^1O_2$ intracelluláris lokalizációja sem teljesen ismert. A $^1O_2$ kioltási mechanizmusai és a $^1O_2$ eliminációjának megértése szintén további vizsgálatokat igényelnek. Ezért munkánk során célul tűztük ki a $^1O_2$ intracelluláris detektálását, a fotoszintetikus apparátusra gyakorolt károsító hatásának, és végül a $^1O_2$ eliminálásának vizsgálatát a sejtkárosító hatás kivédésére.

$^1O_2$ közvetítette fotooxidatív stressz a szimbiózisban élő Symbiodinium sejtekben

Korábbi vizsgálatokban a hisztidin (His) felvétel kinetikáját és a Singlet Oxygen Sensor Green (SOSG) fluoreszcencens festéket alkalmazták $^1O_2$ detektálására a korallokkal szimbiózisban élő algákban, a *Symbiodinium*ban (Symbiodiniaceae) (Rehman *et al.*, 2013, 2016), azonban *Symbiodinium*ban a $^1O_2$ csak az extracelluláris térben volt kimutatható. A munkánk során kidolgoztunk egy módszert, amellyel a $^1O_2$ intracellulárisan is kimutatható SOSG segítségével, protoplaszt technológia alkalmazásával. *Symbiodinium* sejtekből protoplasztokat készítettünk celluláz és macerozym enzimkeverékkel. A protoplaszt képződést és regenerálódást valós időben tanulmányoztuk mikrofluidikai kamrákban, amelyekben egyedi sejtek morfológiai analízise megvalósítható a teljes protoplaszt képződés és regeneráció során. A sejtek térfogata, hossz- és kereszt irányú átmérője növekedett, majd egy egyensúlyi állapot alakult ki; a sejtek eccentricitása csökkent, amely arra utal, hogy a sejtek kerekebbé váltak. Kimutattuk, hogy a protoplaszt képződés folyamata valamelyest felgyorsítható az áramlási sebesség növelésével a mikrofluidikai kamrákban. Egész sejtek nem mutattak alaktani változást az áramlási sebesség megváltoztatásával, de a protoplasztok morfológiai változása felgyorsult nagyobb áramlási sebességnél. Egész sejtek fotoszintetikus aktivitása, a PSII maximális kvantumhatékonyságával (F_v/F_m) kifejezve, nem változott a különböző áramlási sebességeknél, azonban az enzimkezelés során a protoplasztok F_v/F_m értékei az áramlási sebesség függvényében szignifikánsan kisebbek voltak, mint a kontroll egész sejtek F_v/F_m értékei. Az F_v/F_m nagymértékben, de nem teljesen, visszaállt a kezdeti szintre a protoplaszt regeneráció során, amely azt mutatja, hogy az enzimkezelés nem károsította a PSII kvantumhatékonyságát. Egész sejtek jelölése SOSG-vel megerősítették korábbi eredményeinket (Rehman *et al.*,

2016b), miszerint egész sejtekben nem figyelhető meg intracelluláris SOSG fluoreszcencia, a SOSG fluoreszcenciája csak a sejten kívül detektálható *Symbiodinium* esetén. Protoplasztok esetén azonban a SOSG intracelluláris lokalizációja jól megfigyelhető, és a SOSG zöld fluoreszcenciája a kloroplasziszok vörös fluoreszcenciájával együtt lokalizálódott, amely arra utal, hogy a SOSG felhalmozódott a kloroplasztiszokban. Azonban más esetekben a SOSG és a kloroplaszt autofluoreszcenciája nem volt egyértelműen együtt lokalizálható. Annak bizonyítására, hogy a SOSG fluoreszcenciája $^1O_2$-hez köthető a protoplasztokban, a SOSG jelölést His-nel együtt végeztük. Ebben az esetben a SOSG fluoreszcenciája erősen kioltódott $^1O_2$ His általi felvétele miatt. Eredményeink először mutatták ki a SOSG intracelluláris lokalizációját *Symbiodinium*ban, valamint azt is igazolják, hogy a protoplasztok alkalmasak $^1O_2$ vizsgálatára ebben az algafajban.

A prolin $^1O_2$ kioltó in vitro és izolált tilakoidokban

A prolin (Pro) egy fontos antioxidáns molekula, amely nagymennyiségben felhalmozódik a növényi sejtekben stresszkörülmények során, mint pl. vízhiány, sóstressz, UV sugárzás és nehézfémek. A Pro csökkenti a különféle reaktív oxigénformák szintjét, és mint ozmotikusan aktív anyag, a sejtek ozmotikus viszonyainak változásához is vezet. A szakirodalomban ugyan egyetértés van abban, hogy a Pro közvetlen vagy közvetett módon képes eltávolítani a OH és H_2O_2 molekulákat in vivo (Akhter Banu et al., 2010), a $^1O_2$ semlegesítésében betöltött szerepe vitatott: egyes tanulmányokban a Pro-t igen hatékony $^1O_2$ kioltónak találták (Alia *et al.*, 1997; Matysik *et al.*, 2002). Ezzel ellentétben Signorelli és mtsai szerint a Pro nem volt képes a $^1O_2$-t semlegesíteni (Signorelli *et al.*, 2013). A Pro és $^1O_2$ kölcsönhatásiról szóló vita valószínűleg abból ered, hogy a $^1O_2$ fizikai és kémiai úton történő semlegesítése sok félreértésre adhat okot. Háromféle módszer alkalmazásával: TEMPD segítségével történő EPR spin csapdázással, SOSG fluoreszcencia és O_2 felvétel kinetikai mérésekkel kimutattuk, hogy a Proline (Pro) kioltja a $^1O_2$-t in vitro és fotoszintetikusan aktív tilakoid membránokban. A kísérleteinkben a spin csapda egy kissé módosított formáját, a TEMPD (2,2,6,6-tetramethyl-4-piperidone) molekulát használtuk a TEMP (2,2,6,6-tetramethylpiperidine) helyett (utóbbit Mohanty és mtsai alkalmazták). A TEMPD $^1O_2$-nel történő kölcsönhatása során egy stabil paramágneses anyag, TEMPO-D képződik. A TEMPO-D EPR profilja nem változott az általunk alkalmazott körülmények során, amely arra utal, hogy nincs szignifikáns kölcsönhatás TEMPO-D és Pro között. Eredményeink megerősítik Alia et al. 1997 eredményeit, miszerint a TEMPO-D csökkent jele a $^1O_2$ Pro általi eltávolításából ered,

amely csökkenti annak valószínűségét hogy a $^1O_2$ TEMPD által csapdázódjon. Kimutattuk azt is, hogy a $^1O_2$ Pro általi kioltása fizikai mechanizmus útján történik, vagyis nem indukál kémiai (oxidációs) folyamatokat. A $^1O_2$ Pro általi fizikai kioltása töltéstranszfer komplex kialakulása által történik; a Pro alacsony ionizációs potenciálja a O_2 triplet állapotába alakulását eredményezi inter-system crossing által (Alia et al. 2001). Szakirodalmi adatok alapján összehasonlítottuk a Pro $^1O_2$ eltávolítási és a teljes ROS-detoxifikáció sebesség állandóját más antioxidánsokkal ozmotikus vagy só-stresszelt vad típusú *Arabidopsis*ban. Ezek az adatok azt mutatják, hogy a Pro $^1O_2$ kioltó kapacitása az α-tokoferol kapacitásának a kétharmada és az aszkorbát kapacitásának az egynegyede. Ezek alapján a Pro $^1O_2$ kioltó kapacitása fiziológiailag releváns stresszelt növényekben, különösen azokban a sejtkompartmentekben, amelyekben az antioxidáns kapacitás kisebb. A Pro antioxidáns kapacitása relatíve kicsi moláris alapon, azonban figyelembe véve, hogy a mennyisége megnőhet a növényi sejtekben stresszkörülmények során, jelentősen hozzájárulhat a ROS kioltásához, megemelve így más nem-enzimatikus ROS kioltó folyamatok kapacitását növényi sejtekben.

Külsőleg képződött $^1O_2$ a PSII károsodását okozza tilakoid membránokban és Chlorella sorokiniana sejtekben

Kísérleti eredményeink világosan kimutatták, hogy a külsőleg hozzáadott fotoszenzitizáló anyag Rose Bengal (RB) által generált $^1O_2$ a PSII aktivitásának csökkenését okozta izolált tilakoid membránokban, amelyekben a PSII javító mechanizmusok nem működnek. *Chlorella sorokiniana* sejtekben, melyekben a PSII javító mechanizmusok a protein szintézis inhibitor lincomycin által gátolva voltak, a külsőleg képződött $^1O_2$ szintén PSII aktivitás-csökkenést okozott. Ezek az adatok arra utalnak, hogy a $^1O_2$ károsító hatása nem korlátozódik a PSII javító mechanizmusok gátlására, hanem a $^1O_2$ képes a PSII direkt inaktivációjára és ezáltal a fotoszintetikus apparátus fotooxidatív károsodásának mediátora.
Az adataink azt mutatják, hogy *Chlorella* sejtek és tilakoidok megvilágítása RB jelenlétében károsítja a PSII-t még viszonylag kis RB koncentrációknál (1-10 μM) is. A PSII aktivitásának csökkenése külsőleg generált $^1O_2$ által egyezik korábbi tanulmányok eredményeivel, amelyek kimutatták, hogy a $^1O_2$ in vitro hatásai a D1 fehérje fragmentációjához és a D1 fehérje peptidkötéseinek hasadásához (Miyao, 1994; Lupínková & Komenda, 2004), ezáltal az elektron transzport inaktiválódásához (Mishra *et al.*, 1994) vezet. A D1 fehérje degradációja megfigyelhető volt RB-lal infiltrált, megvilágított levelekben is (Hideg *et al.*, 2007; Kovács *et al.*, 2014). A $^1O_2$ károsító hatása sokkal kifejezettebb izolált tilakoid membránokban mint

Chlorella sejtekben, de még utóbbi esetben is a PSII károsodása szignifikáns, és RB koncentráció függő volt, különösen lincomycin jelenlétében, amely gátolja a fehérjeszintézis-függő PSII javító mechanizmust. His hozzáadása RB jelenlétében jelentősen kivédte a PSII aktivitás csökkenését tilakoidokban, igazolva a $^1O_2$ szerepét a PSII károsodásában. *Chlorella* sejtekben a His védő hatása kevésbé volt egyértelmű, valószínűleg a jóval kisebb PSII károsodás miatt. Lehetséges továbbá, hogy a His bejutása a sejtekbe a PSII közvetlen közelébe, ahol a károsító hatást kifejti, meglehetősen limitált. A His erős védő hatása a tilakoidokban arra enged következtezni, hogy a PSII károsító hatása kivédhető *Chlorella* sejtekben is, feltéve, hogy a His bejut az alga sejtek tilakoid membránjaiba. A kísérleti eredményeink ellentmondanak Nishiyama és mtsai eredményeinek (Nishiyama *et al.*, 2004), amelyek azt mutatták, hogy a RB-indukált $^1O_2$ nincs hatással a PSII károsodására. Ezek az eredmények valószínűleg különböző kísérleti körülményekhez is köthetők. Eredményeinkből azt a következtetést vonhatjuk le, hogy a korábbi tanulmányokban bemutatott RB-indukált PSII károsodás hiányának számos oka lehet: i) a RB-indukált $^1O_2$ nem jutott be a tilakoid membránokba ágyazott PSII komponensek közvetlen közelébe, így a $^1O_2$ okozta PSII károsodás detektálása kevésbé volt lehetséges. ii) A korábbi kísérletek során használt erős fehér fény (amely nem szelektív a RB gerjesztésére), együtt a magas chloramphenicol koncentrációkkal nagyon megnövelte a fénykárosítás mértékét, amely így elfedte a $^1O_2$ –indukálta PSII károsodás viszonylag kis mértékét. Ezeket a technikai problémákat elkerültük a RB szelektív gerjesztésével, és a lincomycin mint fehérjeszintézis-gátlószer alkalmazásával, amely a chloramphenicol-lal ellentétben nem lép kölcsönhatásba a PSII elektron transzport aktivitásával, ezáltal alkalmas a $^1O_2$-indukálta PSII aktivitás-csökkenés detektálására tilakoidokban és *Chlorella* sejtekben is.

ACKNOWLEDGEMENTS

All Praise to ALLAH SWT the Almighty, for giving me the blessing, the strength, the chance and endurance to complete this study.

First and foremost I offer my sincerest gratitude to my supervisor, Prof. Dr. *Imre Vass*, for giving me the opportunity to carry out my PhD studies in his lab. I am very thankful for his generous guidance, encouragement and financial support throughout my PhD research work. Without his kind interest and persistent help, this thesis work would not have been possible.

I would like to express my sincere gratitude to my co-supervisor, Dr. *Milán Szabó*. I attribute my doctorate degree to his encouragement and effort and without him this thesis would not have been completed. One simply could not wish for a better or friendlier supervisor. I am very grateful to him for his scientific advice and knowledge and many insightful discussions and suggestions. He is my primary resource for getting my science questions answered and was instrumental in helping me crank out this thesis, all in a couple of months.

I also have to thank the members of my PhD committee, for constructive criticism and for offering advice and guidance on my thesis work. I would like to thank *Dr. Atteq ur Rehman* for his teaching in the lab, valuable support and thoughtful discussions during the initial stage of my PhD. I would also like to thank *László Sass* for his computer simulated work and kind support for the image analysis. I am grateful to *Sándor Kovács* for teaching me the microfluidics technique and his technical support in this project. I would like to thank *Dr. Péter Kós* for his teaching in the lab, valuable support and thoughtful discussions during the thesis work.

I would like to convey my sincere appreciation to *Ágnes Ábrahám* and *Péter Galajda* from the Institute of Biophysics, BRC for preparing and providing me the microfluidics devices whenever I needed it. Thanks to Dr. *Ferhan Ayaydin* and *Ildikó Valkony-Kelemen*, for their assistance during the confocal imaging experiments.

Thanks to the past and present members of the laboratory of Molecular Stress and Photobiology, *Istvan, Sandeesha, Gabor, Barbara, Prithwi, Ivy, Miklos, Sabit, and Priyanka* for their help and friendly working atmosphere in the group. Thanks to the laborortory technicians, *Gyorgyi* and *Lilla* for all your assistance in the lab. I would also like to express my gratitude to *Károlyi Mariann, Tímea Varga,* and other BRC administration staff for their assistance throughout my stay and thesis work. The thesis work is supported by the Hungarian Granting Agency GINOP-

2.3.2-15-2016-00026. I am obliged to GINOP which allowed me to take part in a cutting edge research project.

I also thank my friends (too many to list here but you know who you are!) for providing support and friendship that I needed.

I especially thank my mom, dad, sisters and my brothers. I love them so much, and I would not have made it this far without them. I thank my beloved grandmother and my uncle (Prof. Azeem Kiani), who have both passed on, for their love, support and prayers. I wished they could have lived for another few years for my graduation. Special thanks to the newest additions to my family, Ehsan, my husband as well as his wonderful family who all have been supportive and caring. Ehsan has been a true and great supporter and has unconditionally loved me during my good and bad times. I truly thank my family for sticking by my side, even when I was irritable and depressed. I am also grateful to all those people who have helped morally and socially to accomplish the thesis and made my stay promising.

LIST OF PUBLICATIONS (MTMT: 10074886)

Peer-reviewed publications, for PhD thesis:

Bashir, F., Rehman, AU., Szabó, M., Vass, I. (2021) Singlet oxygen damages the function of Photosystem II in isolated thylakoids and in the green alga *Chlorella sorokiniana. Photosynthesis Research* 149, 93-105. **IF: 3.63**

Rehman, A. U., Bashir, F., Ayaydin, F., Kóta, Z., Páli, T., Vass, I. (2020) Proline is a quencher of singlet oxygen and superoxide both in in vitro systems and isolated thylakoids. *Physiologia Plantarum*, *172*(1), 7-18. **IF: 4.14**

Faiza Bashir, Milán Szabó, Sándor Kovács, Ágnes Ábrahám, Ferhan Ayaydin, Péter Galajda, László Sass, Imre Vass (2021) Microfluidic analysis of viable protoplast formation in the coral endosymbiont alga Symbiodinium sp. (submitted to Lab on a Chip)

Other publications:

Mallick, I., Kirtania, P., Szabó, M., Bashir, F., Domonkos, I., Kós, P. B., & Vass, I. (2020). A simple method to produce Synechocystis PCC6803 biofilm under laboratory conditions for electron microscopic and functional studies. *Plos one*, *15*(7), e0236842. **IF: 2.74**

International conference abstracts and poster presentations

1. **Faiza Bashir**, Ateeq Ur Rehmam, Ildiko Domonkos, Ferhan Ayaydin and Imre Vass (2017) $^1O_2$ induced impairment of EPSs in Synechocystis and Symbiodinium at a Straub conference at Biological Research Center, Hungarian Academy of Sciences, Szeged, Hungary.
2. **Faiza Bashir**, Ateeq Ur Rehmam, Ildiko Domonkos, Ferhan Ayaydin and Imre Vass (2017) Singlet oxygen induced impairment of extracellular polymeric substances in *Synechocystis* and *Symbiodinium* at 19th IUPAB and 11th EBSA Congress, Edinburgh, Scotland
3. Ateeq Ur Rehmam, **Faiza Bashir**, Ferhan Ayaydin, Zoltán Kóta, Tibor Páli and Imre Vass (2018) Proline is an excellent quencher of superoxide, and singlet oxygen in vitro

at a Straub conference at Biological Research Center, Hungarian Academy of Sciences, Szeged, Hungary.

4. Ateeq Ur Rehman, Huiru Li, **Faiza Bashir**, László Kovács, Imre Vass, Christian Wild, Kai Bischof (2018) Effect of high intensity light on Photosystem II function and singlet oxygen production in the brown seaweed *Saccharina latissima* at a Straub conference at Biological Research Center, Hungarian Academy of Sciences, Szeged, Hungary.
5. **Faiza Bashir**, Ferhan Ayaydin, Ildikó Kelemen-Valkony, Györgyi Ferenc, Péter Kós, Milán Szabó, Imre Vass (2019) Application of protoplast technology for Symbiodinium sp. and other microalgae at a Straub conference at Biological Research Center, Hungarian Academy of Sciences, Szeged, Hungary.
6. **Faiza Bashir**, Ferhan Ayaydin, Ildikó Kelemen-Valkony, Györgyi Ferenc, Péter Kós, Milán Szabó, Imre Vass (2019) Protoplast technology as an experimental platform for characterizing oxidative stress in Symbiodinium sp. and other microalgae at 9th Symposium on Microalgae and Seaweed products in Plant/Soil-systems at Mosonmagyaróvár, Hungary.
7. **Faiza Bashir**, Milán Szabó, Imre Vass (2021) Singlet oxygen damages the function of Photosystem II in isolated thylakoids and in the green alga Chlorella sorokiniana at 8th Congress of Hungarian Society of Plant Biology, Szeged, Hungary.

International conference- Oral presentations

Faiza Bashir, Milán Szabó, Imre Vass (2021). Characterization of singlet oxygen in the photosynthetic apparatus of plants and microalgae at 11th Congress of the Hungarian Free Radical Society, Budapest, 27th August, 2021, Hungary.

Declaration

As the corresponding author of the scientific publications, I certify that the results reported in the Ph.D. dissertation and the following publications were not used to acquire any Ph.D. degree previously and will not be used in future either.

Bashir, F., Rehman, AU., Szabó, M., Vass, I. (2021) Singlet oxygen damages the function of Photosystem II in isolated thylakoids and in the green alga *Chlorella sorokiniana. Photosynthesis Research*, 149, 93-105.

Rehman, A. U., Bashir, F., Ayaydin, F., Kóta, Z., Páli, T., Vass, I. (2020) Proline is a quencher of singlet oxygen and superoxide both in in vitro systems and isolated thylakoids. *Physiologia Plantarum*, 172 (1), 7-18.

Szeged, 13-07-2021

Prof. Dr. Imre Vass
Director
Institute of Plant Biology
Biological Research Centre, Szeged
Temesvári krt. 62., H-6726 Szeged, Hungary